Spacecraft Relative Motion Applications to Pursuit-Evasion Games and Control Using Angles-Only Navigation

by

Ashish Jagat

A dissertation submitted to the Graduate Faculty of
Auburn University
in partial fulfillment of the
requirements for the Degree of
Doctor of Philosophy

Auburn, Alabama
August 1, 2015

Approved by

Andrew J. Sinclair, Chair, Associate Professor of Aerospace Engineering
John E. Cochran, Jr., Professor Emeritus of Aerospace Engineering
David A. Cicci, Professor of Aerospace Engineering
Subhash C. Sinha, Professor of Mechanical Engineering

Abstract

Spacecraft relative motion dynamics, guidance, navigation, and control have been studied extensively in the last decade or more owing to the growing interest in proximity operations and formation flying. This dissertation focuses on the control and navigation aspects of spacecraft relative motion by exploring two problems.

The first problem addresses the control of spacecraft relative motion from a pursuit-evasion game perspective. This problem is formulated as a two-player zero-sum differential game. The Euler-Hill reference frame is used to describe the dynamics of the game. The goal is to derive control laws which form a saddle point solution to the game. Both spacecraft use continuous-thrust engines. The linear quadratic differential game theory is applied to derive control laws for a linear pursuit-evasion game. The state-dependent Riccati equation method is applied to extend the linear quadratic differential game theory to derive control laws for a nonlinear pursuit-evasion game. Contributions of this work are development of a state-dependent coefficient model for the game dynamics using the nonlinear spacecraft relative motion equations and derivation of nonlinear pursuit-evasion control laws using this model, the efficacy of which is found to be superior to that of the linear control laws.

The second problem addresses improving the observability of the spacecraft relative-motion state when nonlinear angles-only measurements are used and one of the spacecraft is maneuvering for rendezvous. Results in the literature have shown that the linear homogeneous spacecraft relative motion is unobservable when angles-only

measurements are used. Results have also shown that the linear spacecraft relative motion can be observable when one of the spacecraft undergoes either impulsive or continuous-thrust maneuvers. This dissertation further explores the continuous-thrust feedback control of spacecraft relative motion when an angles-only navigation model is used for state estimation. A typical approach to state feedback control problems when full state knowledge is not available is to separate control and estimation: estimate the state using noisy measurements and implement the control law using the state estimate. Whereas for linear systems, control and estimation are separable, this may not be the case for systems involving nonlinearities. In such systems, control input in addition to affecting the system state also affects the observability of the state and hence affecting the accuracy of its estimate. This is called the dual effect of control.

The dual effect is found in the control of spacecraft relative motion when angles-only measurement model is used for state estimation. Two approaches to address the dual effect are explored. The first approach is the linear quadratic dual control method described in the literature and the second approach is the information-weighted LQG control method presented here as a novel contribution. Both approaches have been found to address the dual effect successfully and provide observability. The contribution of this work is the successful application of a dual control method and a new LQG control approach to gain observability of the spacecraft relative motion when angles-only measurements are used and one of the spacecraft undergoes continuous-thrust maneuvers for rendezvous.

Acknowledgments

This work could not have been completed without the help and support of many individuals. I am forever indebted to my advisor, Dr. Andrew J. Sinclair, for his constant encouragement, guidance, and support. He went above and beyond to help me succeed and was patient when I struggled. His suggestions from time to time have been imperative to this work. Working with him has been a tremendous learning experience for me. I am very thankful for the valuable time of my committee members Dr. John E. Cochran, Jr., Dr. David A. Cicci, and Dr. Subhash C. Sinha. I would also like to appreciate the tremendous support of my friends both during good and tough times. Finally, the support of my parents, my sister Anagha, and the rest of my family in whatever I do is invaluable to me.

Table of Contents

List of Tables

List of Figures

CHAPTER 1

INTRODUCTION

The study of spacecraft relative motion has provoked great interest for many years. Spacecraft relative motion refers to the study of motion of one spacecraft (or multiple spacecraft) with respect to another spacecraft that is designated as the chief/target. The spacecraft whose relative motion is of interest is designated as the deputy/chaser. An understanding of spacecraft relative motion is critical for applications such as spacecraft rendezvous and formation flying. Rendezvous operations have played a key role in many space programs such as Gemini, Apollo, and Space Shuttle. Today there is a growing interest in formation flying missions and associated dynamics, guidance, navigation, and control challenges. These missions are driven by commercial and military applications as well as scientific objectives such as Earth surveillance, remote sensing, stellar imaging, astrometry, space interferometry etc. Some of the formation flying missions include ESA's CLUSTER, PRISMA, and PROBA-3 and joint ESA/NASA missions such as GRACE and LISA.[1]

In this dissertation two problems related to spacecraft relative motion are explored. The first problem studies the control of spacecraft pursuit-evasion games from a differential-game-theory perspective. This problem is motivated by a number of potential applications of differential game theory to orbital problems. Examples are modeling the interaction between hostile space assets such as spy satellites, space situational awareness such as collision avoidance, modeling uncertainty in the motion of

tumbling objects and so on. Linear and nonlinear control laws are derived using the linear and nonlinear equations of spacecraft relative motion, respectively. The linear quadratic differential game theory is applied to derive linear control laws. The state-dependent Riccati equation method is applied to extend the linear quadratic differential game theory to derive nonlinear control laws. These laws are tested and compared in various scenarios to demonstrate the superior efficacy of the nonlinear control laws.

The second problem is to study the range observability issue of spacecraft relative motion when angles-only navigation is used. This problem is motivated by the autonomous spacecraft rendezvous missions possibly involving uncooperative spacecraft. Traditional spacecraft proximity operations use large and expensive on-board sensors in addition to ground support to generate range as well as angles information. Autonomous proximity operations involve smaller spacecraft and require small, inexpensive on-board sensors such as optical cameras, which may be used to generate angles information but have difficulty generating range information. Previous research in the literature has shown that range information can be generated provided one of the spacecraft is thrusting. This dissertation further studies the continuous-thrust control of spacecraft relative motion to improve range observability when angles-only navigation is used.

The linear quadratic Gaussian control method is implemented for control of spacecraft relative motion when both linear as well as nonlinear measurement models are used. It is demonstrated that the control and estimation processes are decoupled when a linear measurement model is used, whereas they are coupled when the nonlinear angles-only measurement model is used. This coupling results in the failure of the linear

quadratic Gaussian control method when the state weighting in the performance criterion is high.

Two approaches are explored and successfully applied to address this failure. The first approach, an existing one in the dual control theory literature, implements a linear quadratic dual control strategy such that the control action consists of two parts. One control action attempts to regulate the state while the other attempts to reduce the uncertainty in the state estimate. The second approach, a new one explored in this dissertation, implements an information-weighted linear quadratic Gaussian control in which the state weighting is not constant but is dependent on the accuracy of the state estimate.

Chapter 2 presents a review of basic orbital mechanics and spacecraft relative motion dynamics. Chapter 3 presents a review of optimal control problems, differential game theory, the state-dependent Riccati equation method for control of nonlinear systems, and sequential state estimation algorithms. Chapter 4 discusses the problem of spacecraft pursuit-evasion games. In Chapter 4, first relevant literature is reviewed followed by the description of the problem and then results are presented. Chapters 5 and 6 discuss the problem of range observability in spacecraft relative motion when angles-only navigation is used. In Chapter 5, first relevant literature is reviewed. The implementation of the linear quadratic Gaussian control method for control of spacecraft relative motion is discussed for both linear as well as nonlinear measurement models. In Chapter 6, the linear quadratic dual control approach and the information-weighted linear quadratic Gaussian control approach are discussed. Finally, Chapter 7 presents contributions and concluding remarks.

CHAPTER 2

ORBITAL MECHANICS

Celestial mechanics is the study of motion of celestial objects. Orbital mechanics applies the principles of celestial mechanics to describe the motion of spacecraft. This chapter first focuses on the basic principles of orbital mechanics which describe the motion of a spacecraft relative to the Earth. Later, these principles are used to describe the relative motion of two spacecraft in neighboring orbits around the Earth.

BASIC PRINCIPLES OF ORBITAL MECHANICS

Kepler's Laws of Planetary Motion

Danish astronomer Tycho Brahe observed the motion of planets and stars. Kepler, a mathematician, studied Brahe's observational data and formulated his laws of planetary motion. In 1609, Kepler published his first two laws. In 1619, Kepler published his third law. Kepler's three laws are stated below.[2]

1. The orbit of each planet is an ellipse with the Sun at one focus.
2. The line from the Sun to a planet sweeps out equal areas inside the ellipse in equal lengths of time.
3. The square of the period of a planet is proportional to the cube of its mean distance from the Sun.

Kepler's first two laws are depicted in Figure 2.1. The planet's orbit around the Sun is an ellipse with the Sun at one focus while the other focus remains empty. The shaded regions are traced in equal amounts of time, demonstrating Kepler's second law. Kepler's

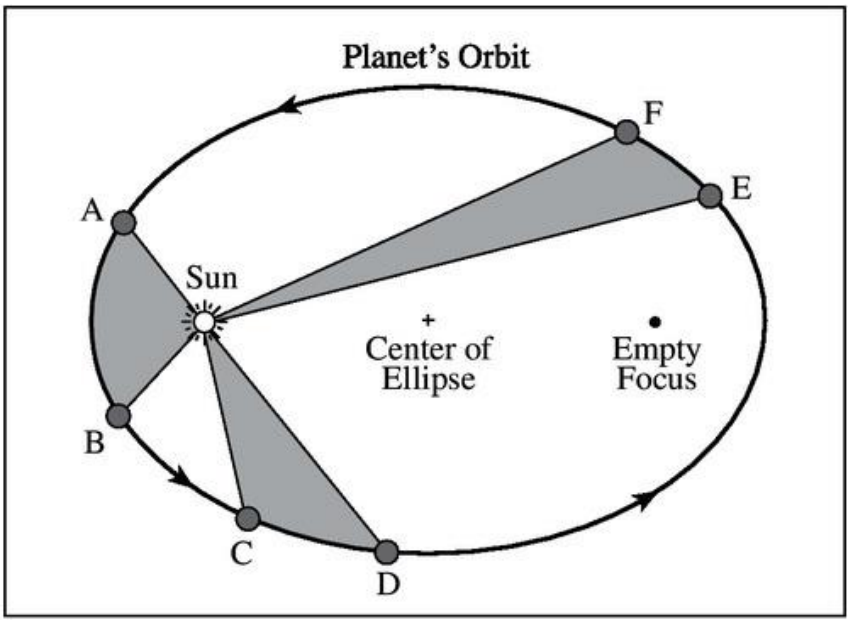

Figure 2.1: Kepler's Laws[3]

laws provide only an empirical description of planetary motion. Their mathematical explanation was provided by Newton's laws.

Newton's Laws

In 1687, Newton introduced his three laws of motion which form the foundation of classical mechanics. These laws are stated below.[2]

1. Every body continues its state of rest or of uniform motion in a straight line unless it is compelled to change that state by forces impressed upon it.
2. The rate of change of momentum is proportional to the force impressed and is in the same direction as that force.
3. To every action there is always opposed an equal reaction.

In addition to the laws of motion, Newton also formulated the law of universal gravitation.[2] According to this law, any two bodies attract one another with a force proportional to the product of their masses and inversely proportional to the square of the

distance between them. Newton's second law of motion along with the law of universal gravitation forms the basis of mathematics of spacecraft orbits.

Two-Body Problem

The two-body problem describes the motion of a spacecraft around a planet. Figure 2.2 depicts the two-body problem.

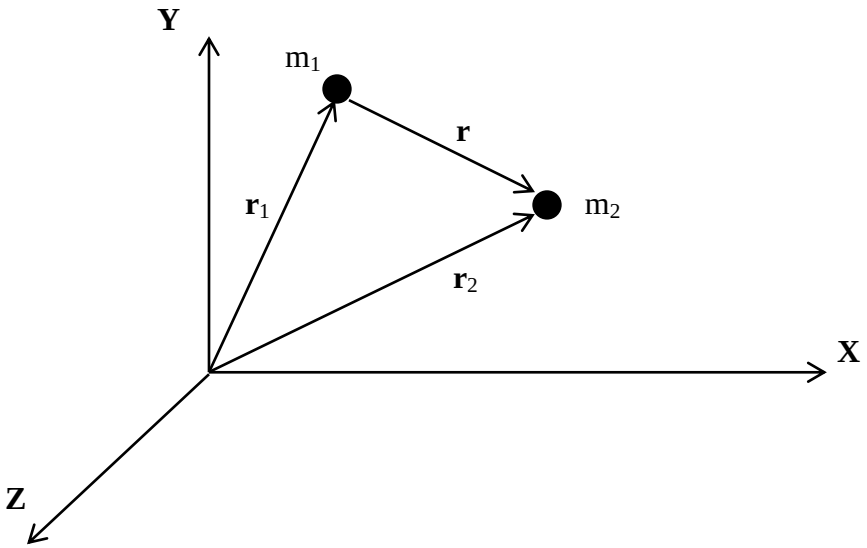

Figure 2.2: Two-Body Problem

Newton's second law can be described mathematically as follows.

$$\Sigma \mathbf{F} = m\mathbf{a} \tag{2.1}$$

Here, **F**, m, and **a** represent the forces acting on a body, the mass of the body, and the acceleration of the body respectively. Consider the motion of two point masses in an inertial coordinate system XYZ. According to Newton's law of universal gravitation, these masses attract each other with a force given by $F = \frac{Gm_1m_2}{r^2}$. Here, G is the universal gravitational constant, $m_1$and m_2 are the masses of two bodies, and r is the distance between their center of masses. The equation of motion for each mass can be written in vector form as follows.

$$m_1\ddot{\mathbf{r}}_1 = \frac{Gm_1m_2}{r^3}\mathbf{r} \tag{2.2}$$

$$m_2\ddot{\mathbf{r}}_2 = -\frac{Gm_1m_2}{r^3}\mathbf{r} \tag{2.3}$$

Here, $\mathbf{r}$ represents the relative motion of the bodies given by $\mathbf{r} = \mathbf{r}_2 - \mathbf{r}_1$. The relative acceleration of the bodies is given by:

$$\ddot{\mathbf{r}} = \ddot{\mathbf{r}}_2 - \ddot{\mathbf{r}}_1 = -\frac{G(m_1 + m_2)}{r^3}\mathbf{r} \tag{2.4}$$

Define the gravitational parameter μ such that $\mu = G(m_1 + m_2)$. Often when calculating the gravitational parameter, the mass of one of the bodies will be negligible compared to the other such as the mass of a spacecraft compared to that of the Earth. If m_1 is the mass of the Earth and m_2 is the mass of a spacecraft then $\mu = Gm_1$. The two-body equation of motion then can be written in the familiar form as follows.

$$\ddot{\mathbf{r}} \cong -\frac{\mu}{r^3}\mathbf{r} \tag{2.5}$$

Classical Orbital Elements

In order to describe the position of a spacecraft in an orbit, a coordinate system must be chosen. One choice is a Cartesian system known as the Earth centered inertial (ECI) coordinate system shown in Figure 2.3. In this system, the fundamental plane is the equatorial plane and the origin is located at the center of the Earth. The X axis is directed along the vernal equinox, the Z axis is normal to the equatorial plane directed along the geographic North Pole, and the Y axis lies in the equatorial plane completing the right-handed orthogonal triad. Using the ECI system, a spacecraft's state can be completely described by six independent parameters: position (x, y, z) and velocity $(\dot{x}, \dot{y}, \dot{z})$.

Visualizing a spacecraft's orbit described in the ECI system can be difficult sometimes. Therefore, it is often advantageous to choose another set of coordinates called

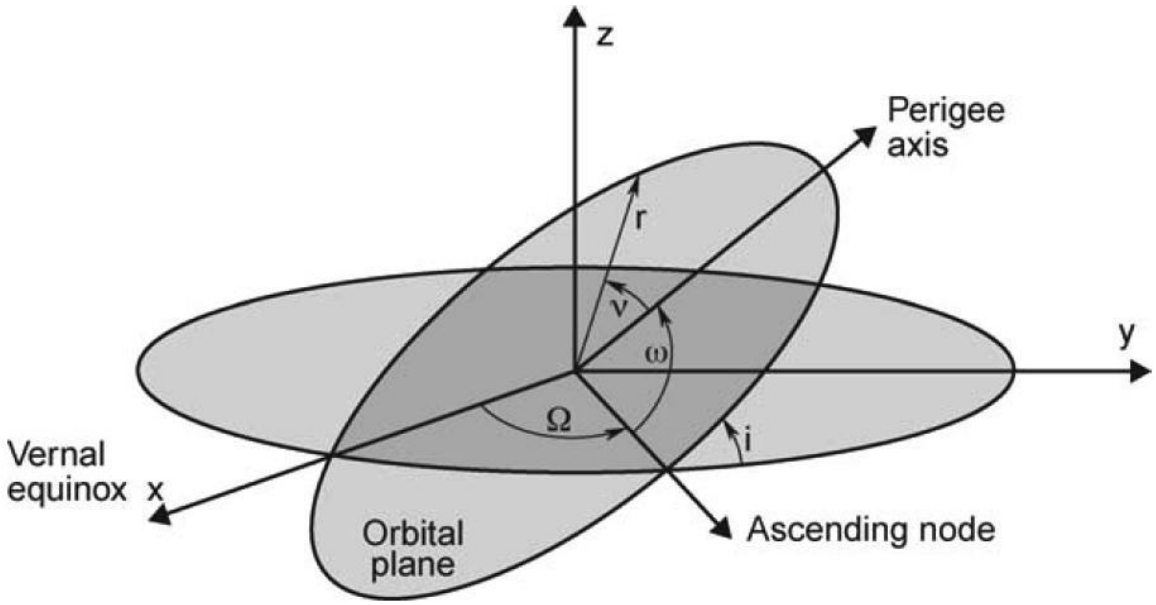

Figure 2.3: Earth Centered Inertial System and Orbital Elements[4]

the classical orbital elements. When using the orbital elements, five of the six parameters needed to describe a spacecraft's Keplerian orbit state are constant and represent the size, shape, and orientation of the orbit. The sixth parameter represents the motion along the orbit. The orbital elements are depicted in Figure 2.3 and are briefly described below.

1. Semi-major axis (a) describes the size of the ellipse.
2. Eccentricity (e) describes the shape of the ellipse.
3. Inclination (i) is the angle between the orbital plane and the equatorial plane.
4. Right ascension of the ascending node (Ω) is the angle from the vernal equinox to the point on the equator where the spacecraft makes its south to north crossing.
5. Argument of Perigee (ω) is the angle from the ascending node to perigee which is the closest point on the ellipse from the focus.
6. True anomaly (ν) is the angle between spacecraft's current position in the orbit and perigee.

The orbital elements contain the same information as the position and velocity vectors at a particular time. It is therefore possible to transform from one set of coordinates to the other.[5]

Orbit Equation

In a polar coordinate system ($\hat{\mathbf{i}}_r$, $\hat{\mathbf{i}}_\theta$, $\hat{\mathbf{i}}_z$) centered at m_1, the position of the spacecraft is given by $\mathbf{r} = r\hat{\mathbf{i}}_r$, and the velocity is given by $\mathbf{v} = \dot{\mathbf{r}} = \dot{r}\hat{\mathbf{i}}_r + r\dot{\nu}\hat{\mathbf{i}}_\theta$. The angular momentum is given by the following.

$$\mathbf{h} = \mathbf{r} \times \mathbf{v} = r^2\dot{\nu}\hat{\mathbf{i}}_z \tag{2.6}$$

The orbital motion lies in a plane perpendicular to **h** which is constant. Taking the cross product of both sides of Equation (2.5) by **h** gives the following.[10]

$$\ddot{\mathbf{r}} \times \mathbf{h} = \frac{d\mathbf{v}}{dt} \times \mathbf{h} = -\frac{\mu}{r^3}\mathbf{r} \times \mathbf{h}$$

$$\frac{d(\mathbf{v} \times \mathbf{h})}{dt} = \mu\frac{d}{dt}\left(\frac{\mathbf{r}}{r}\right) \tag{2.7}$$

Integrating both sides of Equation (2.7) gives the following.[2]

$$\mathbf{v} \times \mathbf{h} = \frac{\mu}{r}\mathbf{r} + \mu\mathbf{e} \tag{2.8}$$

Here, $\mu\mathbf{e}$ is the constant of integration and **e** is the eccentricity vector. The eccentricity vector points towards perigee. The magnitude of the eccentricity vector is given by the following.

$$e^2 = \mathbf{e} \cdot \mathbf{e} = \frac{1}{\mu^2}(\mathbf{v} \times \mathbf{h}) \cdot (\mathbf{v} \times \mathbf{h}) - \frac{2}{\mu r}\mathbf{r} \cdot (\mathbf{v} \times \mathbf{h}) + 1 \tag{2.9}$$

Using the properties of cross product, $\mathbf{v} \times \mathbf{h} = vh$ and $\mathbf{r} \cdot (\mathbf{v} \times \mathbf{h}) = (\mathbf{r} \times \mathbf{v}) \cdot \mathbf{h}$, Equation (2.9) can be written as shown below.

$$e^2 = \frac{1}{\mu^2}h^2v^2 - \frac{2}{\mu r}h^2 + 1$$

$$e^2 - 1 = \frac{h^2}{\mu}\left(\frac{v^2}{\mu} - \frac{2}{r}\right)$$

$$1 - e^2 = \frac{h^2}{\mu}\left(\frac{2}{r} - \frac{v^2}{\mu}\right) \tag{2.10}$$

Define $p = \frac{h^2}{\mu}$ and $a = \left(\frac{2}{r} - \frac{v^2}{\mu}\right)^{-1}$ where p is called the parameter. From Equation (2.10), the parameter is related to a and e by the following.

$$p = \frac{h^2}{\mu} = a(1 - e^2) \tag{2.11}$$

The total energy of the system is related to a by the following.

$$\frac{v^2}{2} - \frac{\mu}{r} = -\frac{\mu}{2a} \tag{2.12}$$

The kinetic energy is given by $\frac{v^2}{2}$, the potential energy is given by $-\frac{\mu}{r}$, and $-\frac{\mu}{2a}$ is the energy constant. Equation (2.12) can be written as the energy integral or the vis-viva equation.

$$v^2 = \mu\left(\frac{2}{r} - \frac{1}{a}\right) \tag{2.13}$$

Solving Equation (2.8) for e and taking the dot product with the position vector gives the following.

$$\mathbf{e} \cdot \mathbf{r} = \frac{1}{\mu}\left(\mathbf{v} \times \mathbf{h} - \mu\frac{\mathbf{r}}{r}\right) \cdot \mathbf{r}$$

$$er\cos\nu = \frac{1}{\mu}(\mathbf{r} \times \mathbf{v} \cdot \mathbf{h} - \mu r)$$

$$er\cos\nu = \frac{h^2}{\mu} - r \tag{2.14}$$

Solving Equation (2.14) for r and substituting for p gives the orbit equation.

$$r = \frac{p}{1 + e\cos\nu} \tag{2.15}$$

Orbital Position as a Function of Time

The orbit equation expresses the position as a function of true anomaly. To express position as a function of time, true anomaly needs to be expressed as a function of time. For this purpose, two new terms of mean anomaly and eccentric anomaly are introduced.[5] The mean anomaly, M, is defined as a function of time as given below.

$$M = n(t - t_p) \tag{2.16}$$

Here, n is the mean motion of the orbit given by $n = \frac{2\pi}{T}$, T is the period of the orbit given by $T = 2\pi\sqrt{\frac{a^3}{\mu}}$, and t_p is a constant of integration known as the time at perigee passage. The eccentric anomaly, E, is depicted in Figure 2.4.

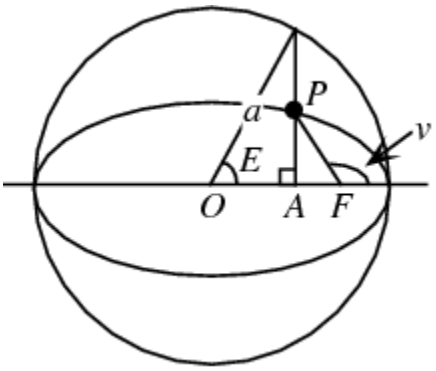

Figure 2.4: Eccentric Anomaly[6]

The mean anomaly is related to the eccentric anomaly by the Kepler's equation given below.

$$M = E - e\sin E \tag{2.17}$$

In order to solve for E, the Kepler's equation needs to be solved using one of the iterative methods such as the Newton-Raphson method. Finally, the eccentric anomaly is related to the true anomaly as follows.

$$\tan\frac{E}{2} = \sqrt{\frac{1-e}{1+e}}\tan\frac{\nu}{2} \tag{2.18}$$

Equations (2.16), (2.17), and (2.18) can be used for the transformation between time and true anomaly.

SPACECRAFT RELATIVE MOTION

While the two-body equation of motion describes the motion of a spacecraft relative to the Earth, it cannot be used directly to describe the relative motion between two spacecraft in neighboring orbits around the Earth. These equations of motion will now be derived using the two-body equation of motion. The spacecraft are assumed to be in Keplerian orbits. The equations of motion are derived in the homogeneous form but can be written in control-affine form if control accelerations are present.

Nonlinear Equations of Spacecraft Relative Motion

Recall that the spacecraft relative motion refers to the study of motion of one spacecraft (or multiple spacecraft) with respect to another spacecraft which is designated as the chief/target. The spacecraft whose relative motion is of interest is designated as the deputy/chaser. The orbit of the chief around the Earth is the reference orbit for describing the relative motion of a deputy with respect to the chief. Thus, the chief may not have to be a physical object in an orbit around the Earth. The reference orbit could be any orbit around the Earth. The equations of spacecraft relative motion are described in a Cartesian coordinate system known as the Euler-Hill (EH) frame depicted in Figure 2.5.

The EH reference frame is a local-vertical local-horizontal (LVLH) rotating reference frame centered at the chief in a reference orbit around the Earth. The x axis is directed along the instantaneous radius vector (with respect to the Earth) of the chief.

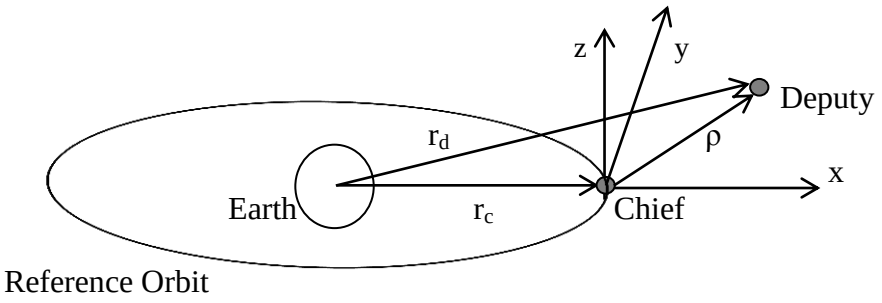

Figure 2.5: Euler-Hill Reference Frame

The z axis is normal to the reference orbital plane and is positive in the direction of the angular momentum vector. The y axis completes the right-handed orthogonal triad. The x and y directions correspond to the in-plane motion and the z direction corresponds to the out-of-plane motion. The transformation matrix for converting a vector from the ECI frame to one in the LVLH frame can be found in Reference 1.

The inertial chief position is expressed through the vector $\mathbf{r}_c$, while the deputy position is given by $\mathbf{r}_d$. The relative orbit position vector is given by $\boldsymbol{\rho}$ and can be expressed in the LVLH reference frame as $\boldsymbol{\rho} = [x\ y\ z]^T$. The relative orbit is described in terms of $\boldsymbol{\rho}$ and the vector components are taken in the chief LVLH frame. To derive the relative equations of motion in the chief LVLH frame, the position of the deputy spacecraft is given by the following.

$$\mathbf{r}_d = \mathbf{r}_c + \boldsymbol{\rho} = (r_c + x)\hat{\mathbf{i}} + y\hat{\mathbf{j}} + z\hat{\mathbf{k}} \tag{2.19}$$

The angular velocity and acceleration of the LVLH frame with respect to the ECI frame are given by $\boldsymbol{\Omega} = \dot{\nu}\hat{\mathbf{k}} = \frac{h}{{r_c}^2}\hat{\mathbf{k}}$ and $\boldsymbol{\alpha} = \ddot{\nu}\hat{\mathbf{k}} = -\frac{2\dot{r}_c\dot{\nu}}{r_c}\hat{\mathbf{k}}$. Here, h is the angular momentum of the chief orbit. Taking two derivatives of Equation (2.19) with respect to the ECI frame, the deputy acceleration vector is given by the following.

$$\ddot{\mathbf{r}}_d = \ddot{\mathbf{r}}_c + \boldsymbol{\alpha} \times \boldsymbol{\rho} + \boldsymbol{\Omega} \times (\boldsymbol{\Omega} \times \boldsymbol{\rho}) + 2\boldsymbol{\Omega} \times \dot{\boldsymbol{\rho}} + \ddot{\boldsymbol{\rho}} \tag{2.20}$$

The chief's position in the LVLH frame can be written as $\mathbf{r}_c = r_c\hat{\mathbf{i}}$. The chief's acceleration vector can be written as the following.

$$\ddot{\mathbf{r}}_c = -\frac{\mu}{{r_c}^3}\mathbf{r}_c = -\frac{\mu}{{r_c}^3}r_c\hat{\mathbf{i}} = -\frac{\mu}{{r_c}^2}\hat{\mathbf{i}}$$

Substituting for $\ddot{\mathbf{r}}_c$, $\boldsymbol{\Omega}$, $\boldsymbol{\alpha}$, and $\boldsymbol{\rho}$ in Equation (2.20) gives the following.

$$\begin{aligned}\ddot{\mathbf{r}}_d &= -\frac{\mu}{{r_c}^2}\hat{\mathbf{i}} + \ddot{\nu}\hat{\mathbf{k}} \times \left(x\hat{\mathbf{i}} + y\hat{\mathbf{j}} + z\hat{\mathbf{k}}\right) + \dot{\nu}\hat{\mathbf{k}} \times \left(\dot{\nu}\hat{\mathbf{k}} \times \left(x\hat{\mathbf{i}} + y\hat{\mathbf{j}} + z\hat{\mathbf{k}}\right)\right) \\ &\quad + 2\dot{\nu}\hat{\mathbf{k}} \times (\dot{x}\hat{\mathbf{i}} + \dot{y}\hat{\mathbf{j}} + \dot{z}\hat{\mathbf{k}}) + (\ddot{x}\hat{\mathbf{i}} + \ddot{y}\hat{\mathbf{j}} + \ddot{z}\hat{\mathbf{k}}) \\ &= -\frac{\mu}{{r_c}^2}\hat{\mathbf{i}} + \ddot{\nu}x\hat{\mathbf{j}} - \ddot{\nu}y\hat{\mathbf{i}} - \dot{\nu}^2 x\hat{\mathbf{i}} - \dot{\nu}^2 y\hat{\mathbf{j}} + 2\dot{\nu}\dot{x}\hat{\mathbf{j}} - 2\dot{\nu}\dot{y}\hat{\mathbf{i}} + \ddot{x}\hat{\mathbf{i}} + \ddot{y}\hat{\mathbf{j}} + \ddot{z}\hat{\mathbf{k}} \\ &= \left(-\frac{\mu}{{r_c}^2} - \dot{\nu}^2 x - \ddot{\nu}y - 2\dot{\nu}\dot{y} + \ddot{x}\right)\hat{\mathbf{i}} + (\ddot{\nu}x - \dot{\nu}^2 y + 2\dot{\nu}\dot{x} + \ddot{y})\hat{\mathbf{j}} + \ddot{z}\hat{\mathbf{k}}\end{aligned} \tag{2.21}$$

The acceleration of the deputy is given by $\ddot{\mathbf{r}}_d = -\frac{\mu}{{r_d}^3}\mathbf{r}_d$ where $\mathbf{r}_d = [(r_c + x)\ y\ z]^T$. Equating coefficients in Equation (2.21) gives the following nonlinear equations of relative motion (NERM).

$$\begin{aligned}\ddot{x} &= \dot{\nu}^2 x + \ddot{\nu}y + 2\dot{\nu}\dot{y} + \frac{\mu}{{r_c}^2} - \frac{\mu}{{r_d}^3}(r_c + x) \\ \ddot{y} &= -\ddot{\nu}x + \dot{\nu}^2 y - 2\dot{\nu}\dot{x} - \frac{\mu}{{r_d}^3}y \\ \ddot{z} &= -\frac{\mu}{{r_d}^3}z\end{aligned} \tag{2.22}$$

If $[x\ y\ z\ \dot{x}\ \dot{y}\ \dot{z}]^T$ is the state vector, then the NERM can be written in the state space form as follows.

$$\dot{\mathbf{x}} = \mathbf{f}(\mathbf{x}) \tag{2.23}$$

A sufficient condition for periodic solutions to the NERM can be derived by satisfying the energy matching criterion on the chief's and deputy's orbit around the Earth.

The derivation of the constraint on the initial condition to satisfy the energy matching criterion can be found in Reference 1.

Linear Equations of Spacecraft Relative Motion

The NERM are valid for arbitrarily large separations and eccentric chief orbits. If the relative orbit coordinates (x, y, z) are small compared to the chief orbit radius r_c, then Equation (2.22) can further be simplified by linearization about small separations between the chief and the deputy. The deputy's radius can be approximated by neglecting the higher order terms.

$$r_d = \sqrt{(r_c + x)^2 + y^2 + z^2} = r_c\sqrt{1 + \frac{2x}{r_c} + \frac{x^2 + y^2 + z^2}{{r_c}^2}} \approx r_c\sqrt{1 + \frac{2x}{r_c}} \tag{2.24}$$

Using the binomial theorem, the term $\frac{\mu}{{r_d}^3}$ can be expanded in terms of r_c. Retaining only the first order terms gives the following.

$$\frac{\mu}{{r_d}^3} \approx \frac{\mu}{\left(r_c\sqrt{1 + \frac{2x}{r_c}}\right)^3} \approx \frac{\mu}{{r_c}^3}\left(\sqrt{1 + \frac{2x}{r_c}}\right)^{-\frac{3}{2}} \approx \frac{\mu}{{r_c}^3}\left(1 - \frac{3x}{r_c}\right) \tag{2.25}$$

Equation (2.25) is used to approximate the deputy's acceleration.

$$-\frac{\mu}{{r_d}^3}\mathbf{r}_d = -\frac{\mu}{{r_d}^3}\begin{bmatrix} r_c + x \\ y \\ z \end{bmatrix} \approx -\frac{\mu}{{r_c}^3}\left(1 - \frac{3x}{r_c}\right)\begin{bmatrix} r_c + x \\ y \\ z \end{bmatrix} \approx -\frac{\mu}{{r_c}^3}\begin{bmatrix} r_c - 2x \\ y \\ z \end{bmatrix} \tag{2.26}$$

Using Equation (2.26), Equation (2.22) can be linearized for small separations between the chief and the deputy. The resulting equations are the linearized equations of relative motion (LERM) given as follows.

$$\ddot{x} = \left(\dot{\nu}^2 + 2\frac{\mu}{{r_c}^3}\right)x + \ddot{\nu}y + 2\dot{\nu}\dot{y}$$

$$\ddot{y} = -\ddot{\nu}x + \left(\dot{\nu}^2 - \frac{\mu}{{r_c}^3}\right)y - 2\dot{\nu}\dot{x} \tag{2.27}$$

$$\ddot{z} = -\frac{\mu}{{r_c}^3}z$$

The in-plane and out-of-plane motion described by the LERM is decoupled. The LERM can be written in the state space form as follows.

$$\begin{bmatrix} \dot{x} \\ \dot{y} \\ \dot{z} \\ \ddot{x} \\ \ddot{y} \\ \ddot{z} \end{bmatrix} = \begin{bmatrix} 0 & 0 & 0 & 1 & 0 & 0 \\ 0 & 0 & 0 & 0 & 1 & 0 \\ 0 & 0 & 0 & 0 & 0 & 1 \\ \dot{\nu}^2 + 2\frac{\mu}{{r_c}^3} & \ddot{\nu} & 0 & 0 & 2\dot{\nu} & 0 \\ -\ddot{\nu} & \dot{\nu}^2 - \frac{\mu}{{r_c}^3} & 0 & -2\dot{\nu} & 0 & 0 \\ 0 & 0 & -\frac{\mu}{{r_c}^3} & 0 & 0 & 0 \end{bmatrix} \begin{bmatrix} x \\ y \\ z \\ \dot{x} \\ \dot{y} \\ \dot{z} \end{bmatrix}$$

$$\dot{\mathbf{x}} = \mathbf{A}_{\mathrm{LERM}}(t)\mathbf{x}(t) \tag{2.28}$$

The LERM are time varying as r_c, $\dot{\nu}$, and $\ddot{\nu}$ vary with time. For elliptic orbits, all these quantities are time-periodic with the orbital period T.

Initial conditions corresponding to periodic solutions to the LERM can be derived by following the similar procedure as used for the NERM. Solutions to the LERM are available; however, they require a coordinate scaling and a change in independent variable from time to true anomaly. After the coordinate scaling and the change in the independent variable, the LERM are transformed into the well-known Tschauner-Hempel (TH) equations.[7] In this dissertation, the LERM are used to represent the linearized relative dynamics when the chief orbit is elliptic. Therefore, the TH equations are not discussed here. A detailed discussion of the TH equations and their solutions can be found in Reference 1.

Hill-Clohessy-Wiltshire Equations

While studying spacecraft rendezvous, Clohessy and Wiltshire[8] published one of the most frequently used equations of spacecraft relative motion. These equations are frequently called Hill-Clohessy-Wiltshire (HCW) equations, as Hill[9] in 1878 was the first to linearize a set of equations to describe the motion of the Moon relative to the Earth. Assuming the chief orbit to be circular (e = 0), the LERM reduce to the HCW equations given below.

$$\begin{aligned} \ddot{x} - 3n^2 x - 2n\dot{y} &= 0 \\ \ddot{y} + 2n\dot{x} &= 0 \\ \ddot{z} + n^2 z &= 0 \end{aligned} \tag{2.29}$$

Recall that n represents the mean motion of the chief orbit. The HCW equations are time-invariant and can be written in the state space form as follows.

$$\begin{bmatrix} \dot{x} \\ \dot{y} \\ \dot{z} \\ \ddot{x} \\ \ddot{y} \\ \ddot{z} \end{bmatrix} = \begin{bmatrix} 0 & 0 & 0 & 1 & 0 & 0 \\ 0 & 0 & 0 & 0 & 1 & 0 \\ 0 & 0 & 0 & 0 & 0 & 1 \\ 3n^2 & 0 & 0 & 0 & 2n & 0 \\ 0 & 0 & 0 & -2n & 0 & 0 \\ 0 & 0 & -n^2 & 0 & 0 & 0 \end{bmatrix} \begin{bmatrix} x \\ y \\ z \\ \dot{x} \\ \dot{y} \\ \dot{z} \end{bmatrix}$$

$$\dot{\mathbf{x}} = \mathbf{A}_{\mathrm{HCW}}\mathbf{x}(t) \tag{2.30}$$

The homogeneous HCW equations have a closed form solution given in Equation (2.31), where, s(nt) and c(nt) represent sin(nt) and cos(nt) respectively.

$$\mathbf{x}(t) = \begin{bmatrix} 4 - 3c(nt) & 0 & 0 & \frac{s(nt)}{n} & \frac{2}{n} - \frac{2c(nt)}{n} & 0 \\ -6nt + 6s(nt) & 1 & 0 & -\frac{2}{n} + \frac{2c(nt)}{n} & \frac{4s(nt)}{n} - 3t & 0 \\ 0 & 0 & c(nt) & 0 & 0 & \frac{s(nt)}{n} \\ 3ns(nt) & 0 & 0 & c(nt) & 2s(nt) & 0 \\ -6n + 6nc(nt) & 0 & 0 & -2s(nt) & -3 + 4c(nt) & 0 \\ 0 & 0 & -ns(nt) & 0 & 0 & c(nt) \end{bmatrix} \mathbf{x}(0) \tag{2.31}$$

The in-plane and out-of-plane motion described by the HCW equations is decoupled. The out-of-plane solution is periodic and takes the form of a harmonic oscillator with the amplitude of its terms dependent on its initial position and velocity. The state matrix corresponding to the in-plane equations has eigenvalues 0, 0, and ±in, resulting in periodic terms and secular terms. The secular terms cause a drift along y direction which grows linearly with time. For a periodic solution, the secular drift term can be eliminated by enforcing the following constraint.

$$\dot{y}(0) + 2nx(0) = 0 \tag{2.32}$$

The accuracy of the HCW equations is limited by a number of simplifying assumptions made during their derivation, such as small separation, Keplerian two-body motion, and circular chief orbit around the Earth. Despite their limitations, however, the HCW equations are useful for controller design and their periodic solutions offer basic reference trajectories for a controller to track during formation flying in a near-circular orbit.

Orbital Element Difference Description

Instead of describing the relative orbit in terms of the Cartesian state vector **x** defined in the EH frame, an alternative way to describe it is in terms of the orbital element difference vector. An orbital element vector is defined as follows.

$$\mathbf{e} = [\mathrm{a}\ \mathrm{e}\ \mathrm{i}\ \Omega\ \omega\ \nu]^{\mathrm{T}}$$

The orbital element difference vector is given as follows.

$$\delta\mathbf{e} = \mathbf{e}_{\mathrm{d}} - \mathbf{e}_{\mathrm{c}} = [\delta\mathrm{a}\ \delta\mathrm{e}\ \delta\mathrm{i}\ \delta\Omega\ \delta\omega\ \delta\nu]^{\mathrm{T}} \tag{2.33}$$

Here, $\mathbf{e}_d$ and $\mathbf{e}_c$ are the orbital element vectors for the deputy and the chief. There exists a linear mapping between $\mathbf{x}$ and $\delta\mathbf{e}$.[10] For this mapping, in order to avoid numerical difficulties, the orbital element vector $\mathbf{e}$ is defined as follows.

$$\mathbf{e} = [a\ \theta\ i\ q_1\ q_2\ \Omega\ ]^T$$

Here, $\theta = \omega + \nu$ is the argument of latitude and q_1 and q_2 are defined as follows.

$$q_1 = e\cos\omega, \quad q_2 = e\sin\omega$$

The orbital element difference vector is given as follows.

$$\delta\mathbf{e} = \mathbf{e}_d - \mathbf{e}_c = [\delta a\ \delta\theta\ \delta i\ \delta q_1\ \delta q_2\ \delta\Omega]^T \tag{2.34}$$

The linear mapping between $\mathbf{x}$ and $\delta\mathbf{e}$ is

$$\mathbf{x} = \mathbf{A}(\mathbf{e}_c)\delta\mathbf{e} \tag{2.35}$$

The mapping matrix $\mathbf{A}$ is a function of the chief's orbital element vector $\mathbf{e}_c$ and can be found in Reference 10.

CHAPTER 3

OPTIMAL CONTROL, DIFFERENTIAL GAMES, AND ESTIMATION

This chapter reviews basic principles of optimal control theory, differential game theory, and estimation algorithms. These principles are later applied to the research problems explored in Chapters 4 and 5. First, based on the basic principles of optimal control theory, the linear quadratic regulator (LQR) control law is derived. Differential game theory is an extension of optimal control theory. Thus, the linear quadratic differential game control laws are derived next by following the same procedure used for deriving the LQR control law. The state-dependent Riccati equation method which extends the LQR method to control of nonlinear systems is discussed next. Finally, state estimation algorithms are discussed.

OPTIMAL CONTROL PROBLEM

Optimal control problems arise in many branches of engineering including aerospace, chemical, and electrical engineering. In aerospace engineering, optimal control theory has applications in areas such as trajectory optimization, attitude control, and vehicle guidance. As defined by Kirk[11], the objective of an optimal control problem is to determine the control signals that will minimize (or maximize) some performance index and at the same time cause a process to satisfy the physical constraints. Possible performance indices include time, fuel consumption, or any other parameter of interest in a given application.

There are three common approaches to solve optimal control problems. The first approach is that of deriving the first-order necessary conditions for optimality using the calculus of variations and Pontryagin's minimum principle. This approach leads to a two-point boundary value problem (TPBVP). The second approach is dynamic programming, which requires solving the Hamilton-Jacobi-Bellman (HJB) equation which is a partial differential equation (PDE). The third approach is direct numerical methods in which the continuous-time optimal control problem is transcribed directly into a nonlinear programming problem (NLP) without formulating an alternate set of optimality conditions. The resulting NLP can be solved numerically by various algorithms.

Except for special cases, the TPBVP and the HJB equation cannot be solved analytically and numerical methods must be employed. Commonly used approaches for solving the TPBVP are shooting, multiple shooting, finite difference, and collocation. Numerically solving the HJB equation is a challenging task and approaches like series solution methods have been explored for this purpose. However, in this dissertation, only the optimal control problems of linear quadratic (LQ) nature, where the dynamics are linear and the performance index is quadratic, are considered. An advantage of LQ problems is that they can be solved analytically. In case of LQ problems, both the TPBVP and the HJB equation reduce to solving a differential Riccati equation which can be solved numerically without much difficulty.

First-Order Necessary Conditions for Optimality

The optimal control problem is to find an optimal control input $\mathbf{u}^*$ for a set of generally nonlinear, coupled differential equations of the form

$$\dot{\mathbf{x}} = \mathbf{f}(\mathbf{x}(t), \mathbf{u}(t), t), \qquad t \in [t_0, t_f] \tag{3.1}$$

subject to the boundary conditions

$$\boldsymbol{\Psi}(\mathbf{x}(t_0), \mathbf{x}(t_f), t_0, t_f) = \mathbf{0} \tag{3.2}$$

and the inequality path constraints

$$\mathbf{C}(\mathbf{x}(t), \mathbf{u}(t), t) \leq \mathbf{0} \tag{3.3}$$

such that the associated cost function

$$J = \Phi(\mathbf{x}(t_f), t_f) + \int_{t_o}^{t_f} L(\mathbf{x}(t), \mathbf{u}(t), t)dt \tag{3.4}$$

is minimized. Here, $\mathbf{x}(t) \in \mathbb{R}^n$ is the state and $\mathbf{u}(t) \in \mathbb{R}^m$ is the control. The first-order necessary conditions for the solution of the problem given in Equations (3.1)-(3.4) are derived by using the calculus of variations. Here, these conditions are directly given but their derivation can be found, for example, in Reference 11. Define the Hamiltonian with $\boldsymbol{\lambda}$ as Lagrange multipliers or co-states as follows.

$$H(\mathbf{x}(t), \mathbf{u}(t), \boldsymbol{\lambda}(t), t) = L(\mathbf{x}(t), \mathbf{u}(t), t) + \boldsymbol{\lambda}^T \mathbf{f}(\mathbf{x}(t), \mathbf{u}(t), t) \tag{3.5}$$

The co-states represent the sensitivity of the cost to the states. The first-order necessary conditions are given as follows.

$$\begin{aligned} \dot{\mathbf{x}} &= \frac{\partial H}{\partial \boldsymbol{\lambda}} \\ \dot{\boldsymbol{\lambda}} &= -\frac{\partial H}{\partial \mathbf{x}} \\ \frac{\partial H}{\partial \mathbf{u}} &= \mathbf{0} \end{aligned} \tag{3.6}$$

Generally, the boundary conditions for states and co-states are split leading to the TPBVP. The optimal control law $\mathbf{u}^*$ can be written as follows.

$$\mathbf{u}^* = \arg\min_{\mathbf{u}(t)} H(\mathbf{x}^*, \boldsymbol{\lambda}^*, \mathbf{u}), \qquad \forall t \geq 0 \tag{3.7}$$

Hamilton-Jacobi-Bellman Equation

The HJB equation which is an alternative to the first-order optimality conditions is stated here. Its derivation can be found in Reference 11. For the problem given in Equations (3.1)-(3.4), let $J^*(\mathbf{x}(t), t)$ be the optimal cost function. Define the Hamiltonian as follows.

$$\begin{aligned} H\left(\mathbf{x}(t), \mathbf{u}(t), \frac{\partial J^*}{\partial \mathbf{x}}, t\right) &= L(\mathbf{x}(t), \mathbf{u}(t), t) + \left[\frac{\partial J^*}{\partial \mathbf{x}}\right]^T \mathbf{f}(\mathbf{x}(t), \mathbf{u}(t), t) \\ H\left(\mathbf{x}(t), \mathbf{u}^*\left(\mathbf{x}(t), \frac{\partial J^*}{\partial \mathbf{x}}, t\right), \frac{\partial J^*}{\partial \mathbf{x}}, t\right) &= \min_{\mathbf{u}(t)} H\left(\mathbf{x}(t), \mathbf{u}(t), \frac{\partial J^*}{\partial \mathbf{x}}, t\right) \end{aligned} \tag{3.8}$$

The HJB equation is given as follows.

$$\frac{\partial J^*}{\partial t} + H\left(\mathbf{x}(t), \mathbf{u}^*\left(\mathbf{x}(t), \frac{\partial J^*}{\partial \mathbf{x}}, t\right), \frac{\partial J^*}{\partial \mathbf{x}}, t\right) = 0 \tag{3.9}$$

The boundary condition is as follows.

$$J^*(\mathbf{x}(t_f), t_f) = \Phi(\mathbf{x}(t_f), t_f) \tag{3.10}$$

LINEAR QUADRATIC REGULATOR CONTROL LAW

Derivation Using the First-Order Necessary Conditions

For the LQ optimal control problem, the state equation and the cost function are given as follows.

$$\dot{\mathbf{x}} = \mathbf{A}(t)\mathbf{x}(t) + \mathbf{B}\mathbf{u}(t) \tag{3.11}$$

$$J = \frac{1}{2}\mathbf{x}^T(t_f)\mathbf{S}_f\mathbf{x}(t_f) + \frac{1}{2}\int_{t_o}^{t_f} (\mathbf{x}^T(t)\mathbf{Q}\mathbf{x}(t) + \mathbf{u}^T(t)\mathbf{R}\mathbf{u}(t))dt \tag{3.12}$$

Here, $\mathbf{S}_f$ and $\mathbf{Q}$ are symmetric positive semi-definite matrices, and $\mathbf{R}$ is a symmetric positive definite matrix. Matrix $\mathbf{S}_f$ represents the weighting on the final state, $\mathbf{Q}$

represents weighting on the state, and **R** represents weighting on the control. The Hamiltonian for this system is as follows.

$$\mathrm{H}(\mathbf{x}(\mathrm{t}), \mathbf{u}(\mathrm{t}), \boldsymbol{\lambda}(\mathrm{t}), \mathrm{t}) = \frac{1}{2}(\mathbf{x}^{\mathrm{T}}\mathbf{Q}\mathbf{x} + \mathbf{u}^{\mathrm{T}}\mathbf{R}\mathbf{u}) + \boldsymbol{\lambda}^{\mathrm{T}}(\mathbf{A}\mathbf{x} + \mathbf{B}\mathbf{u}) \tag{3.13}$$

The first-order necessary conditions are as follows.

$$\begin{aligned} \dot{\mathbf{x}} &= \frac{\partial \mathrm{H}}{\partial \boldsymbol{\lambda}} = \mathbf{A}\mathbf{x} + \mathbf{B}\mathbf{u} \\ \dot{\boldsymbol{\lambda}} &= -\frac{\partial \mathrm{H}}{\partial \mathbf{x}} = -\mathbf{Q}\mathbf{x} - \mathbf{A}^{\mathrm{T}}\boldsymbol{\lambda} \\ \frac{\partial \mathrm{H}}{\partial \mathbf{u}} &= \mathbf{0} = \mathbf{R}\mathbf{u} + \mathbf{B}^{\mathrm{T}}\boldsymbol{\lambda} \end{aligned} \tag{3.14}$$

From above conditions the control function and the closed-loop dynamics can be written as follows.

$$\mathbf{u} = -\mathbf{R}^{-1}\mathbf{B}^{\mathrm{T}}\boldsymbol{\lambda} \tag{3.15}$$

$$\dot{\mathbf{x}} = \mathbf{A}\mathbf{x} - \mathbf{B}\mathbf{R}^{-1}\mathbf{B}^{\mathrm{T}}\boldsymbol{\lambda} \tag{3.16}$$

The system including state and co-state dynamics can be written as follows.

$$\begin{bmatrix} \dot{\mathbf{x}} \\ \dot{\boldsymbol{\lambda}} \end{bmatrix} = \begin{bmatrix} \mathbf{A} & -\mathbf{B}\mathbf{R}^{-1}\mathbf{B}^{\mathrm{T}} \\ -\mathbf{Q} & -\mathbf{A}^{\mathrm{T}} \end{bmatrix} \begin{bmatrix} \mathbf{x} \\ \boldsymbol{\lambda} \end{bmatrix} \tag{3.17}$$

The above system is linear and a transformation $\boldsymbol{\lambda}(\mathrm{t}) = \mathbf{P}(\mathrm{t})\mathbf{x}(\mathrm{t})$ is proposed. Matrix $\mathbf{P}(\mathrm{t})$ which is symmetric and positive definite is to be determined. Taking derivative of this transformation and using the expression for $\dot{\boldsymbol{\lambda}}$ we get the following equation.

$$\begin{aligned} \dot{\boldsymbol{\lambda}} &= \dot{\mathbf{P}}\mathbf{x} + \mathbf{P}\dot{\mathbf{x}} = -\mathbf{Q}\mathbf{x} - \mathbf{A}^{\mathrm{T}}\boldsymbol{\lambda} \\ \dot{\mathbf{P}}\mathbf{x} + \mathbf{P}(\mathbf{A}\mathbf{x} - \mathbf{B}\mathbf{R}^{-1}\mathbf{B}^{\mathrm{T}}\boldsymbol{\lambda}) &= -\mathbf{Q}\mathbf{x} - \mathbf{A}^{\mathrm{T}}\mathbf{P}\mathbf{x} \\ \left(\dot{\mathbf{P}} + \mathbf{P}\mathbf{A} + \mathbf{A}^{\mathrm{T}}\mathbf{P} - \mathbf{P}\mathbf{B}\mathbf{R}^{-1}\mathbf{B}^{\mathrm{T}}\mathbf{P} + \mathbf{Q}\right)\mathbf{x} &= \mathbf{0} \end{aligned} \tag{3.17}$$

Since $\mathbf{x}(t) \neq \mathbf{0}$, Equation (3.17) gives the differential Riccati equation (DRE).

$$\dot{\mathbf{P}} + \mathbf{PA} + \mathbf{A}^{\mathrm{T}}\mathbf{P} - \mathbf{PBR}^{-1}\mathbf{B}^{\mathrm{T}}\mathbf{P} + \mathbf{Q} = \mathbf{0}, \qquad \mathbf{P}(t_f) = \mathbf{S}_f \tag{3.18}$$

For a time-periodic $\mathbf{A}$ matrix such as $\mathbf{A}_{\mathrm{LERM}}(t)$, as $t_f \to \infty$, solution of the DRE is a time-periodic matrix $\mathbf{P}(t)$. For a constant $\mathbf{A}$ matrix such as $\mathbf{A}_{\mathrm{HCW}}$, as $t_f \to \infty$, solution of the DRE is a constant matrix $\mathbf{P}$. Constant matrix $\mathbf{P}$ can be obtained by solving the algebraic Riccati equation (ARE) given below.

$$\mathbf{PA} + \mathbf{A}^{\mathrm{T}}\mathbf{P} - \mathbf{PBR}^{-1}\mathbf{B}^{\mathrm{T}}\mathbf{P} + \mathbf{Q} = \mathbf{0} \tag{3.19}$$

Defining $\mathbf{K} = -\mathbf{R}^{-1}\mathbf{B}^{\mathrm{T}}\mathbf{P}$ and using $\boldsymbol{\lambda} = \mathbf{Px}$, the optimal control law and the closed-loop dynamics can be written as follows.

$$\mathbf{u}^{*} = -\mathbf{Kx} \tag{3.20}$$

$$\dot{\mathbf{x}} = (\mathbf{A} - \mathbf{BK})\mathbf{x} \tag{3.21}$$

Derivation Using the HJB Equation

To use the HJB equation, the Hamiltonian is written as follows.

$$\mathrm{H}\left(\mathbf{x}(t), \mathbf{u}(t), \frac{\partial \mathrm{J}^{*}}{\partial \mathbf{x}}, t\right) = \frac{1}{2}\mathbf{x}^{\mathrm{T}}\mathbf{Q}\mathbf{x} + \frac{1}{2}\mathbf{u}^{\mathrm{T}}\mathbf{R}\mathbf{u} + \left[\frac{\partial \mathrm{J}^{*}}{\partial \mathbf{x}}\right]^{\mathrm{T}}(\mathbf{Ax} + \mathbf{Bu}) \tag{3.22}$$

The necessary condition $\frac{\partial \mathrm{H}}{\partial \mathbf{u}} = \mathbf{0}$ gives the following.

$$\frac{\partial \mathrm{H}}{\partial \mathbf{u}} = \mathbf{Ru} + \mathbf{B}^{\mathrm{T}}\left[\frac{\partial \mathrm{J}^{*}}{\partial \mathbf{x}}\right] = \mathbf{0} \tag{3.23}$$

Solving above equation gives the following expression for control.

$$\mathbf{u} = -\mathbf{R}^{-1}\mathbf{B}^{\mathrm{T}}\left[\frac{\partial \mathrm{J}^{*}}{\partial \mathbf{x}}\right] \tag{3.24}$$

Substituting above expression in Equation (3.22) gives the following.

$$H\left(\mathbf{x}(t),\mathbf{u}(t),\frac{\partial J^*}{\partial \mathbf{x}},t\right)=\frac{1}{2}\mathbf{x}^T\mathbf{Q}\mathbf{x}+\frac{1}{2}\left[\frac{\partial J^*}{\partial \mathbf{x}}\right]^T\mathbf{B}\mathbf{R}^{-1}\mathbf{B}^T\frac{\partial J^*}{\partial \mathbf{x}}$$

$$+\left[\frac{\partial J^*}{\partial \mathbf{x}}\right]^T\mathbf{A}\mathbf{x}-\left[\frac{\partial J^*}{\partial \mathbf{x}}\right]^T\mathbf{B}\mathbf{R}^{-1}\mathbf{B}^T\frac{\partial J^*}{\partial \mathbf{x}}$$

$$=\frac{1}{2}\mathbf{x}^T\mathbf{Q}\mathbf{x}-\frac{1}{2}\left[\frac{\partial J^*}{\partial \mathbf{x}}\right]^T\mathbf{B}\mathbf{R}^{-1}\mathbf{B}^T\frac{\partial J^*}{\partial \mathbf{x}}+\left[\frac{\partial J^*}{\partial \mathbf{x}}\right]^T\mathbf{A}\mathbf{x} \quad (3.25)$$

The HJB equation can be written as follows.

$$\frac{\partial J^*}{\partial t}+\frac{1}{2}\mathbf{x}^T\mathbf{Q}\mathbf{x}-\frac{1}{2}\left[\frac{\partial J^*}{\partial \mathbf{x}}\right]^T\mathbf{B}\mathbf{R}^{-1}\mathbf{B}^T\frac{\partial J^*}{\partial \mathbf{x}}+\left[\frac{\partial J^*}{\partial \mathbf{x}}\right]^T\mathbf{A}\mathbf{x}=0 \quad (3.26)$$

From Equation (3.12), the boundary condition is as follows.

$$J^*(\mathbf{x}(t_f),t_f)=\frac{1}{2}\mathbf{x}^T(t_f)\mathbf{S}_f\mathbf{x}(t_f)$$

Let us guess the following solution for the cost function.

$$J^*(\mathbf{x}(t),t)=\frac{1}{2}\mathbf{x}^T(t)\mathbf{P}(t)\mathbf{x}(t)$$

Matrix $\mathbf{P}(t)$ which is symmetric and positive definite is to be determined. The partial derivatives of above cost function with respect to time and state are as follows.

$$\frac{\partial J^*}{\partial t}=\frac{1}{2}\mathbf{x}^T\dot{\mathbf{P}}\mathbf{x}$$

$$\frac{\partial J^*}{\partial \mathbf{x}}=\mathbf{P}\mathbf{x}$$

Substituting above expressions in Equation (3.26) gives the following.

$$\frac{1}{2}\mathbf{x}^T\dot{\mathbf{P}}\mathbf{x}+\mathbf{x}^T\mathbf{P}\mathbf{A}\mathbf{x}-\frac{1}{2}\mathbf{x}^T\mathbf{P}\mathbf{B}\mathbf{R}^{-1}\mathbf{B}^T\mathbf{P}\mathbf{x}+\frac{1}{2}\mathbf{x}^T\mathbf{Q}\mathbf{x}=\mathbf{0}$$

$$\frac{1}{2}\mathbf{x}^T\dot{\mathbf{P}}\mathbf{x}+\frac{1}{2}\mathbf{x}^T\mathbf{P}\mathbf{A}\mathbf{x}+\frac{1}{2}\mathbf{x}^T\mathbf{A}^T\mathbf{P}\mathbf{x}-\frac{1}{2}\mathbf{x}^T\mathbf{P}\mathbf{B}\mathbf{R}^{-1}\mathbf{B}^T\mathbf{P}\mathbf{x}+\frac{1}{2}\mathbf{x}^T\mathbf{Q}\mathbf{x}=\mathbf{0} \quad (3.27)$$

Since $\mathbf{x}(t)\neq\mathbf{0}$, Equation (3.27) gives the DRE which is the same as Equation (3.18).

$$\dot{\mathbf{P}}+\mathbf{P}\mathbf{A}+\mathbf{A}^T\mathbf{P}-\mathbf{P}\mathbf{B}\mathbf{R}^{-1}\mathbf{B}^T\mathbf{P}+\mathbf{Q}=\mathbf{0},\qquad \mathbf{P}(t_f)=\mathbf{S}_f \quad (3.28)$$

DIFFERNTIAL GAME THEORY

The two-player spacecraft pursuit-evasion game problem to be explored in this dissertation involves two competing players with opposite objectives. This problem can be modeled as a two-player zero-sum differential game. Zero-sum differential games were first introduced by Isaacs.[12] The two-player zero-sum differential game problem can be considered as an extension of the optimal control problem. Thus, the principles of calculus of variations and dynamic programming can also be applied to the differential game problem. Particularly, the dynamic programming approach requires solving the Hamilton-Jacobi-Isaacs (HJI) PDE.[13] For LQ problems, the HJI equation also reduces to a DRE or an ARE for infinite-horizon problem.[14]

Hamilton-Jacobi-Isaacs Equation

The two-player zero-sum differential game problem is to find optimal control inputs $\mathbf{u}_p{}^*$ and $\mathbf{u}_e{}^*$ for a set of generally nonlinear, coupled differential equations of the form

$$\dot{\mathbf{x}} = \mathbf{f}\big(\mathbf{x}(t), \mathbf{u}_p(t), \mathbf{u}_e(t), t\big), \qquad t \in [t_0, t_f] \tag{3.29}$$

such that $\mathbf{u}_p$ minimizes and $\mathbf{u}_e$ maximizes the associated cost function.

$$J = \Phi(\mathbf{x}(t_f), t_f) + \int_{t_0}^{t_f} L\big(\mathbf{x}(t), \mathbf{u}_p(t), \mathbf{u}_e(t), t\big)dt \tag{3.30}$$

Here, $\mathbf{x}(t) \in \mathbb{R}^n$ is the game state and $\mathbf{u}_p(t) \in \mathbb{R}^m$ and $\mathbf{u}_e(t) \in \mathbb{R}^m$ are the controls of the two players. The optimal control laws correspond to a saddle point solution of the zero-sum differential game. The saddle point solution is such that if a player deviates unilaterally from this solution then this would worsen that particular player's situation as a result of a change contrary to that player's objective.

$$J(\mathbf{u}_p{}^*, \mathbf{u}_e) \le J(\mathbf{u}_p{}^*, \mathbf{u}_e{}^*) \le J(\mathbf{u}_p, \mathbf{u}_e{}^*) \tag{3.31}$$

Define the Hamiltonian as follows.

$$\begin{aligned} H\left(\mathbf{x}(t), \mathbf{u}_p(t), \mathbf{u}_e(t), \frac{\partial J^*}{\partial \mathbf{x}}, t\right) &= L\left(\mathbf{x}(t), \mathbf{u}_p(t), \mathbf{u}_e(t), t\right) + \left[\frac{\partial J^*}{\partial \mathbf{x}}\right]^T \mathbf{f}\left(\mathbf{x}(t), \mathbf{u}_p(t), \mathbf{u}_e(t), t\right) \\ H\left(\mathbf{x}(t), \mathbf{u}_p{}^*(t), \mathbf{u}_e{}^*(t), \frac{\partial J^*}{\partial \mathbf{x}}, t\right) &= \min_{\mathbf{u}_p(t)} \max_{\mathbf{u}_e(t)} H\left(\mathbf{x}(t), \mathbf{u}_p(t), \mathbf{u}_e(t), \frac{\partial J^*}{\partial \mathbf{x}}, t\right) \\ &= \max_{\mathbf{u}_e(t)} \min_{\mathbf{u}_p(t)} H\left(\mathbf{x}(t), \mathbf{u}_p(t), \mathbf{u}_e(t), \frac{\partial J^*}{\partial \mathbf{x}}, t\right) \end{aligned} \tag{3.32}$$

The HJI equation is given as follows.

$$\frac{\partial J^*}{\partial t} + H\left(\mathbf{x}(t), \mathbf{u}_p{}^*(t), \mathbf{u}_e{}^*(t), \frac{\partial J^*}{\partial \mathbf{x}}, t\right) = 0 \tag{3.33}$$

The boundary condition is as follows.

$$J^*(\mathbf{x}(t_f), t_f) = \Phi(\mathbf{x}(t_f), t_f) \tag{3.34}$$

Linear Quadratic Zero-Sum Differential Game

For the LQ zero-sum differential game problem, the dynamics equation and the cost function are given as follows.

$$\dot{\mathbf{x}} = \mathbf{A}(t)\mathbf{x}(t) + \mathbf{B}_p\mathbf{u}_p(t) + \mathbf{B}_e\mathbf{u}_e(t) \tag{3.35}$$

$$J = \frac{1}{2}\mathbf{x}^T(t_f)\mathbf{S}_f\mathbf{x}(t_f) + \frac{1}{2}\int_{t_0}^{t_f}\left(\mathbf{x}^T(t)\mathbf{Q}\mathbf{x}(t) + \mathbf{u}_p{}^T(t)\mathbf{R}\mathbf{u}_p(t) - \gamma^2\mathbf{u}_e{}^T(t)\mathbf{R}\mathbf{u}_e(t)\right)dt \tag{3.36}$$

The control weighting for two players differs by the scaling factor γ. The Hamiltonian for this system is as follows.

$$\begin{aligned} H\left(\mathbf{x}(t), \mathbf{u}_p(t), \mathbf{u}_e(t), \frac{\partial J^*}{\partial \mathbf{x}}, t\right) &= \frac{1}{2}\mathbf{x}^T\mathbf{Q}\mathbf{x} + \frac{1}{2}\mathbf{u}_p{}^T\mathbf{R}\mathbf{u}_p - \frac{1}{2}\gamma^2\mathbf{u}_e{}^T\mathbf{R}\mathbf{u}_e \\ &\quad + \left[\frac{\partial J^*}{\partial \mathbf{x}}\right]^T\left(\mathbf{A}\mathbf{x} + \mathbf{B}_p\mathbf{u}_p + \mathbf{B}_e\mathbf{u}_e\right) \end{aligned} \tag{3.37}$$

The necessary condition $\frac{\partial \mathrm{H}}{\partial \mathbf{u}} = \mathbf{0}$ gives the following.

$$\frac{\partial \mathrm{H}}{\partial \mathbf{u}_\mathrm{p}} = \mathbf{R}\mathbf{u}_\mathrm{p} + \mathbf{B}_\mathrm{p}{}^\mathrm{T}\left[\frac{\partial \mathrm{J}^*}{\partial \mathbf{x}}\right] = \mathbf{0}$$
$$\frac{\partial \mathrm{H}}{\partial \mathbf{u}_\mathrm{e}} = -\gamma^2\mathbf{R}\mathbf{u}_\mathrm{e} + \mathbf{B}_\mathrm{e}{}^\mathrm{T}\left[\frac{\partial \mathrm{J}^*}{\partial \mathbf{x}}\right] = \mathbf{0} \tag{3.38}$$

Solving above equations gives the following expressions for the controls.

$$\mathbf{u}_\mathrm{p} = -\mathbf{R}^{-1}\mathbf{B}_\mathrm{p}{}^\mathrm{T}\left[\frac{\partial \mathrm{J}^*}{\partial \mathbf{x}}\right]$$
$$\mathbf{u}_\mathrm{e} = \frac{1}{\gamma^2}\mathbf{R}^{-1}\mathbf{B}_\mathrm{e}{}^\mathrm{T}\left[\frac{\partial \mathrm{J}^*}{\partial \mathbf{x}}\right] \tag{3.39}$$

Substituting above expressions in Equation (3.37) gives the following.

$$\mathrm{H}\left(\mathbf{x}(\mathrm{t}), \mathbf{u}_\mathrm{p}(\mathrm{t}), \mathbf{u}_\mathrm{e}(\mathrm{t}), \frac{\partial \mathrm{J}^*}{\partial \mathbf{x}}, \mathrm{t}\right) = \frac{1}{2}\mathbf{x}^\mathrm{T}\mathbf{Q}\mathbf{x} + \frac{1}{2}\left[\frac{\partial \mathrm{J}^*}{\partial \mathbf{x}}\right]^\mathrm{T}\mathbf{B}_\mathrm{p}\mathbf{R}^{-1}\mathbf{B}_\mathrm{p}{}^\mathrm{T}\frac{\partial \mathrm{J}^*}{\partial \mathbf{x}}$$
$$-\frac{1}{2\gamma^2}\left[\frac{\partial \mathrm{J}^*}{\partial \mathbf{x}}\right]^\mathrm{T}\mathbf{B}_\mathrm{e}\mathbf{R}^{-1}\mathbf{B}_\mathrm{e}{}^\mathrm{T}\frac{\partial \mathrm{J}^*}{\partial \mathbf{x}} + \left[\frac{\partial \mathrm{J}^*}{\partial \mathbf{x}}\right]^\mathrm{T}\mathbf{A}\mathbf{x}$$
$$-\left[\frac{\partial \mathrm{J}^*}{\partial \mathbf{x}}\right]^\mathrm{T}\mathbf{B}_\mathrm{p}\mathbf{R}^{-1}\mathbf{B}_\mathrm{p}{}^\mathrm{T}\frac{\partial \mathrm{J}^*}{\partial \mathbf{x}} + \frac{1}{\gamma^2}\left[\frac{\partial \mathrm{J}^*}{\partial \mathbf{x}}\right]^\mathrm{T}\mathbf{B}_\mathrm{e}\mathbf{R}^{-1}\mathbf{B}_\mathrm{e}{}^\mathrm{T}\frac{\partial \mathrm{J}^*}{\partial \mathbf{x}}$$

$$\mathrm{H}\left(\mathbf{x}(\mathrm{t}), \mathbf{u}_\mathrm{p}(\mathrm{t}), \mathbf{u}_\mathrm{e}(\mathrm{t}), \frac{\partial \mathrm{J}^*}{\partial \mathbf{x}}, \mathrm{t}\right) = \frac{1}{2}\mathbf{x}^\mathrm{T}\mathbf{Q}\mathbf{x} + \left[\frac{\partial \mathrm{J}^*}{\partial \mathbf{x}}\right]^\mathrm{T}\mathbf{A}\mathbf{x} - \frac{1}{2}\left[\frac{\partial \mathrm{J}^*}{\partial \mathbf{x}}\right]^\mathrm{T}\mathbf{B}_\mathrm{p}\mathbf{R}^{-1}\mathbf{B}_\mathrm{p}{}^\mathrm{T}\frac{\partial \mathrm{J}^*}{\partial \mathbf{x}}$$
$$+\frac{1}{2\gamma^2}\left[\frac{\partial \mathrm{J}^*}{\partial \mathbf{x}}\right]^\mathrm{T}\mathbf{B}_\mathrm{e}\mathbf{R}^{-1}\mathbf{B}_\mathrm{e}{}^\mathrm{T}\frac{\partial \mathrm{J}^*}{\partial \mathbf{x}} \tag{3.40}$$

The HJI equation can be written as follows.

$$\frac{\partial \mathrm{J}^*}{\partial \mathrm{t}} + \frac{1}{2}\mathbf{x}^\mathrm{T}\mathbf{Q}\mathbf{x} - \frac{1}{2}\left[\frac{\partial \mathrm{J}^*}{\partial \mathbf{x}}\right]^\mathrm{T}\mathbf{B}_\mathrm{p}\mathbf{R}^{-1}\mathbf{B}_\mathrm{p}{}^\mathrm{T}\frac{\partial \mathrm{J}^*}{\partial \mathbf{x}} + \frac{1}{2\gamma^2}\left[\frac{\partial \mathrm{J}^*}{\partial \mathbf{x}}\right]^\mathrm{T}\mathbf{B}_\mathrm{e}\mathbf{R}^{-1}\mathbf{B}_\mathrm{e}{}^\mathrm{T}\frac{\partial \mathrm{J}^*}{\partial \mathbf{x}} + \left[\frac{\partial \mathrm{J}^*}{\partial \mathbf{x}}\right]^\mathrm{T}\mathbf{A}\mathbf{x} = 0 \tag{3.41}$$

From the Equation (3.30) the boundary condition is as follows.

$$\mathrm{J}^*(\mathbf{x}(\mathrm{t_f}), \mathrm{t_f}) = \frac{1}{2}\mathbf{x}^\mathrm{T}(\mathrm{t_f})\mathbf{S}_\mathrm{f}\mathbf{x}(\mathrm{t_f})$$

Let us guess the following solution for the cost function.

$$J^*(\mathbf{x}(t), t) = \frac{1}{2}\mathbf{x}^T(t)\mathbf{P}(t)\mathbf{x}(t)$$

Matrix $\mathbf{P}(t)$ which is symmetric and positive definite is to be determined. The partial derivatives of above function with respect to time and state are as follows.

$$\frac{\partial J^*}{\partial t} = \frac{1}{2}\mathbf{x}^T\dot{\mathbf{P}}\mathbf{x}$$

$$\frac{\partial J^*}{\partial \mathbf{x}} = \mathbf{P}\mathbf{x}$$

Substituting above expressions in Equation (3.41) gives the following.

$$\frac{1}{2}\mathbf{x}^T\dot{\mathbf{P}}\mathbf{x} + \mathbf{x}^T\mathbf{P}\mathbf{A}\mathbf{x} - \frac{1}{2}\mathbf{x}^T\mathbf{P}\mathbf{B}_p\mathbf{R}^{-1}\mathbf{B}_p{}^T\mathbf{P}\mathbf{x} + \frac{1}{2\gamma^2}\mathbf{x}^T\mathbf{B}_e\mathbf{R}^{-1}\mathbf{B}_e{}^T\mathbf{x} + \frac{1}{2}\mathbf{x}^T\mathbf{Q}\mathbf{x} = \mathbf{0}$$

$$\frac{1}{2}\mathbf{x}^T\dot{\mathbf{P}}\mathbf{x} + \frac{1}{2}\mathbf{x}^T\mathbf{P}\mathbf{A}\mathbf{x} + \frac{1}{2}\mathbf{x}^T\mathbf{A}^T\mathbf{P}\mathbf{x} - \frac{1}{2}\mathbf{x}^T\mathbf{P}\mathbf{B}_p\mathbf{R}^{-1}\mathbf{B}_p{}^T\mathbf{P}\mathbf{x} + \frac{1}{2\gamma^2}\mathbf{x}^T\mathbf{B}_e\mathbf{R}^{-1}\mathbf{B}_e{}^T\mathbf{x} + \frac{1}{2}\mathbf{x}^T\mathbf{Q}\mathbf{x} = \mathbf{0} \quad (3.42)$$

Since $\mathbf{x}(t) \neq \mathbf{0}$, Equation (3.42) gives the game DRE.

$$\dot{\mathbf{P}} + \mathbf{P}\mathbf{A} + \mathbf{A}^T\mathbf{P} - \mathbf{P}\mathbf{B}_p\mathbf{R}^{-1}\mathbf{B}_p{}^T\mathbf{P} + \frac{1}{\gamma^2}\mathbf{P}\mathbf{B}_e\mathbf{R}^{-1}\mathbf{B}_e{}^T\mathbf{P} + \mathbf{Q} = \mathbf{0}, \qquad \mathbf{P}(t_f) = \mathbf{S}_f \quad (3.43)$$

The game ARE is given below.

$$\mathbf{P}\mathbf{A} + \mathbf{A}^T\mathbf{P} - \mathbf{P}\mathbf{B}_p\mathbf{R}^{-1}\mathbf{B}_p{}^T\mathbf{P} + \frac{1}{\gamma^2}\mathbf{P}\mathbf{B}_e\mathbf{R}^{-1}\mathbf{B}_e{}^T\mathbf{P} + \mathbf{Q} = \mathbf{0} \quad (3.44)$$

Equation (3.44) can be written as follows.

$$\mathbf{P}\mathbf{A} + \mathbf{A}^T\mathbf{P} - \mathbf{P}\left(\mathbf{B}_p\mathbf{R}^{-1}\mathbf{B}_p{}^T - \frac{1}{\gamma^2}\mathbf{B}_e\mathbf{R}^{-1}\mathbf{B}_e{}^T\right)\mathbf{P} + \mathbf{Q} = \mathbf{0}$$

$$\mathbf{P}\mathbf{A} + \mathbf{A}^T\mathbf{P} - \mathbf{P}[\mathbf{B}_p \quad \mathbf{B}_e]\begin{bmatrix}\mathbf{R} & \mathbf{0} \\ \mathbf{0} & -\gamma^2\mathbf{R}\end{bmatrix}^{-1}\begin{bmatrix}\mathbf{B}_p \\ \mathbf{B}_e\end{bmatrix}^T\mathbf{P} + \mathbf{Q} = \mathbf{0}$$

$$\mathbf{P}\mathbf{A} + \mathbf{A}^T\mathbf{P} - \mathbf{P}\mathbf{B}_g\mathbf{R}_g{}^{-1}\mathbf{B}_g{}^T\mathbf{P} + \mathbf{Q} = \mathbf{0} \quad (3.45)$$

Equation (3.45) can be solved using the "*care*" function in MATLAB™. From Equation (3.39), the optimal control laws are given as follows.

$$\mathbf{u}_p{}^* = -\mathbf{R}^{-1}\mathbf{B}_p{}^T\mathbf{P}\mathbf{x}$$
$$\mathbf{u}_e{}^* = \frac{1}{\gamma^2}\mathbf{R}^{-1}\mathbf{B}_e{}^T\mathbf{P}\mathbf{x} \tag{3.46}$$

STATE-DEPENDENT RICCATI EQUATION METHOD

The solution of a nonlinear optimal control problem or a nonlinear differential game problem involves the challenging task of numerically solving the TPBVP or the HJB/HJI equation. This has lead researchers to develop methods to obtain near-optimal solutions without directly solving the TPBVP or the HJB/HJI equation. One such method is the well-known and popular state-dependent Riccati Equation (SDRE) method for control of nonlinear systems.[15-21] The SDRE method employs factorization of the nonlinear dynamics into a state vector and state-dependent matrix-valued function. This factorization transforms the nonlinear system into a linear-like system that is dependent on the current state and is capable of capturing the nonlinear system dynamics. The optimal control problem of this linear-like system with a quadratic performance index leads to an ARE in terms of the state-dependent matrices. This ARE needs to be solved at each point in state space.

Nonlinear Control Using SDRE Method

Consider a nonlinear control-affine dynamic system given below.

$$\dot{\mathbf{x}} = \mathbf{f}(\mathbf{x}) + \mathbf{B}\mathbf{u}(t) \tag{3.47}$$

In the SDRE method, state-dependent coefficient (SDC) parameterization (also known as extended linearization or apparent linearization) is the process of factorizing a nonlinear system into a linear-like structure which contains SDC matrices. For a nonlinear system

$\mathbf{f}(\mathbf{x})$, under the assumption $\mathbf{f}(\mathbf{0}) = \mathbf{0}$, a continuous matrix-valued function $\mathbf{A}(\mathbf{x})$ always exists such that $\mathbf{f}(\mathbf{x}) = \mathbf{A}(\mathbf{x})\mathbf{x}$. The matrix $\mathbf{A}(\mathbf{x})$ is found by mathematical factorization and is non-unique for multivariable systems. The control law obtained may be slightly sub-optimal. Equation (3.47) can now be written as follows.

$$\dot{\mathbf{x}} = \mathbf{A}(\mathbf{x})\mathbf{x} + \mathbf{B}\mathbf{u}(\mathrm{t}) \tag{3.48}$$

Consider the following cost function for an infinite-horizon problem.

$$\mathrm{J} = \frac{1}{2}\int_{\mathrm{t_0}}^{\infty} (\mathbf{x}^{\mathrm{T}}(\mathrm{t})\mathbf{Q}(\mathbf{x})\mathbf{x}(\mathrm{t}) + \mathbf{u}^{\mathrm{T}}(\mathrm{t})\mathbf{R}(\mathbf{x})\mathbf{u}(\mathrm{t}))\mathrm{dt} \tag{3.49}$$

The nonlinear control law is given as follows.

$$\mathbf{u}(\mathbf{x}) = -\mathbf{R}^{-1}(\mathbf{x})\mathbf{B}^{\mathrm{T}}\mathbf{P}(\mathbf{x})\mathbf{x} \tag{3.50}$$

Matrix $\mathbf{P}(\mathbf{x})$ is obtained by solving the following SDRE at each point in state space.

$$\mathbf{P}(\mathbf{x})\mathbf{A}(\mathbf{x}) + \mathbf{A}^{\mathrm{T}}(\mathbf{x})\mathbf{P}(\mathbf{x}) - \mathbf{P}(\mathbf{x})\mathbf{B}\mathbf{R}^{-1}(\mathbf{x})\mathbf{B}^{\mathrm{T}}\mathbf{P}(\mathbf{x}) + \mathbf{Q}(\mathbf{x}) = \mathbf{0} \tag{3.51}$$

Nonlinear Zero-Sum Differential Game Using SDRE Method

Consider a nonlinear control-affine dynamic system given below.

$$\dot{\mathbf{x}} = \mathbf{f}(\mathbf{x}) + \mathbf{B}_{\mathrm{p}}\mathbf{u}_{\mathrm{p}}(\mathrm{t}) + \mathbf{B}_{\mathrm{e}}\mathbf{u}_{\mathrm{e}}(\mathrm{t}) \tag{3.52}$$

Using SDC parameterization, above system can be written as follows.

$$\dot{\mathbf{x}} = \mathbf{A}(\mathbf{x})\mathbf{x}(\mathrm{t}) + \mathbf{B}_{\mathrm{p}}\mathbf{u}_{\mathrm{p}}(\mathrm{t}) + \mathbf{B}_{\mathrm{e}}\mathbf{u}_{\mathrm{e}}(\mathrm{t}) \tag{3.53}$$

Consider the following cost function.

$$\mathrm{J} = \frac{1}{2}\int_{\mathrm{t_0}}^{\infty} \left(\mathbf{x}^{\mathrm{T}}(\mathrm{t})\mathbf{Q}(\mathbf{x})\mathbf{x}(\mathrm{t}) + \mathbf{u}_{\mathrm{p}}{}^{\mathrm{T}}(\mathrm{t})\mathbf{R}(\mathbf{x})\mathbf{u}_{\mathrm{p}}(\mathrm{t}) - \gamma^2\mathbf{u}_{\mathrm{e}}{}^{\mathrm{T}}(\mathrm{t})\mathbf{R}(\mathbf{x})\mathbf{u}_{\mathrm{e}}(\mathrm{t})\right)\mathrm{dt} \tag{3.54}$$

The nonlinear control laws can be given as follows.

$$\begin{aligned} \mathbf{u}_{\mathrm{p}}(\mathbf{x}) &= -\mathbf{R}^{-1}(\mathbf{x})\mathbf{B}_{\mathrm{p}}{}^{\mathrm{T}}\mathbf{P}(\mathbf{x})\mathbf{x} \\ \mathbf{u}_{\mathrm{e}}(\mathbf{x}) &= \frac{1}{\gamma^2}\mathbf{R}^{-1}(\mathbf{x})\mathbf{B}_{\mathrm{e}}{}^{\mathrm{T}}\mathbf{P}(\mathbf{x})\mathbf{x} \end{aligned} \tag{3.55}$$

Matrix $\mathbf{P}(\mathbf{x})$ is obtained by solving the following SDRE at each point in state space.

$$\mathbf{P}(\mathbf{x})\mathbf{A}(\mathbf{x}) + \mathbf{A}^{\mathrm{T}}(\mathbf{x})\mathbf{P}(\mathbf{x}) - \mathbf{P}(\mathbf{x})\mathbf{B}_{\mathrm{p}}\mathbf{R}^{-1}(\mathbf{x}){\mathbf{B}_{\mathrm{p}}}^{\mathrm{T}}\mathbf{P}(\mathbf{x}) + \frac{1}{\gamma^2}\mathbf{P}(\mathbf{x})\mathbf{B}_{\mathrm{e}}\mathbf{R}^{-1}(\mathbf{x}){\mathbf{B}_{\mathrm{e}}}^{\mathrm{T}}\mathbf{P}(\mathbf{x}) + \mathbf{Q}(\mathbf{x}) = \mathbf{0} \tag{3.56}$$

Similar to Equation (3.45), above equation can be written as follows.

$$\mathbf{P}(\mathbf{x})\mathbf{A}(\mathbf{x}) + \mathbf{A}^{\mathrm{T}}(\mathbf{x})\mathbf{P}(\mathbf{x}) - \mathbf{P}(\mathbf{x})\mathbf{B}_{\mathrm{g}}{\mathbf{R}_{\mathrm{g}}}^{-1}(\mathbf{x}){\mathbf{B}_{\mathrm{g}}}^{\mathrm{T}}\mathbf{P}(\mathbf{x}) + \mathbf{Q}(\mathbf{x}) = \mathbf{0} \tag{3.57}$$

SEQUENTIAL STATE ESTIMATION ALGORITHMS

State estimation techniques estimate the orbit of a celestial body or a spacecraft from measurement sensor data. The simplest state estimation algorithm is the least-squares method which processes a batch of measurement data and minimizes the sum of squares of the residuals. A sequential state estimation algorithm processes measurements as they are received.

Kalman Filter

The Kalman filter (KF) is a sequential estimation algorithm for linear systems.[22] The KF is a minimum mean square error (MMSE) estimator that minimizes mean square of the estimation error. The KF is used to estimate the system state vector **x** consisting of state variables such as position, velocity, and any other system parameters. The KF needs a system dynamics model and a measurement model. The system dynamics model may be inadequate to capture all the dynamics present in a real world case. The KF attempts to account for this by adding zero-mean Gaussian white noise **w** to the model. The strength of this noise is captured in the process noise covariance matrix **Q**. Zero-mean Gaussian white noise **v** is also added to the measurement model to account for sensor noise. The strength of this noise is captured in the measurement noise covariance matrix **R**. The KF requires that **w** and **v** are not correlated. The KF stores the current estimate of the state

vector $\hat{\mathbf{x}}$ and also maintains a state covariance matrix $\mathbf{P}$ that represents the uncertainty in the estimate and how errors in one state variable co-vary with other state variables. The KF needs to be initialized with an estimate of the initial state vector $\hat{\mathbf{x}}_0$ and an associated state covariance matrix $\mathbf{P}_0$.

The KF updates and maintains the state estimate and the state covariance matrix with a two-step process. The first step is to propagate the state estimate and the state covariance matrix forward in time using the system dynamics model. As the state estimate is propagated, it will tend to drift away from the true state. This is due to the imperfections in both the initial state estimate and the system dynamics model. The propagated state covariance matrix also reflects this reduced accuracy of the state estimate. The second step processes any available measurement and updates the state estimate and the state covariance matrix. The KF combines the state estimate obtained by propagation with the information gained from the measurement to generate a better state estimate. When generating the new state estimate, the KF uses the state covariance and the measurement noise covariance to weight the estimate towards the more accurate source.

The KF can be derived in a discrete-time form, a continuous-time form, and a continuous-discrete form. The KF is not derived here. The derivation can be found in Reference 23. The steps to implement the continuous-time KF are as follows.

Initialize: $\mathbf{x}(t_0) = \mathbf{x}_0, \hat{\mathbf{x}}(t_0) = \hat{\mathbf{x}}_0, \mathbf{P}(t_0) = \mathbf{P}_0$

Model: $\dot{\mathbf{x}} = \mathbf{A}\mathbf{x} + \mathbf{B}\mathbf{u} + \mathbf{w}$

$\mathbf{y} = \mathbf{C}\mathbf{x} + \mathbf{v}$

Gain: $\mathbf{K} = \mathbf{P}\mathbf{C}^{\mathrm{T}}\mathbf{R}^{-1}$

Covariance: $\dot{\mathbf{P}} = \mathbf{P}\mathbf{A}^{\mathrm{T}} + \mathbf{A}\mathbf{P} + \mathbf{Q} - \mathbf{P}\mathbf{C}^{\mathrm{T}}\mathbf{R}^{-1}\mathbf{C}\mathbf{P}$

Estimate: $\dot{\hat{\mathbf{x}}} = \mathbf{A}\hat{\mathbf{x}} + \mathbf{B}\mathbf{u} + \mathbf{K}[\mathbf{y} - \mathbf{C}\hat{\mathbf{x}}]$

The steps to implement the continuous-discrete KF are as follows.

Initialize: $\mathbf{x}(\mathrm{t}_0) = \mathbf{x}_0, \hat{\mathbf{x}}(\mathrm{t}_0) = \hat{\mathbf{x}}_0, \mathbf{P}(\mathrm{t}_0) = \mathbf{P}_0$

Model: $\dot{\mathbf{x}} = \mathbf{A}\mathbf{x} + \mathbf{B}\mathbf{u} + \mathbf{w}$

$\mathbf{y}_{\mathrm{k}} = \mathbf{C}\mathbf{x}_{\mathrm{k}} + \mathbf{v}$

Gain: $\mathbf{K}_{\mathrm{k}} = \mathbf{P}_{\mathrm{k}}{}^{-}\mathbf{C}^{\mathrm{T}}[\mathbf{C}\mathbf{P}_{\mathrm{k}}{}^{-}\mathbf{C}^{\mathrm{T}} + \mathbf{R}]^{-1}$

Update: $\hat{\mathbf{x}}_{\mathrm{k}}{}^{+} = \hat{\mathbf{x}}_{\mathrm{k}}{}^{-} + \mathbf{K}_{\mathrm{k}}[\mathbf{y}_{\mathrm{k}} - \mathbf{C}\hat{\mathbf{x}}_{\mathrm{k}}{}^{-}]$

$\mathbf{P}_{\mathrm{k}}{}^{+} = [\mathbf{I} - \mathbf{K}_{\mathrm{k}}\mathbf{C}]\mathbf{P}_{\mathrm{k}}{}^{-}$

Propagate: $\dot{\hat{\mathbf{x}}} = \mathbf{A}\hat{\mathbf{x}} + \mathbf{B}\mathbf{u}$

$\dot{\mathbf{P}} = \mathbf{P}\mathbf{A}^{\mathrm{T}} + \mathbf{A}\mathbf{P} + \mathbf{Q}$

Extended Kalman Filter

The extended Kalman filter (EKF) is a sequential estimation algorithm for nonlinear systems. Although not considered optimal, the EKF has been successfully applied to many nonlinear problems. The steps to implement the continuous-time EKF are as follows.

Initialize: $\mathbf{x}(\mathrm{t}_0) = \mathbf{x}_0, \hat{\mathbf{x}}(\mathrm{t}_0) = \hat{\mathbf{x}}_0, \mathbf{P}(\mathrm{t}_0) = \mathbf{P}_0$

Model: $\dot{\mathbf{x}} = \mathbf{f}(\mathbf{x}, \mathbf{u}, \mathrm{t}) + \mathbf{w}$

$\mathbf{y} = \mathbf{h}(\mathbf{x}) + \mathbf{v}$

Gain: $\mathbf{K} = \mathbf{P}\mathbf{H}^{\mathrm{T}}\mathbf{R}^{-1}, \mathbf{H} = \left.\frac{\partial \mathbf{h}}{\partial \mathbf{x}}\right|_{\hat{\mathbf{x}}}$

Covariance: $\dot{\mathbf{P}} = \mathbf{P}\mathbf{A}^{\mathrm{T}} + \mathbf{A}\mathbf{P} + \mathbf{Q} - \mathbf{P}\mathbf{H}^{\mathrm{T}}\mathbf{R}^{-1}\mathbf{H}\mathbf{P}, \mathbf{A} = \left.\frac{\partial \mathbf{f}}{\partial \mathbf{x}}\right|_{\hat{\mathbf{x}}}$

Estimate: $\dot{\hat{\mathbf{x}}} = \mathbf{f}(\hat{\mathbf{x}}, \mathbf{u}, \mathrm{t}) + \mathbf{K}[\mathbf{y} - \mathbf{h}(\hat{\mathbf{x}})]$

The steps to implement the continuous-discrete EKF are as follows.

Initialize: $\mathbf{x}(t_0) = \mathbf{x}_0, \hat{\mathbf{x}}(t_0) = \hat{\mathbf{x}}_0, \mathbf{P}(t_0) = \mathbf{P}_0$

Model: $\dot{\mathbf{x}} = \mathbf{f}(\mathbf{x}, \mathbf{u}, t) + \mathbf{w}$

$\mathbf{y}_k = \mathbf{h}(\mathbf{x}_k) + \mathbf{v}$

Gain: $\mathbf{K}_k = \mathbf{P}_k^{-}\mathbf{H}^T[\mathbf{H}\mathbf{P}_k^{-}\mathbf{H}^T + \mathbf{R}]^{-1}, \mathbf{H} = \left.\frac{\partial \mathbf{h}}{\partial \mathbf{x}}\right|_{\hat{\mathbf{x}}_k^{-}}$

Update: $\hat{\mathbf{x}}_k^{+} = \hat{\mathbf{x}}_k^{-} + \mathbf{K}_k[\mathbf{y}_k - \mathbf{h}(\hat{\mathbf{x}}_k^{-})]$

$\mathbf{P}_k^{+} = [\mathbf{I} - \mathbf{K}_k\mathbf{H}]\mathbf{P}_k^{-}$

Propagate: $\dot{\hat{\mathbf{x}}} = \mathbf{f}(\hat{\mathbf{x}}, \mathbf{u}, t)$

$\dot{\mathbf{P}} = \mathbf{P}\mathbf{A}^T + \mathbf{A}\mathbf{P} + \mathbf{Q}, \mathbf{A} = \left.\frac{\partial \mathbf{f}}{\partial \mathbf{x}}\right|_{\hat{\mathbf{x}}}$

CHAPTER 4

SPACECRAFT PURSUIT-EVASION GAMES

In a two-player spacecraft pursuit-evasion (PE) game, one spacecraft is the pursuer and the other is the evader. Typically, the objective of the pursuer is to intercept/rendezvous with the evader and the objective of the evader is to avoid or delay the interception/rendezvous. This problem of two competing players with opposite objectives can be formulated as a two-player zero-sum differential game. In this chapter, the LQ zero-sum differential game results from the previous Chapter are applied to derive control laws for an infinite-horizon LQ PE game. The results obtained from the application of the SDRE method to the nonlinear zero-sum differential game are used to derive control laws for an infinite-horizon nonlinear PE game.

In almost all of the previous research in spacecraft PE games, spacecraft dynamics are described in an Earth-centered reference frame. Using the calculus of variations approach, Woodward[24] and Bohn[25] derived near-optimal feedback control laws while Pontani and Conway[26] applied a direct numerical method for a saddle point solution. Menon and Calise used the feedback linearization method to obtain the solution of the spacecraft PE game defined by nonlinear dynamics and quadratic objective function.[27]

Kelly et al. used the EH reference frame and used the linear HCW equations to describe the dynamics of the spacecraft PE problem.[28] In Reference 28, however, the problem is not set up as a differential game and impulsive thrusts are used for control.

Recently, the EH reference frame has been used to describe the dynamics of the spacecraft PE game.[29] In Reference 29, the linear HCW equations are used to describe the dynamics and the objective function of both the players is the time to intercept. The pursuer tries to minimize the time to intercept while the evader tries to maximize it. The game terminates at the interception. Both spacecraft use constant-thrust engines and the control is provided by varying the thrust direction. The calculus of variations approach is used.

The novel contribution of this chapter is using the nonlinear spacecraft relative motion dynamics to derive the nonlinear PE control laws, the efficacy of which is found to be superior to that of the linear PE control laws. In this chapter, the EH reference frame is used to describe the game dynamics. Both the pursuer and the evader are deputies of the chief. The schematic of a PE game in the EH frame is depicted in Figure 4.1. Both spacecraft use continuous-thrust engines and the control is provided by varying the thrust magnitude and direction. However, the masses of both spacecraft are assumed to remain constant throughout the game time interval which is fixed a priori. A perfect information structure is assumed.

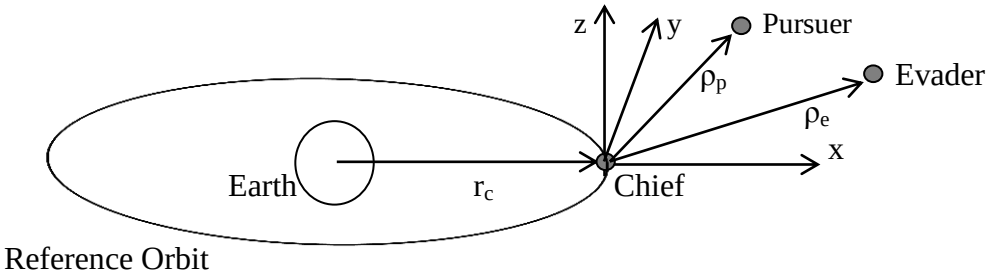

Figure 4.1: PE Game in the EH Frame

LINEAR QUADRATIC PURSUIT-EVASION GAME

An infinite-horizon LQ PE game is considered. The linear dynamics of the pursuer and the evader relative to the chief can be described by the LERM. The linear game dynamics is the difference between the pursuer dynamics and the evader dynamics.

The LERM of a deputy with respect to the chief along with control accelerations can be written as follows.

$$\ddot{x} = \left(\dot{\nu}^2 + 2\frac{\mu}{{r_c}^3}\right)x + \ddot{\nu}y + 2\dot{\nu}\dot{y} + u_x$$

$$\ddot{y} = -\ddot{\nu}x + \left(\dot{\nu}^2 - \frac{\mu}{{r_c}^3}\right)y - 2\dot{\nu}\dot{x} + u_y$$

$$\ddot{z} = -\frac{\mu}{{r_c}^3}z + u_z$$

If $\begin{bmatrix} u_x & u_y & u_z \end{bmatrix}^T$ is the control vector, then above equations can be written in the state space form as follows.

$$\begin{bmatrix} \dot{x} \\ \dot{y} \\ \dot{z} \\ \ddot{x} \\ \ddot{y} \\ \ddot{z} \end{bmatrix} = \begin{bmatrix} 0 & 0 & 0 & 1 & 0 & 0 \\ 0 & 0 & 0 & 0 & 1 & 0 \\ 0 & 0 & 0 & 0 & 0 & 1 \\ \dot{\nu}^2 + 2\frac{\mu}{{r_c}^3} & \ddot{\theta} & 0 & 0 & 2\dot{\nu} & 0 \\ -\ddot{\nu} & \dot{\nu}^2 - \frac{\mu}{{r_c}^3} & 0 & -2\dot{\nu} & 0 & 0 \\ 0 & 0 & -\frac{\mu}{{r_c}^3} & 0 & 0 & 0 \end{bmatrix} \begin{bmatrix} x \\ y \\ z \\ \dot{x} \\ \dot{y} \\ \dot{z} \end{bmatrix} + \begin{bmatrix} 0 & 0 & 0 \\ 0 & 0 & 0 \\ 0 & 0 & 0 \\ 1 & 0 & 0 \\ 0 & 1 & 0 \\ 0 & 0 & 1 \end{bmatrix} \begin{bmatrix} u_x \\ u_y \\ u_z \end{bmatrix}$$

$$\dot{\mathbf{x}} = \mathbf{A}_{\text{LERM}}(t)\mathbf{x}(t) + \mathbf{B}\mathbf{u}(t)$$

Thus, the pursuer and the evader dynamics can be written as follows.

$$\dot{\mathbf{x}}_p = \mathbf{A}_{\text{LERM}}(t)\mathbf{x}_p(t) + \mathbf{B}\mathbf{u}_p(t) \tag{4.1}$$

$$\dot{\mathbf{x}}_e = \mathbf{A}_{\text{LERM}}(t)\mathbf{x}_e(t) + \mathbf{B}\mathbf{u}_e(t) \tag{4.2}$$

Let the game state be $\mathbf{x} = \mathbf{x}_p - \mathbf{x}_e$. The game dynamics can then be written as follows.

$$\dot{\mathbf{x}} = \dot{\mathbf{x}}_{\mathrm{p}} - \dot{\mathbf{x}}_{\mathrm{e}} = \mathbf{A}_{\mathrm{LERM}}(\mathrm{t})\mathbf{x}_{\mathrm{p}}(\mathrm{t}) + \mathbf{B}\mathbf{u}_{\mathrm{p}}(\mathrm{t}) - \mathbf{A}_{\mathrm{LERM}}(\mathrm{t})\mathbf{x}_{\mathrm{e}}(\mathrm{t}) - \mathbf{B}\mathbf{u}_{\mathrm{e}}(\mathrm{t})$$

$$\dot{\mathbf{x}} = \mathbf{A}_{\mathrm{LERM}}(\mathrm{t})\mathbf{x}(\mathrm{t}) + \mathbf{B}_{\mathrm{p}}\mathbf{u}_{\mathrm{p}}(\mathrm{t}) + \mathbf{B}_{\mathrm{e}}\mathbf{u}_{\mathrm{e}}(\mathrm{t}) \tag{4.3}$$

$$\mathbf{B}_{\mathrm{p}} = \mathbf{B}, \mathbf{B}_{\mathrm{e}} = -\mathbf{B}$$

Each player tries to minimize a cost function which is a quadratic function of the game state and the controls of both players. The cost function of the pursuer is given as follows.

$$\mathrm{J}_{\mathrm{p}} = \frac{1}{2}\int_{\mathrm{t}_0}^{\infty} \left(\mathbf{x}^{\mathrm{T}}(\mathrm{t})\mathbf{Q}\mathbf{x}(\mathrm{t}) + \mathbf{u}_{\mathrm{p}}{}^{\mathrm{T}}(\mathrm{t})\mathbf{R}\mathbf{u}_{\mathrm{p}}(\mathrm{t}) - \gamma^2\mathbf{u}_{\mathrm{e}}{}^{\mathrm{T}}(\mathrm{t})\mathbf{R}\mathbf{u}_{\mathrm{e}}(\mathrm{t})\right)\mathrm{dt} \tag{4.4}$$

The cost function for the evader is opposite of that of the pursuer.

$$\mathrm{J}_{\mathrm{e}} = -\mathrm{J}_{\mathrm{p}} \tag{4.5}$$

The optimal control laws are given as follows.

$$\mathbf{u}_{\mathrm{p}}{}^{*} = -\mathbf{R}^{-1}\mathbf{B}_{\mathrm{p}}{}^{\mathrm{T}}\mathbf{P}\mathbf{x}$$

$$\mathbf{u}_{\mathrm{e}}{}^{*} = \frac{1}{\gamma^2}\mathbf{R}^{-1}\mathbf{B}_{\mathrm{e}}{}^{\mathrm{T}}\mathbf{P}\mathbf{x} \tag{4.6}$$

Instead of solving for the periodic solution of **P**, the symmetric matrix **P** is obtained by solving the following game ARE at each time step.

$$\mathbf{P}\mathbf{A}_{\mathrm{LERM}} + \mathbf{A}_{\mathrm{LERM}}{}^{\mathrm{T}}\mathbf{P} - \mathbf{P}\mathbf{B}_{\mathrm{p}}\mathbf{R}^{-1}\mathbf{B}_{\mathrm{p}}{}^{\mathrm{T}}\mathbf{P} + \frac{1}{\gamma^2}\mathbf{P}\mathbf{B}_{\mathrm{e}}\mathbf{R}^{-1}\mathbf{B}_{\mathrm{e}}{}^{\mathrm{T}}\mathbf{P} + \mathbf{Q} = \mathbf{0} \tag{4.7}$$

This approach solves for a sub-optimal control in elliptic reference orbits. The ARE can have a conjugate point on the game time interval, where its solution does not exist (tends to infinity). The necessary condition for not having a conjugate point is that the matrix **P** be positive semi-definite throughout the game time interval.[30] Generally, a sufficiently large value of $\gamma > 0$ ensures that the ARE does not have a conjugate point.[31] In this chapter, the value of γ is $\sqrt{2}$. Appropriate values of γ depend on the game time interval and one may have to decide on a certain value by trial and error.

NONLINEAR PURSUIT-EVASION GAME

An infinite-horizon nonlinear PE game is considered. The nonlinear dynamics of the pursuer and the evader relative to the chief can be described by the NERM. The NERM of a deputy with respect to the chief along with control accelerations in a control-affine form can be written as follows.

$$\ddot{x} = \dot{\nu}^2 x + \ddot{\nu} y + 2\dot{\nu}\dot{y} + \frac{\mu}{{r_c}^2} - \frac{\mu}{{r_d}^3}(r_c + x) + u_x$$

$$\ddot{y} = -\ddot{\nu} x + \dot{\nu}^2 y - 2\dot{\nu}\dot{x} - \frac{\mu}{{r_d}^3} y + u_y$$

$$\ddot{z} = -\frac{\mu}{{r_d}^3} z + u_z$$

$$\dot{\mathbf{x}} = \mathbf{f}(\mathbf{x}) + \mathbf{B}\mathbf{u}(t) \tag{4.8}$$

The pursuer and the evader dynamics can be written as follows.

$$\dot{\mathbf{x}}_p = \mathbf{f}(\mathbf{x}_p) + \mathbf{B}\mathbf{u}_p(t) \tag{4.9}$$

$$\dot{\mathbf{x}}_e = \mathbf{f}(\mathbf{x}_e) + \mathbf{B}\mathbf{u}_e(t) \tag{4.10}$$

The nonlinear game dynamics is the difference between the pursuer dynamics and the evader dynamics.

$$\dot{\mathbf{x}} = \mathbf{f}(\mathbf{x}_p) - \mathbf{f}(\mathbf{x}_e) + \mathbf{B}_p\mathbf{u}_p(t) + \mathbf{B}_e\mathbf{u}_e(t)$$

$$\ddot{x} = \dot{\nu}^2 x + \ddot{\nu} y + 2\dot{\nu}\dot{y} + \left(-\frac{\mu(r_c + x_p)}{{r_p}^3} + \frac{\mu(r_c + x_e)}{{r_e}^3}\right) + u_{xp} - u_{xe}$$

$$\ddot{y} = -\ddot{\nu} x + \dot{\nu}^2 y - 2\dot{\nu}\dot{x} + \left(-\frac{\mu y_p}{{r_p}^3} + \frac{\mu y_e}{{r_e}^3}\right) + u_{yp} - u_{ye} \tag{4.11}$$

$$\ddot{z} = \left(-\frac{\mu z_p}{{r_p}^3} + \frac{\mu z_e}{{r_e}^3}\right) + u_{zp} - u_{ze}$$

The terms in parenthesis on the RHS of Equation (4.11), unlike the rest of the terms, are functions of the states of the pursuer and the evader individually and not the game state.

These terms prevent a direct factorization of the nonlinear game dynamics into $\mathbf{A}(\mathbf{x})\mathbf{x}$. To enable this factorization the terms in parenthesis are multiplied and divided by the magnitude squared of the difference between the position vector of the pursuer and the evader which is $\mathbf{r} = [x_p - x_e \quad y_p - y_e \quad z_p - z_e]^T$. Denoting the terms in parenthesis Equations (4.11) by b_x, b_y, and b_z respectively the game dynamics can be written as follows.

$$\begin{aligned}
\ddot{x} &= \dot{\nu}^2 x + \ddot{\nu} y + 2\dot{\nu}\dot{y} + (b_x)\frac{\mathbf{r}^T\mathbf{r}}{\mathbf{r}^T\mathbf{r}} + u_{xp} - u_{xe} \\
\ddot{y} &= -\ddot{\nu} x + \dot{\nu}^2 y - 2\dot{\nu}\dot{x} + (b_y)\frac{\mathbf{r}^T\mathbf{r}}{\mathbf{r}^T\mathbf{r}} + u_{yp} - u_{ye} \\
\ddot{z} &= (b_z)\frac{\mathbf{r}^T\mathbf{r}}{\mathbf{r}^T\mathbf{r}} + u_{zp} - u_{ze}
\end{aligned} \tag{4.12}$$

Above equations can be expanded as follows.

$$\begin{aligned}
\ddot{x} &= \dot{\nu}^2 x + \ddot{\nu} y + 2\dot{\nu}\dot{y} + \left(\frac{b_x x}{r^2}\right)x + \left(\frac{b_x y}{r^2}\right)y + \left(\frac{b_x z}{r^2}\right)z + u_{xp} - u_{xe} \\
\ddot{y} &= -\ddot{\nu} x + \dot{\nu}^2 y - 2\dot{\nu}\dot{x} + \left(\frac{b_y x}{r^2}\right)x + \left(\frac{b_y y}{r^2}\right)y + \left(\frac{b_y z}{r^2}\right)z + u_{yp} - u_{ye} \\
\ddot{z} &= \left(\frac{b_z x}{r^2}\right)x + \left(\frac{b_z y}{r}\right)y + \left(\frac{b_z z}{r^2}\right)z + u_{zp} - u_{ze}
\end{aligned} \tag{4.13}$$

Finally the nonlinear game dynamics can be written in the state space form as follows.

$$\begin{bmatrix} \dot{x} \\ \dot{y} \\ \dot{z} \\ \ddot{x} \\ \ddot{y} \\ \ddot{z} \end{bmatrix} = \begin{bmatrix} 0 & 0 & 0 & 1 & 0 & 0 \\ 0 & 0 & 0 & 0 & 1 & 0 \\ 0 & 0 & 0 & 0 & 0 & 1 \\ \dot{\nu}^2 + \frac{b_x x}{r^2} & \ddot{\nu} + \frac{b_x y}{r^2} & \frac{b_x z}{r^2} & 0 & 2\dot{\nu} & 0 \\ -\ddot{\nu} + \frac{b_y x}{r^2} & \dot{\nu}^2 + \frac{b_y y}{r^2} & \frac{b_y z}{r^2} & -2\dot{\nu} & 0 & 0 \\ \frac{b_z x}{r^2} & \frac{b_z y}{r^2} & \frac{b_z z}{r^2} & 0 & 0 & 0 \end{bmatrix} \begin{bmatrix} x \\ y \\ z \\ \dot{x} \\ \dot{y} \\ \dot{z} \end{bmatrix} + \mathbf{B}_p\mathbf{u}_p + \mathbf{B}_e\mathbf{u}_p \tag{4.14}$$

$$\dot{\mathbf{x}} = \mathbf{A}_{\mathrm{SDC}}(\mathbf{x})\mathbf{x} + \mathbf{B}_{\mathrm{p}}\mathbf{u}_{\mathrm{p}} + \mathbf{B}_{\mathrm{e}}\mathbf{u}_{\mathrm{p}}$$

Thus, the SDRE method entails factorization or parameterization of the nonlinear dynamics into the product of the state vector and a matrix-valued function which depends on the state. In so doing, the nonlinearities of the system are fully captured and the nonlinear system has a non-unique linear-like structure consisting of SDC matrices. The pursuer and the evader minimize the following cost functions respectively.

$$\mathrm{J_p} = \frac{1}{2}\int_{\mathrm{t_o}}^{\infty} \left(\mathbf{x}^{\mathrm{T}}(\mathrm{t})\mathbf{Q}\mathbf{x}(\mathrm{t}) + \mathbf{u_p}^{\mathrm{T}}(\mathrm{t})\mathbf{R}\mathbf{u}_{\mathrm{p}}(\mathrm{t}) - \gamma^2\mathbf{u_e}^{\mathrm{T}}(\mathrm{t})\mathbf{R}\mathbf{u}_{\mathrm{e}}(\mathrm{t})\right)\mathrm{dt} \tag{4.15}$$

$$\mathrm{J_e} = -\mathrm{J_p}$$

The nonlinear sub-optimal control laws are given as follows.

$$\begin{aligned} \mathbf{u}_{\mathrm{p}}(\mathbf{x}) &= -\mathbf{R}^{-1}\mathbf{B_p}^{\mathrm{T}}\mathbf{P}(\mathbf{x})\mathbf{x} \\ \mathbf{u}_{\mathrm{e}}(\mathbf{x}) &= \frac{1}{\gamma^2}\mathbf{R}^{-1}\mathbf{B_e}^{\mathrm{T}}\mathbf{P}(\mathbf{x})\mathbf{x} \end{aligned} \tag{4.16}$$

The symmetric matrix $\mathbf{P}(\mathbf{x})$ is obtained by solving the following ARE at each point in state space.

$$\begin{aligned} \mathbf{P}(\mathbf{x})\mathbf{A}_{\mathrm{SDC}}(\mathbf{x}) + \mathbf{A_{SDC}}^{\mathrm{T}}(\mathbf{x})\mathbf{P}(\mathbf{x}) - \mathbf{P}(\mathbf{x})\left(\mathbf{B_p}\mathbf{R}^{-1}\mathbf{B_p}^{\mathrm{T}} - \frac{1}{\gamma^2}\mathbf{B_e}\mathbf{R}^{-1}\mathbf{B_e}^{\mathrm{T}}\right)\mathbf{P}(\mathbf{x}) + \mathbf{Q} \\ = \mathbf{0} \end{aligned} \tag{4.17}$$

The coefficients of this ARE vary with the given point in state space. The SDRE method thus involves solving, at a given point in state space, an algebraic SDRE whose point wise stabilizing solution during state evolution yields nonlinear control laws.

NUMERICAL EXAMPLES

MATLAB$^{\mathrm{TM}}$ simulations are performed to test and compare the performance of the linear and nonlinear control laws. Parameters used in the simulations are given in Table 4.1.

Parameter	Value
a_c (km)	15000
e_c	0.5
$\mathbf{Q}$	$\mathbf{I}_{6\times6}$
γ^2	2
$\mathbf{x}_p(0)$	$[500\ 500\ 500\ 0.01\ 0.01\ 0.01]^T$
$\mathbf{x}_e(0)$	$[0\ 0\ 0\ 0\ 0\ 0]^T$
Test Case 1	
t_f (sec)	2000
$\mathbf{R}_1$	$\mathbf{I}_{3\times3} \times 10^9$
Test Case 2	
t_f (sec)	36560 (two periods of the chief orbit)
$\mathbf{R}_2$	$\mathbf{I}_{3\times3} \times 10^{13}$

Table 4.1: Game Simulation Parameters

Dynamics are propagated forward in time using the fourth-order Runge-Kutta (RK4) numerical integration method. A time step of 20 seconds is used. Two test cases are considered. In test case 1, the duration of the game is short and high control usage is permitted by placing low weighting on the controls. In test case 2, the duration of the game is long and high control usage is prohibited by placing high weighting on control.

Linear Quadratic Pursuit-Evasion Game

The LERM system matrix $\mathbf{A}_{\mathrm{LERM}}(t)$ is calculated at every RK4 step (every 5 seconds), and then the ARE given by Equation (4.7) is solved. The linear control laws are given by Equation (4.6). Thus, in the LQ PE game, the control laws are derived using linear game dynamics and are implemented using the LERM of the pursuer and the evader.

Test Case 1

For test case 1, plots of the position vector components of the pursuer and the evader state are shown in Figure 4.2. It can be seen that as the game goes on, the pursuer converges on the position of the evader. Plots comparing the control vector components

of the pursuer and the evader are shown in Figure 4.3. It can be seen that the pursuer applies a greater control effort than the evader. A 3-D plot of the position vector components of the pursuer and the evader state is shown in Figure 4.4. A 3-D plot of the position vector components of the game state is shown in Figure 4.5.

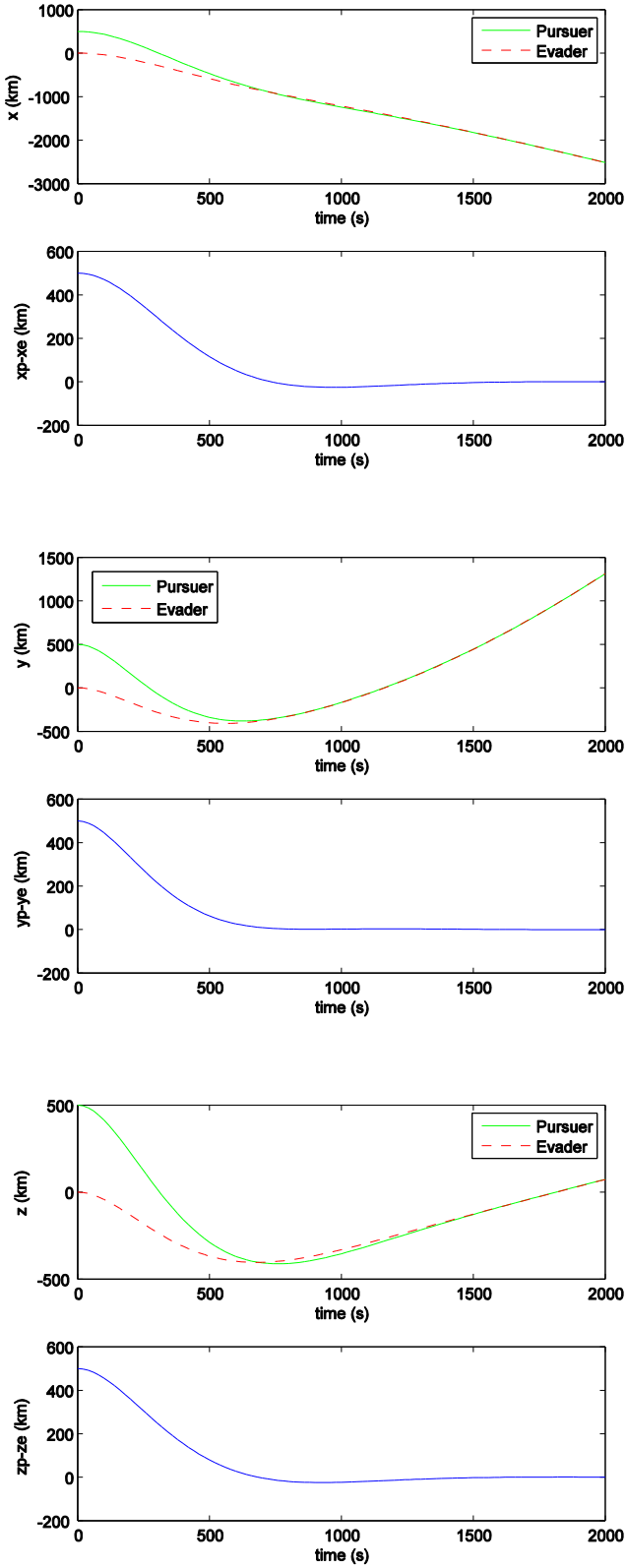

Figure 4.2: Test Case 1: LQ PE Game Position Vector Components

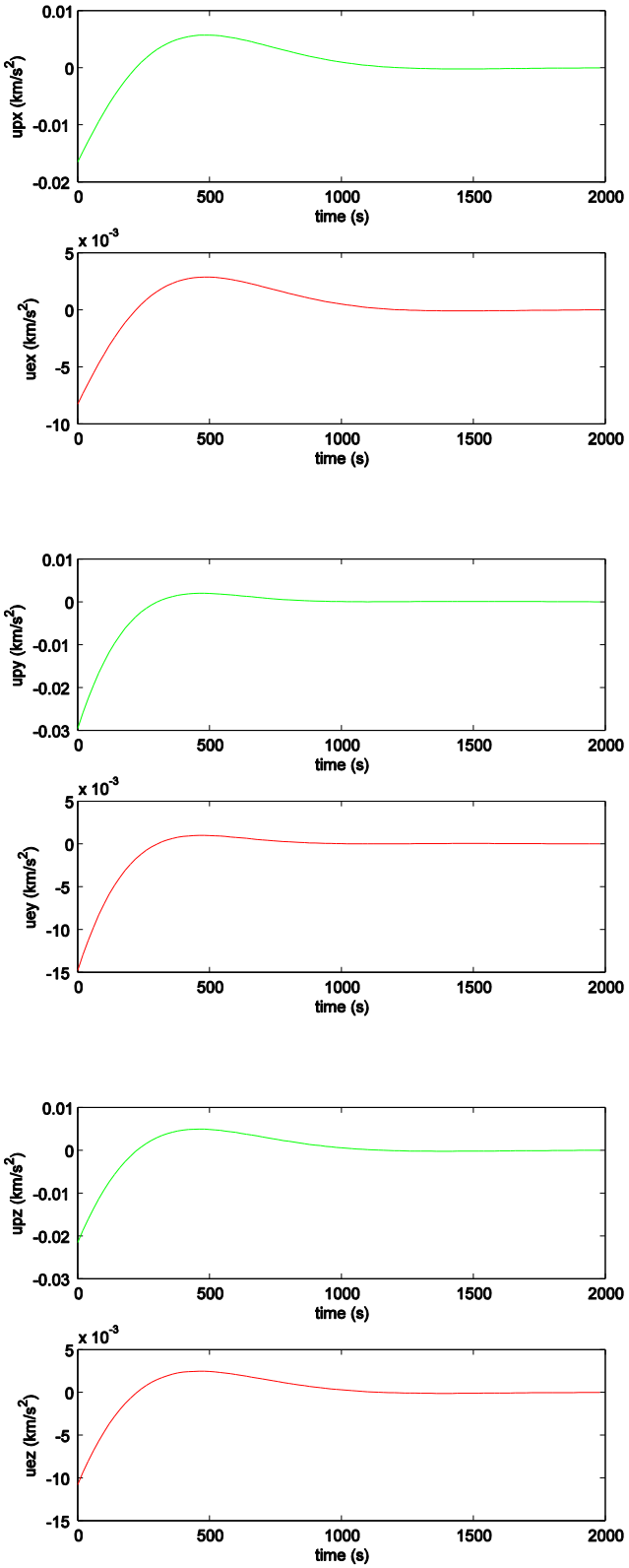

Figure 4.3: Test Case 1: LQ PE Game Control Vector Components

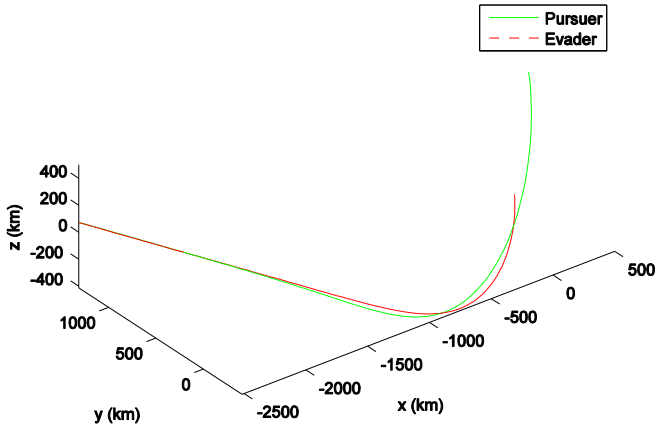

Figure 4.4: Test Case 1: LQ PE Game Pursuer and Evader State in 3-D

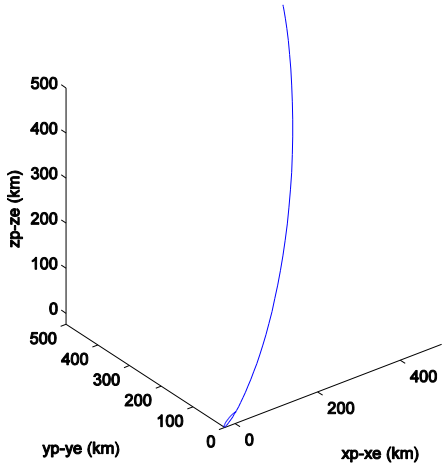

Figure 4.5: Test Case 1: LQ PE Game State in 3-D

Test Case 2

Similar plots for test case 2 are shown in Figures 4.6, 4.7, 4.8, and 4.9. It can be seen that as the game goes on, the pursuer converges on the position of the evader. Also, the pursuer needs a greater control effort than the evader. In this case, because of low control usage, the orbital dynamics plays a greater role and it can be seen from Figure 4.9 that the game state trajectory follows a more curved path.

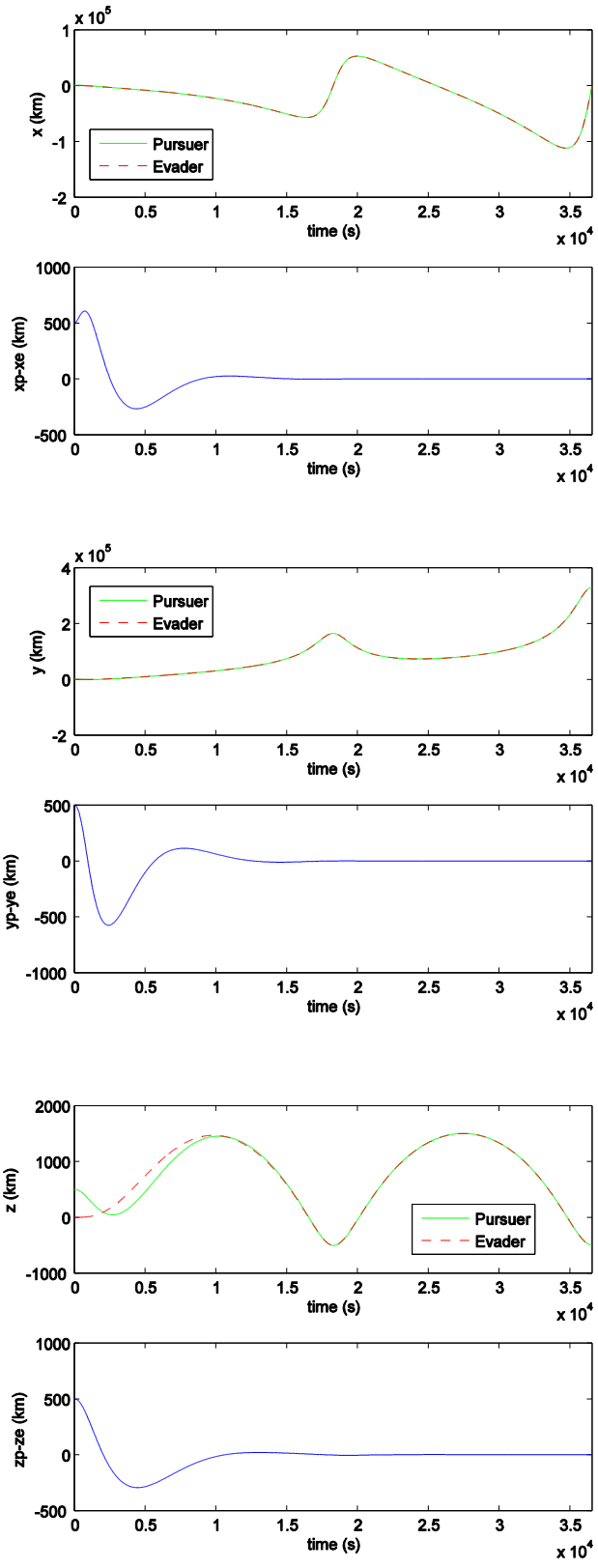

Figure 4.6: Test Case 2: LQ PE Game Position Vector Components

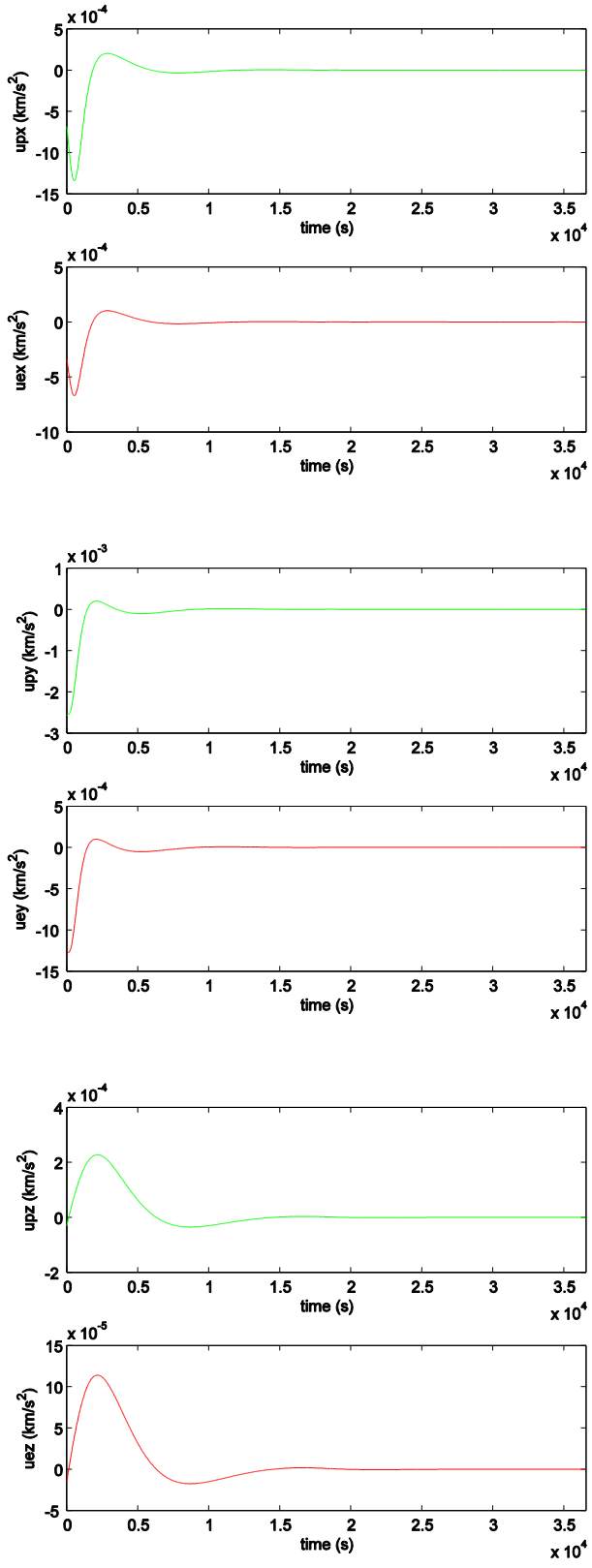

Figure 4.7: Test Case 2: LQ PE Game Control Vector Components

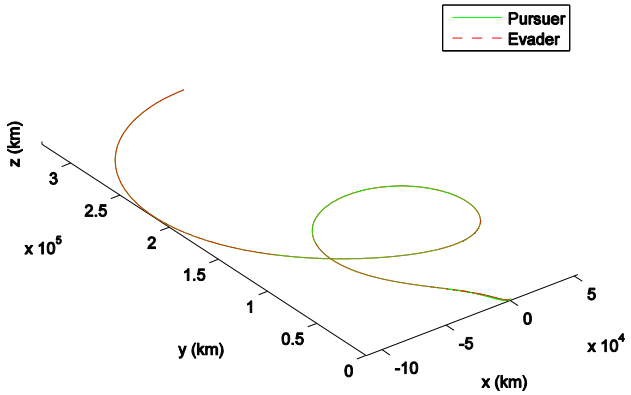

Figure 4.8: Test Case 2: LQ PE Game Pursuer and Evader State in 3-D

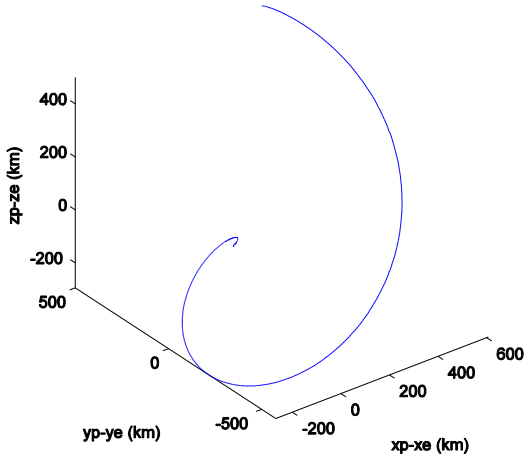

Figure 4.9: Test Case 2: LQ PE Game State in 3-D

Nonlinear Pursuit-Evasion Game

The nonlinear game dynamics is propagated forward in time using the fourth RK4 method. A time step of 20 seconds is used. The SDC matrix $\mathbf{A}_{\mathrm{SDC}}(\mathbf{x})$ is calculated at every RK4 step, and then the SDRE given by Equation (4.17) is solved. The nonlinear control laws are given by Equation (4.16). Thus, in the nonlinear PE game, the control laws are derived using SDC matrix and are implemented using the NERM of the pursuer and the evader.

Test Case 1

For test case 1, plots of the position vector components of the pursuer and the evader state are shown in Figure 4.10. It can be seen that as the game goes on, the pursuer converges on the position of the evader. Plots comparing the control vector components of the pursuer and the evader are shown in Figure 4.11. It can be seen that the pursuer applies a greater control effort than the evader. A 3-D plot of the position vector components of the pursuer and the evader state is shown in Figure 4.12. A 3-D plot of the position vector components of the game state is shown in Figure 4.13.

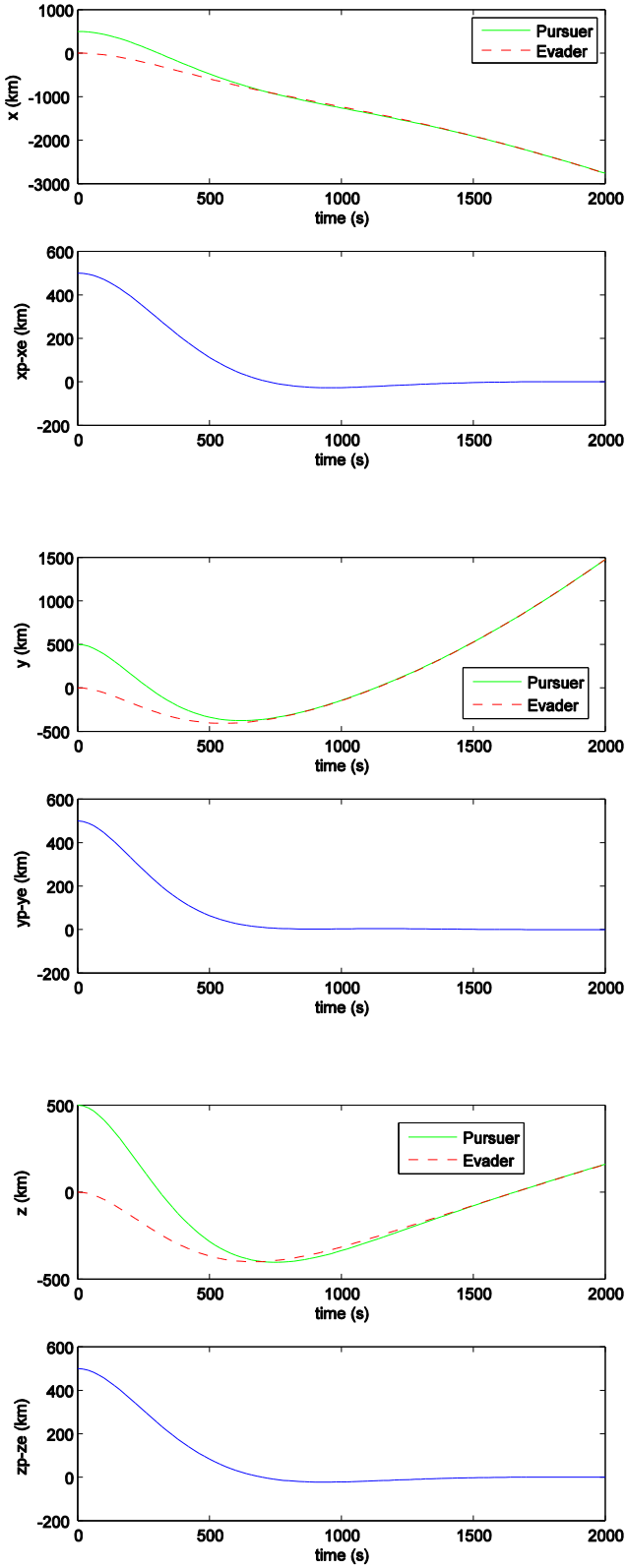

Figure 4.10: Test Case 1: Nonlinear PE Game Position Vector Components

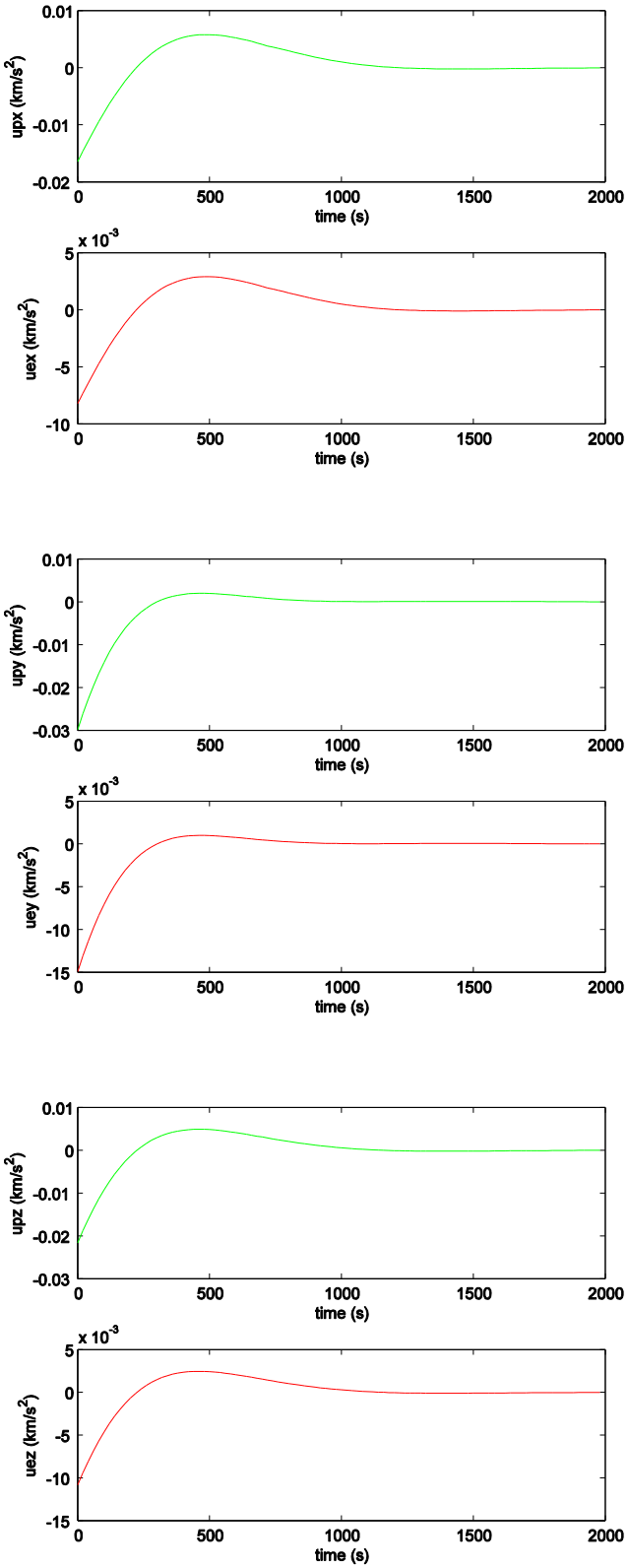

Figure 4.11: Test Case 1: Nonlinear PE Game Control Vector Components

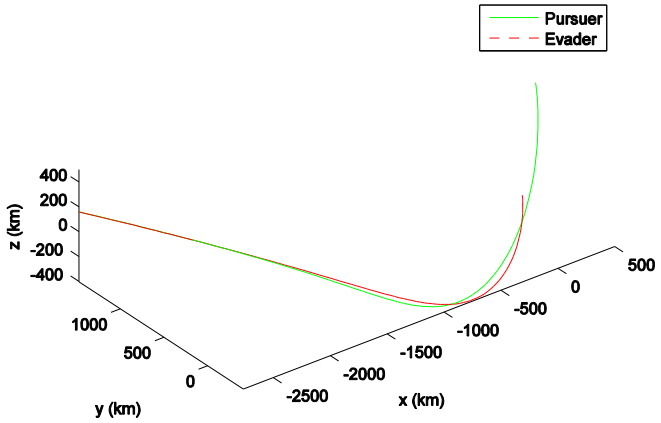

Figure 4.12: Test Case 1: Nonlinear PE Game Pursuer and Evader State in 3-D

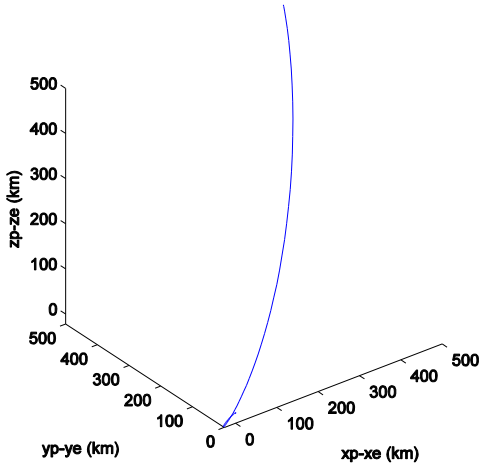

Figure 4.13: Test Case 1: Nonlinear PE Game State in 3-D

Test Case 2

Similar plots for test case 2 are shown in Figures 4.14, 4.15, 4.16, and 4.17. It can be seen that as the game goes on, the pursuer converges on the position of the evader. Also, the pursuer needs a greater control effort than the evader. Since the orbital dynamics plays a greater role, it can be seen from Figure 4.17 that the game state trajectory follows a spiral path.

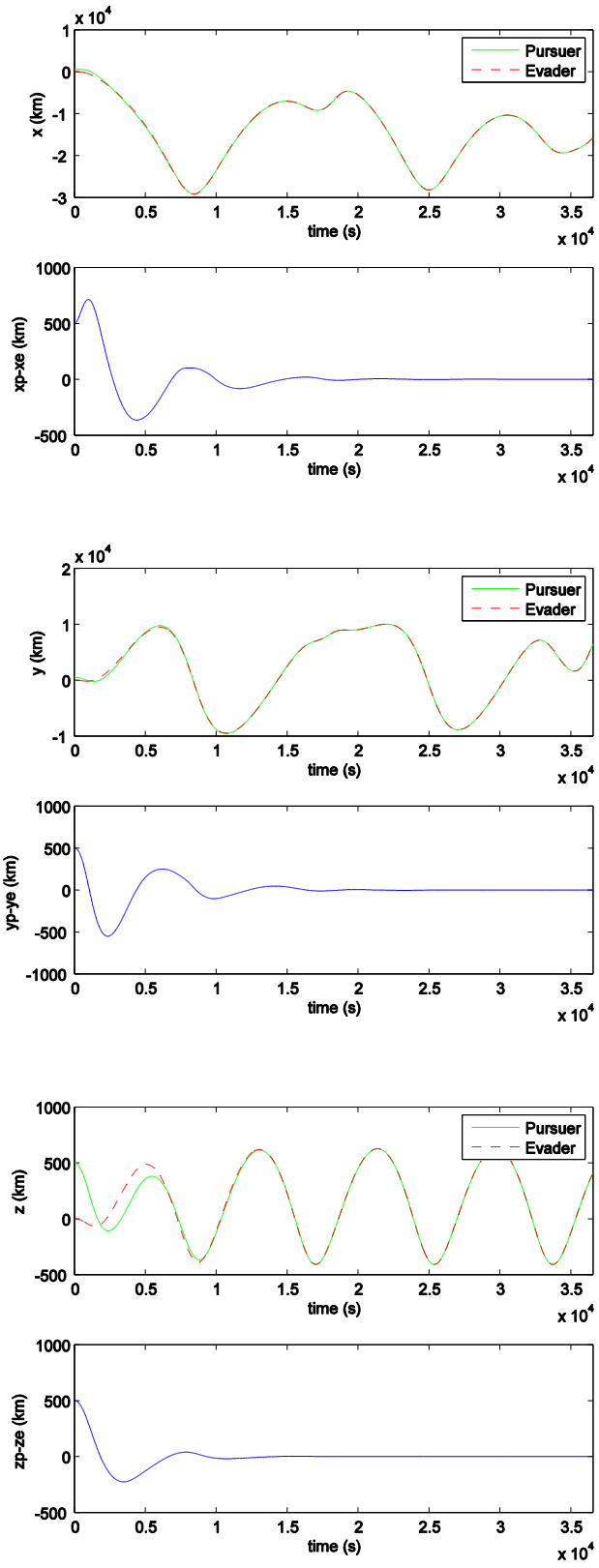

Figure 4.14: Test Case 2: Nonlinear PE Game Position Vector Components

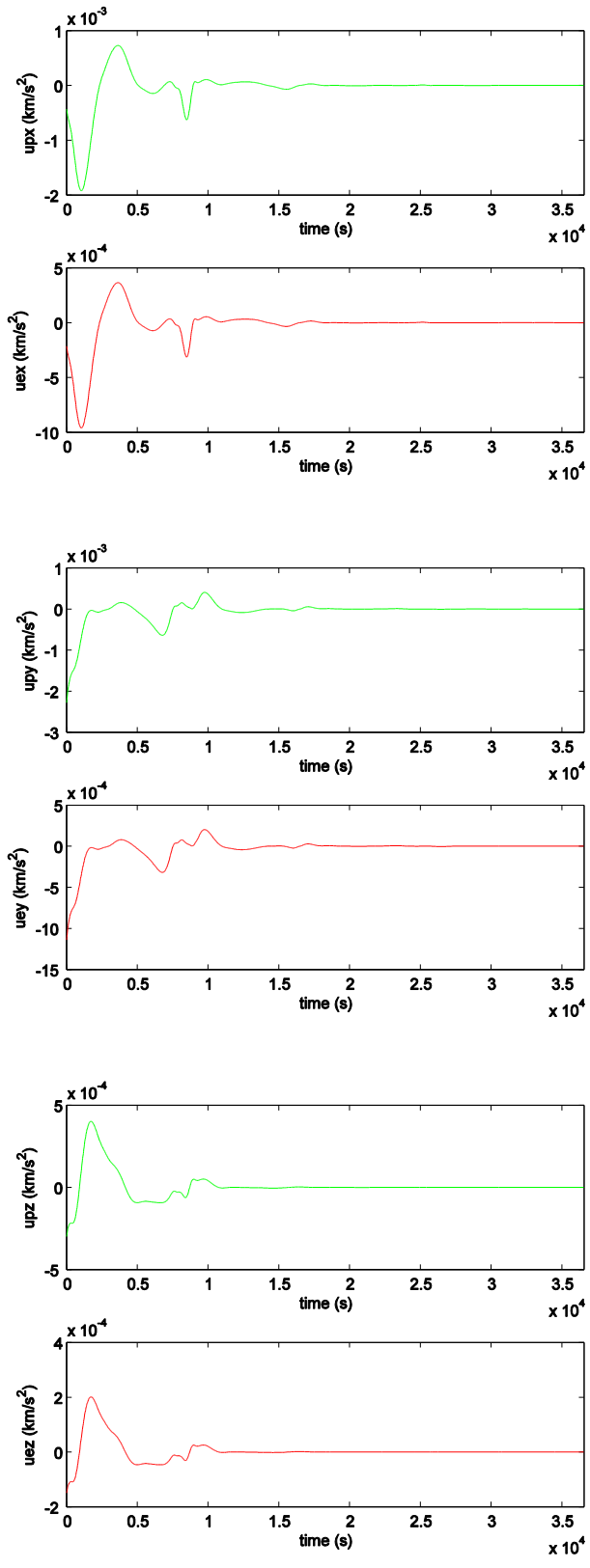

Figure 4.15: Test Case 2: Nonlinear PE Game Control Vector Components

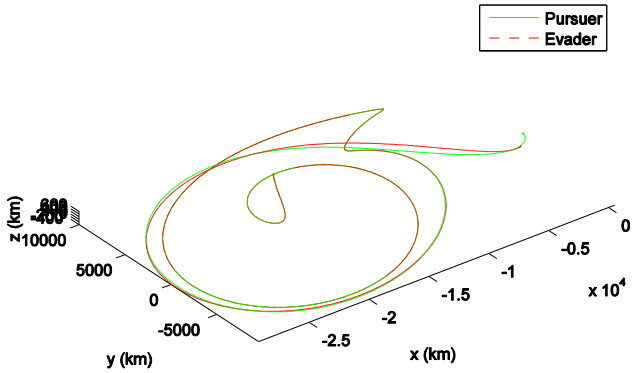

Figure 4.16: Test Case 2: Nonlinear PE Game Pursuer and Evader State in 3-D

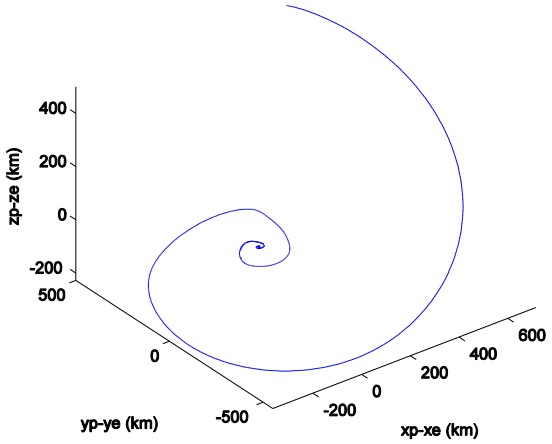

Figure 4.17: Test Case 2: Nonlinear PE Game State in 3-D

Comparison of the Linear and Nonlinear Control Laws

It has been demonstrated that the linear control laws perform well when the dynamics are linear and the nonlinear control laws perform well when the dynamics are nonlinear. A test for the efficacy of the linear control laws could be to see how they perform when the dynamics are nonlinear. Three scenarios are considered for comparison. In all the three scenarios, the dynamics are nonlinear. Therefore, each player

implements the control law using its NERM. In scenario 1, both the pursuer and the evader implement the linear control laws. In scenario 2, the pursuer implements the nonlinear control law whereas the evader implements the linear control law. In scenario 3, the pursuer implements the linear control law whereas the evader implements the nonlinear control law.

Test Case 1

Performances in scenario 1 and scenario 2 are compared first. The performance of the pursuer should be better in scenario 2 as the pursuer is using the better controller. Plots of the position vector components of the game state are shown below in Figure 4.18. The nonlinear controller distinguishes itself from the linear one in the beginning of the game when the separation is larger. It can be seen that in the beginning of the game, the separations in scenario 2 are smaller than those in scenario 1 indicating the fact that the pursuer is being more effective in achieving its objective. Figure 4.19 shows the cost accumulated by the pursuer over time. It is interesting to note that in the beginning of the game the cost accumulated in scenario 2 is higher than that accumulated in scenario 1 and as the game goes on the cost accumulated in scenario 2 becomes lower than that accumulated in scenario 1. Therefore, to achieve superior efficacy as compared to the linear controller, the nonlinear controller initially accepts a higher cumulative cost.

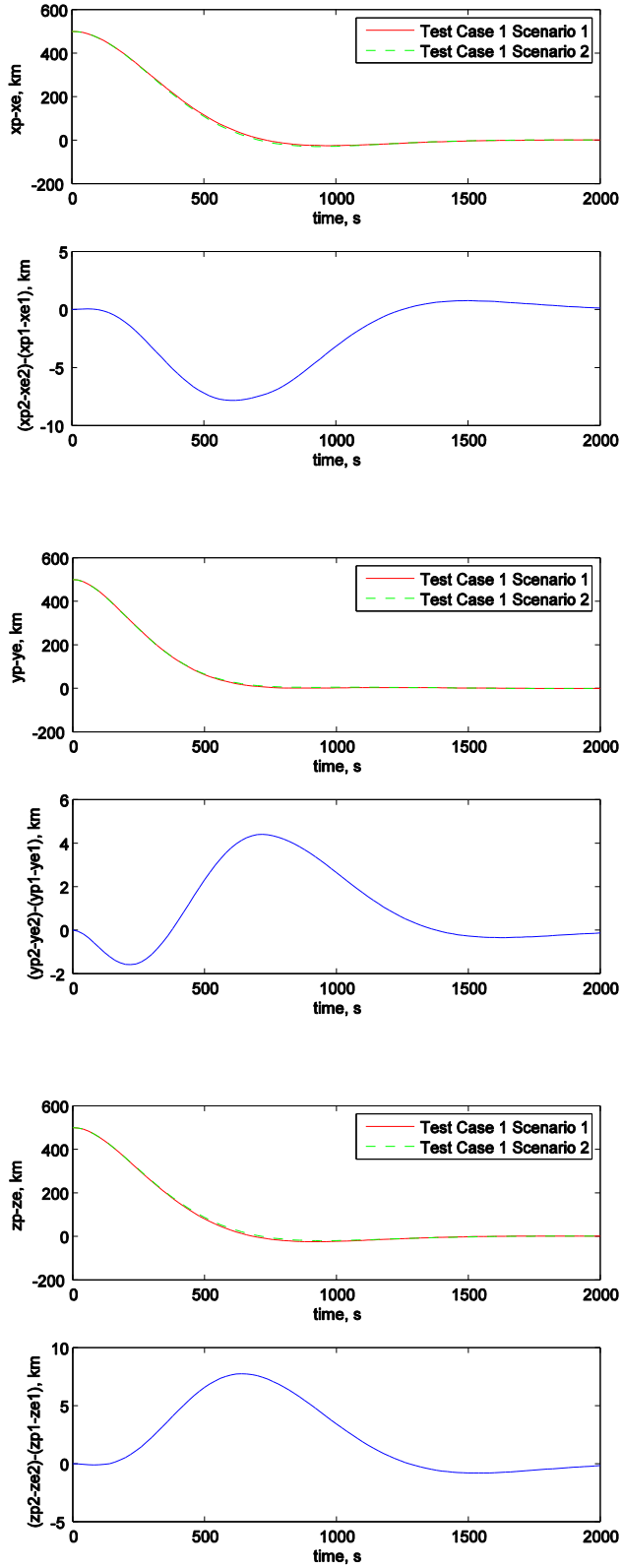

Figure 4.18: Test Case 1: Game State Comparison for Scenario 1 and 2

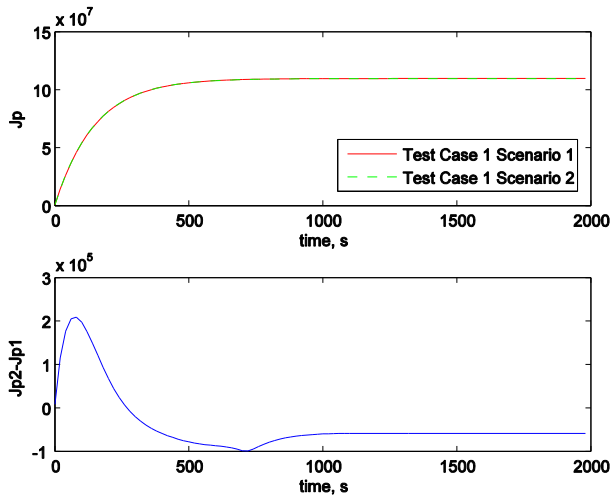

Figure 4.19: Test Case 1: Pursuer Cost Comparison for Scenario 1 and 2

Next, performances in scenario 1 and scenario 3 are compared. The performance of the evader should be better in scenario 3 as the evader is using the better controller. Plots of the position vector components of the game state are shown below in Figure 4.20. The same phenomenon of the nonlinear controller distinguishing itself from the linear one in the beginning of the game when the separation is larger is observed here. It can be seen that in the beginning of the game the separations in scenario 3 are greater than those in scenario 1 indicating the fact that the evader is being more effective in achieving its objective. Figure 4.21 shows the cost accumulated by the evader over time. As in the earlier case, in the beginning of the game the cost accumulated in scenario 3 is higher than that accumulated in scenario 1 and as the game goes on the cost accumulated in scenario 3 becomes lower than that accumulated in scenario 1. Therefore, to achieve superior efficacy as compared to the linear controller, the nonlinear controller initially accepts a higher cumulative cost.

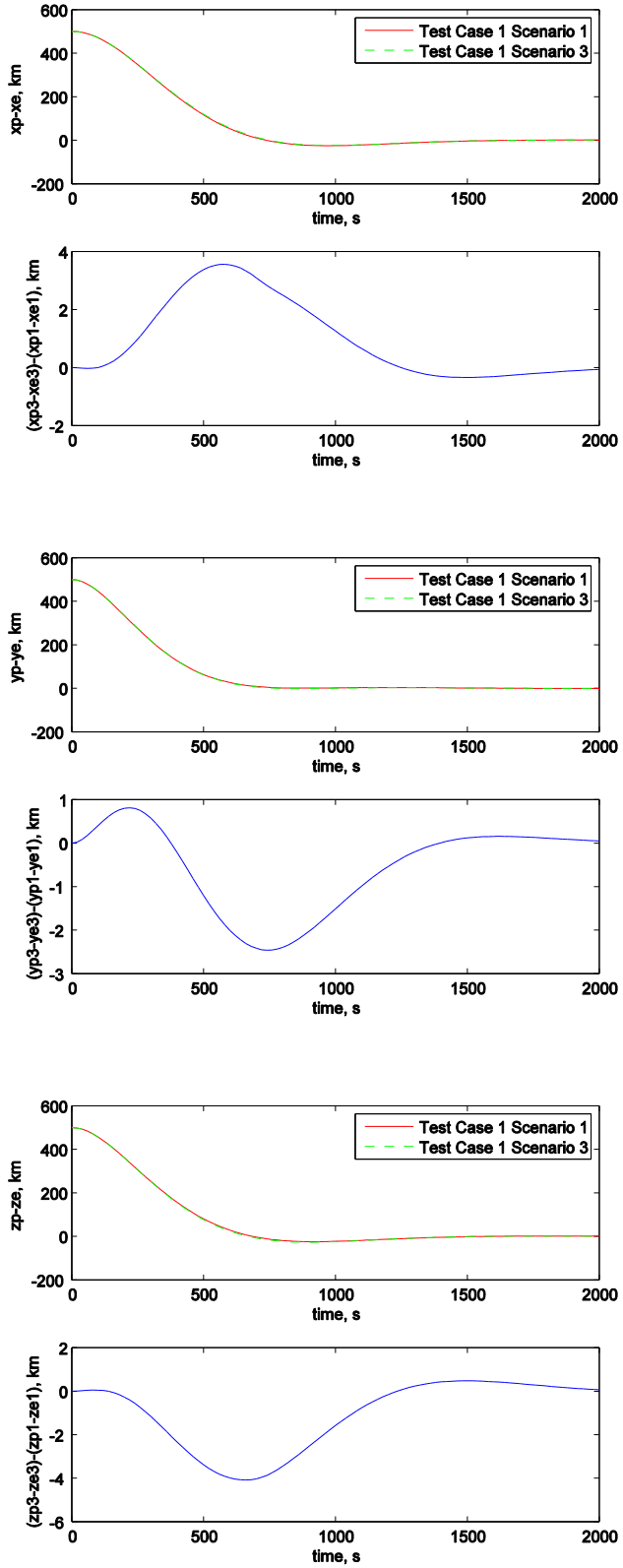

Figure 4.20: Test Case 1: Game State Comparison for Scenario 1 and 3

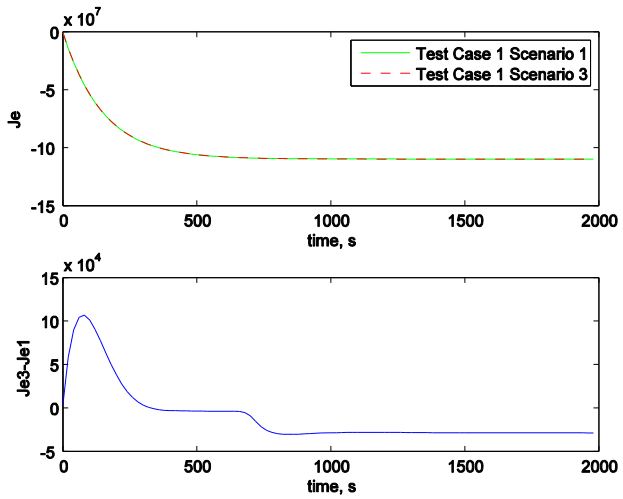

Figure 4.21: Test Case 1: Evader Cost Comparison for Scenario 1 and 3

Test Case 2

Performances in scenario 1 and scenario 2 are compared first. The performance of the pursuer should be better in scenario 2 as the pursuer is using the better controller. Plots of the position vector components of the game state are shown below in Figure 4.22. In this case, the nonlinear controller distinguishes itself from the linear one. Almost throughout the game, the separations in scenario 2 are smaller than those in scenario 1 indicating the fact that the pursuer is being more effective in achieving its objective. Although at the end of the game the game state trajectory in scenario 1 goes to the origin indicating that the pursuer has been able to converge on the position of the evader, the game state trajectory in scenario 2 has settled quicker than in scenario 1. Figure 4.23 shows the cost accumulated by the pursuer over time. In the earlier part of the game, the cost accumulated in scenario 2 is higher than that accumulated in scenario 1 and as the game goes on the cost accumulated in scenario 2 becomes lower than that accumulated in scenario 1. Therefore, to achieve superior efficacy as compared to the linear controller, the nonlinear controller initially accepts a higher cumulative cost.

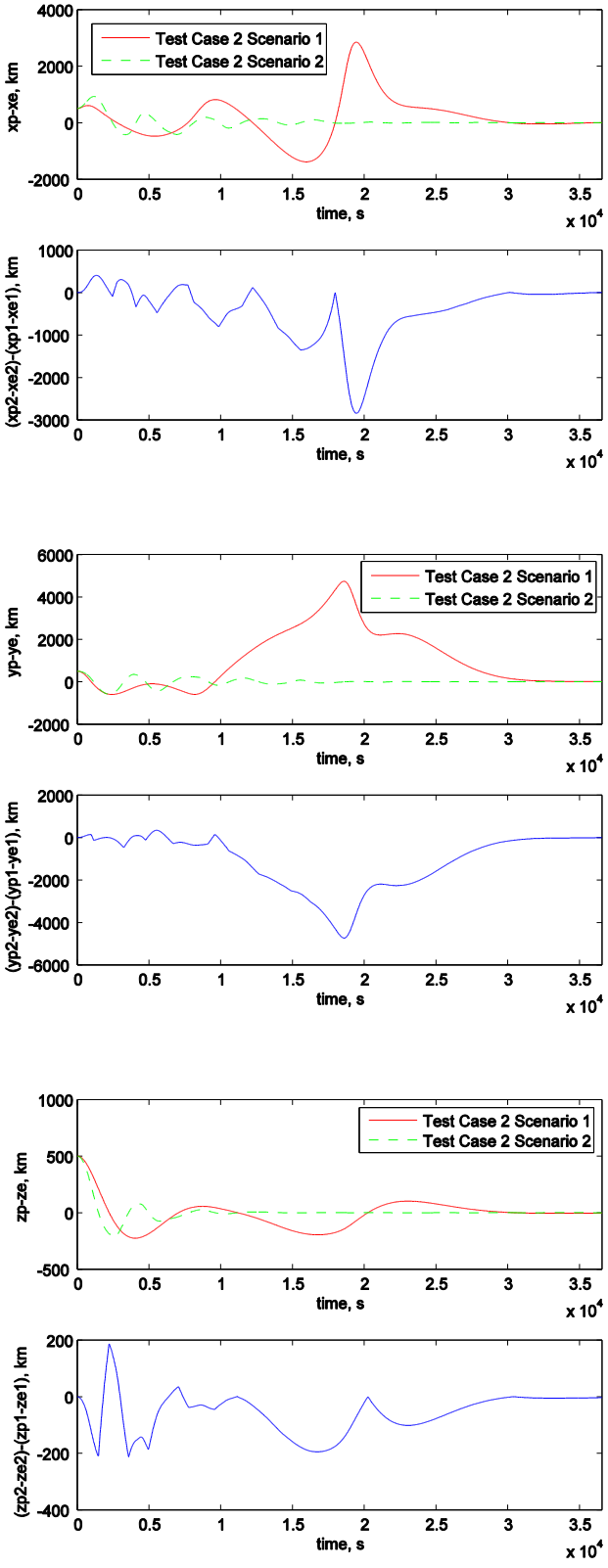

Figure 4.22: Test Case 2: Game State Comparison for Scenario 1 and 2

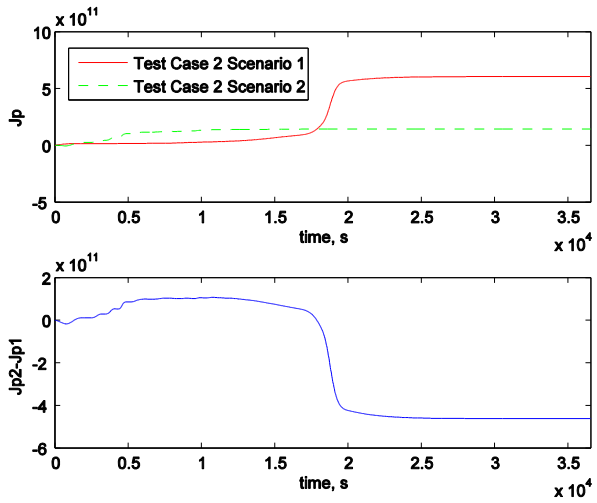

Figure 4.23: Test Case 2: Pursuer Cost Comparison for Scenario 1 and 2

Next, performances in scenario 1 and scenario 3 are compared. The performance of the evader should be better in scenario 3 as the evader is using the better controller. Plots of the position vector components of the game state are shown below in Figure 4.24. The same phenomenon of the nonlinear controller distinguishing itself from the linear one almost throughout the game is observed here. Almost throughout the game, the separations in scenario 3 are greater than those in scenario 1 indicating the fact that the evader is being more effective in achieving its objective. Although at the end of the game the game state trajectory in scenario 3 goes to the origin indicating that the pursuer has been able to converge on the position of the evader, the game state trajectory in scenario 3 takes longer to settle than in scenario 1. Figure 4.25 shows the cost accumulated by the evader over time. In the earlier part of the game the cost accumulated in scenario 3 is higher than that accumulated in scenario 1 and as the game goes on the cost accumulated in scenario 3 becomes lower than that accumulated in scenario 1. Therefore, to achieve superior efficacy as compared to the linear controller, the nonlinear controller initially accepts a higher cumulative cost.

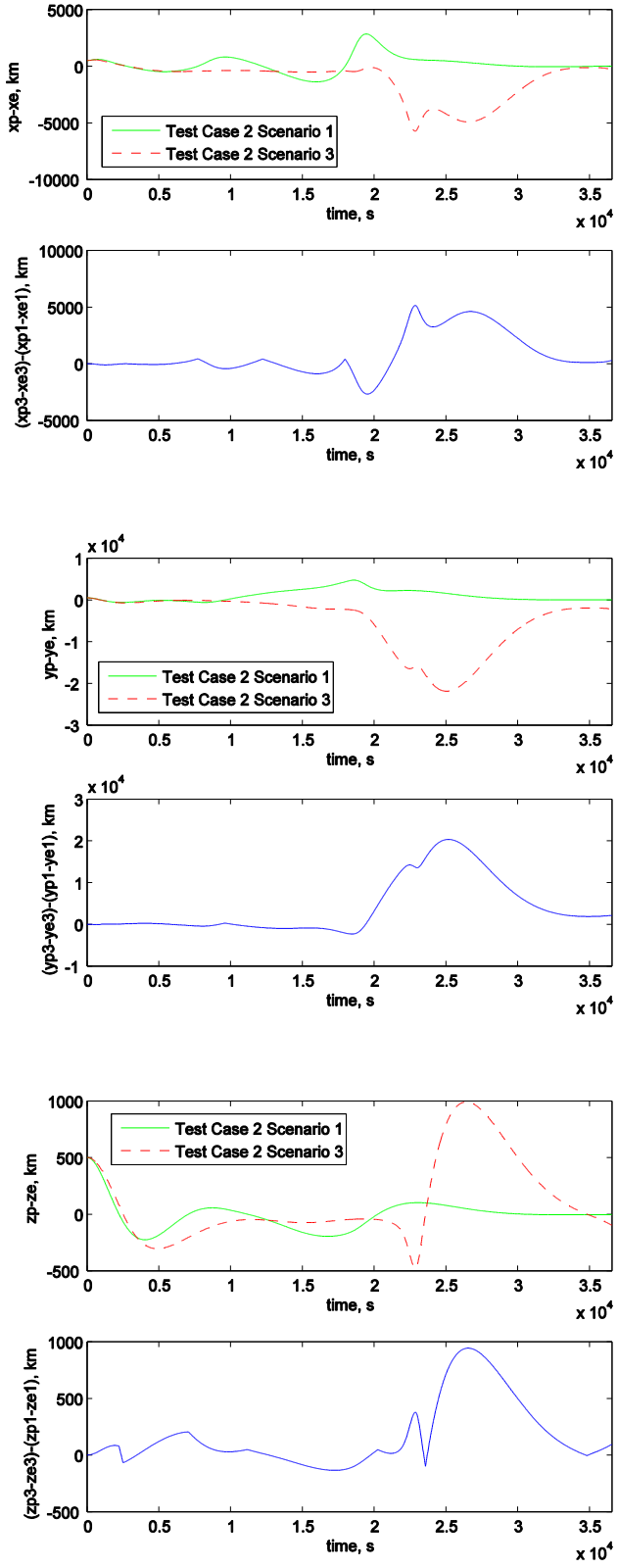

Figure 4.24: Test Case 2: Game State Comparison for Scenario 1 and 3

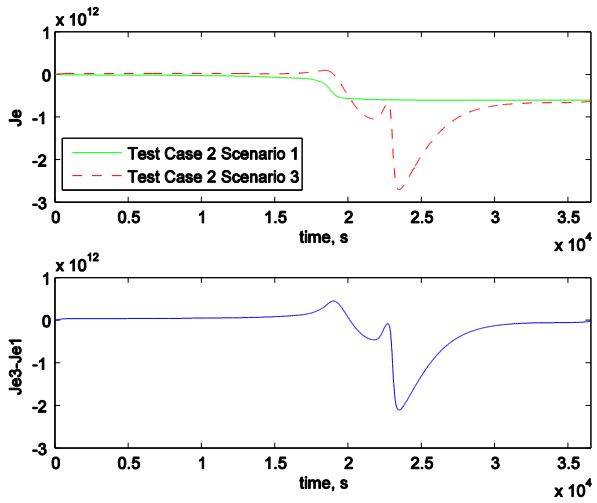

Figure 4.25: Test Case 2: Evader Cost Comparison for Scenario 1 and 3

Orbital Element Difference Comparison

Another way to compare the performances is to compare how the orbital elements of the pursuer and the evader change. The orbital element difference description of the relative orbit given in Chapter 2 can be used for this purpose. The orbital element difference vectors of the pursuer and the evader are given as follows.

$$\delta\mathbf{e}_p = \mathbf{e}_p - \mathbf{e}_c = [\delta a_p \; \delta\theta_p \; \delta i_p \; \delta q_{1_p} \; \delta q_{2_p} \; \delta\Omega_p]^T$$

$$\delta\mathbf{e}_e = \mathbf{e}_e - \mathbf{e}_c = [\delta a_e \; \delta\theta_e \; \delta i_e \; \delta q_{1_e} \; \delta q_{2_e} \; \delta\Omega_e]^T$$

The orbital element difference vector can be obtained from the Cartesian state vector by using the linear mapping.

$$\delta\mathbf{e}_p = \mathbf{A}^{-1}(\mathbf{e}_c)\mathbf{x}_p$$

$$\delta\mathbf{e}_e = \mathbf{A}^{-1}(\mathbf{e}_c)\mathbf{x}_e$$

The difference between the orbital elements of the pursuer and the evader can be obtained as follows.

$$\mathbf{e}_p - \mathbf{e}_e = \delta\mathbf{e}_p - \delta\mathbf{e}_e$$

For the test case 2, the difference between the semi-major axis of the pursuer and the evader orbit is compared in Figure 4.26 for scenarios 1 and 2. By virtue of the pursuer using the better controller in scenario 2, the spike in the difference found in scenario 1 is avoided. Figure 4.27 shows the comparison for scenarios 1 and 3. By virtue of the evader using the better controller in scenario 3, there is a broader spike in the difference almost at the same time as that of scenario 1.

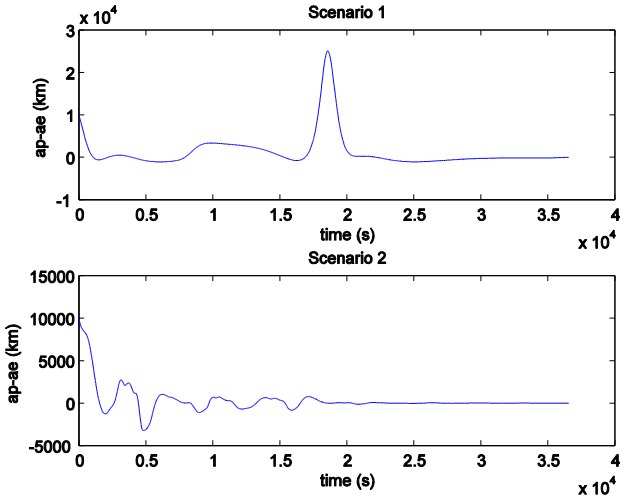

Figure 4.26: Test Case 2: Difference in Semi-Major Axis for Scenario 1 and 2

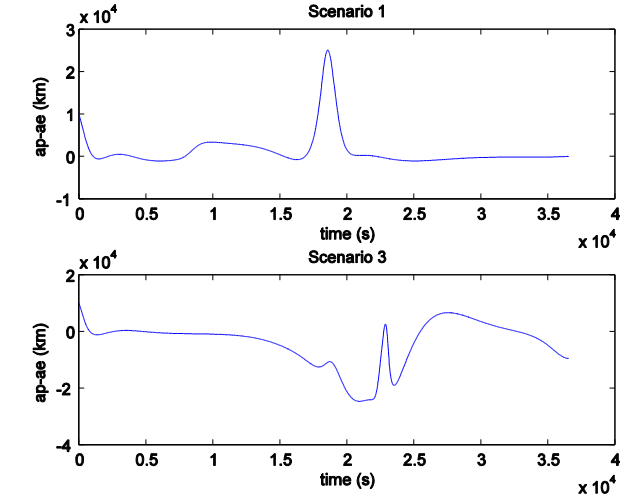

Figure 4.27: Test Case 2: Difference in Semi-Major Axis for Scenario 1 and 3

Comparison of Control Gain Matrices

Control gain matrices, $\mathbf{K}_{\mathrm{p}}$ and $\mathbf{K}_{\mathrm{e}}$, for the pursuer and the evader are

$$\mathbf{K}_{\mathrm{p}} = -\mathbf{R}^{-1}\mathbf{B}_{\mathrm{p}}{}^{\mathrm{T}}\mathbf{P}$$

$$\mathbf{K}_{\mathrm{e}} = \frac{1}{\gamma^2}\mathbf{R}^{-1}\mathbf{B}_{\mathrm{e}}{}^{\mathrm{T}}\mathbf{P}$$

Matrix **P** is obtained by solving Equation (4.7) for linear control laws and Equation (4.17) for nonlinear control laws. Control gain matrices at the initial time are compared for the test case two. Explicitly, these matrices for the pursuer in scenarios 1 and 2 are

$$\mathbf{K}_{\mathrm{p1}} = \begin{bmatrix} -2.0956\times10^{-6} & 7.6491\times10^{-7} & 0 \\ -4.8507\times10^{-6} & -2.3235\times10^{-7} & 0 \\ 0 & 0 & -5.2198\times10^{-8} \end{bmatrix}$$

$$\begin{bmatrix} -1.3803\times10^{-3} & -6.3744\times10^{-4} & 0 \\ -6.3744\times10^{-4} & -2.5678\times10^{-3} & 0 \\ 0 & 0 & -4.5694\times10^{-4} \end{bmatrix}$$

$$\mathbf{K}_{\mathrm{p2}} = \begin{bmatrix} -1.4062\times10^{-6} & 1.2893\times10^{-6} & -6.9952\times10^{-7} \\ -2.5502\times10^{-6} & -1.374\times10^{-6} & -5.737\times10^{-7} \\ -3.9616\times10^{-7} & 2.071\times10^{-7} & -3.7673\times10^{-7} \end{bmatrix}$$

$$\begin{bmatrix} -2.126\times10^{-3} & -1.1287\times10^{-4} & -1.3017\times10^{-4} \\ -1.1287\times10^{-4} & -2.5352\times10^{-3} & -3.6162\times10^{-4} \\ -1.3017\times10^{-4} & -3.6162\times10^{-4} & -1.1658\times10^{-3} \end{bmatrix}$$

The corresponding gain matrices for the evader in scenarios 1 and 3 are

$$\mathbf{K}_{\mathrm{e1}} = \begin{bmatrix} -1.0478\times10^{-6} & 3.8246\times10^{-7} & 0 \\ -2.4253\times10^{-6} & -1.1617\times10^{-7} & 0 \\ 0 & 0 & -2.6099\times10^{-8} \end{bmatrix}$$

$$\begin{bmatrix} -6.902\times10^{-4} & -3.1872\times10^{-4} & 0 \\ -3.1872\times10^{-4} & -1.2839\times10^{-3} & 0 \\ 0 & 0 & -2.2847\times10^{-4} \end{bmatrix}$$

$$\mathbf{K}_{e3} = \begin{bmatrix} -7.0312 \times 10^{-7} & 6.4468 \times 10^{-7} & -3.4976 \times 10^{-7} \\ -1.2751 \times 10^{-6} & -6.8701 \times 10^{-7} & -2.8685 \times 10^{-7} \\ -1.9808 \times 10^{-7} & 1.0355 \times 10^{-7} & -1.8837 \times 10^{-7} \end{bmatrix}$$

$$\begin{matrix} -1.063 \times 10^{-3} & -5.6438 \times 10^{-5} & -6.509 \times 10^{-5} \\ -5.6438 \times 10^{-5} & -1.2676 \times 10^{-3} & -1.8081 \times 10^{-4} \\ -6.509 \times 10^{-5} & -1.8081 \times 10^{-4} & -5.8294 \times 10^{-4} \end{matrix}\Bigg]$$

It can be seen that the gains, in particular, for the y and z position components (represented by the second and the third columns of the gain matrices) for the nonlinear control laws are higher than those for the linear control laws.

Using the linear mapping, the control laws can be written in terms of the orbital element difference vector as follows.

$$\delta\mathbf{e}_g = \delta\mathbf{e}_p - \delta\mathbf{e}_e = \mathbf{A}^{-1}(\mathbf{x}_p - \mathbf{x}_e) = \mathbf{A}^{-1}\mathbf{x}$$

$$\mathbf{x} = \mathbf{A}\delta\mathbf{e}_g$$

$$\mathbf{u}_p = \mathbf{K}_p\mathbf{A}\delta\mathbf{e}_g = \mathbf{K}_p\mathbf{A}(\mathbf{e}_p - \mathbf{e}_e)$$

$$\mathbf{u}_e = \mathbf{K}_e\mathbf{A}\delta\mathbf{e}_g = \mathbf{K}_e\mathbf{A}(\mathbf{e}_p - \mathbf{e}_e)$$

Gain matrices given by matrix products $\mathbf{K}_p\mathbf{A}$ and $\mathbf{K}_e\mathbf{A}$ at the initial time are compared for the test case two. These matrices for the pursuer in scenarios 1 and 2 are given below.

$$\mathbf{K}_{p1}\mathbf{A} = \begin{bmatrix} -4.7868 \times 10^{-7} & 1.6285 \times 10^{-3} & 0 \\ -1.3257 \times 10^{-7} & -3.6398 \times 10^{-3} & 0 \\ 0 & 0 & -4.0858 \times 10^{-3} \end{bmatrix}$$

$$\begin{matrix} 1.0847 \times 10^{-2} & 1.0256 \times 10^{-2} & 5.0416 \times 10^{-3} \\ -4.2684 \times 10^{-3} & 3.1001 \times 10^{-3} & -1.5314 \times 10^{-3} \\ 0 & 0 & -1.5408 \times 10^{-4} \end{matrix}\Bigg]$$

$$\mathbf{K}_{p2}\mathbf{A} = \begin{bmatrix} -6.0232 \times 10^{-7} & 3.3424 \times 10^{-3} & -2.0556 \times 10^{-3} \\ 9.8854 \times 10^{-7} & -1.064 \times 10^{-2} & -3.9269 \times 10^{-3} \\ 1.2479 \times 10^{-7} & 1.1658 \times 10^{-3} & -1.0742 \times 10^{-2} \end{bmatrix}$$

$$\begin{matrix} 1.5266 \times 10^{-2} & 1.5542 \times 10^{-2} & 1.0867 \times 10^{-2} \\ -3.6753 \times 10^{-2} & -5.7983 \times 10^{-3} & -7.3018 \times 10^{-3} \\ -4.8815 \times 10^{-3} & -7.3915 \times 10^{-5} & 1.8303 \times 10^{-3} \end{matrix}\Bigg]$$

Gain matrices for the evader in scenarios 1 and 3 are given below.

$$\mathbf{K}_{e1}\mathbf{A} = \begin{bmatrix} -2.3934 \times 10^{-7} & 8.1428 \times 10^{-4} & 0 \\ -6.6289 \times 10^{-8} & -1.8199 \times 10^{-3} & 0 \\ 0 & 0 & -2.0429 \times 10^{-3} \end{bmatrix}$$

$$\begin{matrix} 5.4237 \times 10^{-3} & 5.1281 \times 10^{-3} & 2.5208 \times 10^{-3} \\ -2.1342 \times 10^{-3} & 1.5501 \times 10^{-3} & -7.6575 \times 10^{-4} \\ 0 & 0 & -7.7043 \times 10^{-5} \end{matrix}\Bigg]$$

$$\mathbf{K}_{e3}\mathbf{A} = \begin{bmatrix} -3.0117 \times 10^{-7} & 1.6712 \times 10^{-3} & -1.0278 \times 10^{-3} \\ 4.9428 \times 10^{-7} & -5.3205 \times 10^{-3} & -1.9635 \times 10^{-3} \\ 6.2399 \times 10^{-8} & 5.8295 \times 10^{-4} & -5.3711 \times 10^{-3} \end{bmatrix}$$

$$\begin{matrix} 7.6336 \times 10^{-3} & 7.7714 \times 10^{-3} & 5.4337 \times 10^{-3} \\ -1.8377 \times 10^{-2} & -2.8992 \times 10^{-3} & -3.6509 \times 10^{-3} \\ -2.4408 \times 10^{-3} & -3.6958 \times 10^{-5} & 9.1517 \times 10^{-4} \end{matrix}\Bigg]$$

It can be seen that the gains for δa and δi (represented by the first and the third columns of the gain matrices) for the nonlinear control laws are higher than those for the linear control laws.

It should be noted that the in-plane and the out-of-plane motions are coupled in the nonlinear dynamics case, whereas they are decoupled in case of linear dynamics. Thus, initially, the nonlinear control laws attempt to influence the in-plane as well as out-of-plane motion aggressively. This observation is consistent with the earlier observation that, initially, the nonlinear control laws accept higher cost.

Effect of Frequency of Solving the SDRE on the Nonlinear Controller Performance

In earlier simulations, the SDRE was being solved every 5 seconds. From a real-time application perspective, considering the availability of computing power on-board, it is important to look at the performance of the nonlinear controller if the SDRE is solved less frequently. Results are presented only for test case 2, as the effect of frequency of solving the SDRE is greater when the game duration is longer and the control usage is lower.

Results are presented for the nonlinear PE game. Each player implements nonlinear control law using its NERM. Three scenarios are considered for comparison. In scenario 1, both players solve the SDRE every 5 seconds. In scenario 2, the pursuer solves the SDRE every 5 seconds whereas the evader computes solutions every 10 minutes. In scenario 3, the pursuer solves the SDRE for every 10 minutes whereas the evader computes solutions every 5 seconds.

Performances in scenario 1 and scenario 2 are compared first. The performance of the pursuer should be better in scenario 2 as the pursuer is using the better controller by virtue of solving the SDRE more frequently. Plots of the position vector components of the game state are shown in Figure 4.28. The frequency of the SDRE solving clearly affects the performance of the controller. Almost throughout the game, the separations in scenario 2 are smaller than those in scenario 1 indicating the fact that the pursuer is being more effective in achieving its objective.

Performances in scenario 1 and scenario 3 are compared next. The performance of the evader should be better in scenario 3 as the evader is using the better controller by virtue of solving the SDRE more frequently. Plots of the position vector components of the game state are shown in Figure 4.29. Again, the frequency of the SDRE solving affects the performance of the controller. Almost throughout the game, the separations in scenario 3 are greater than those in scenario 1 indicating the fact that the evader is being more effective in achieving its objective.

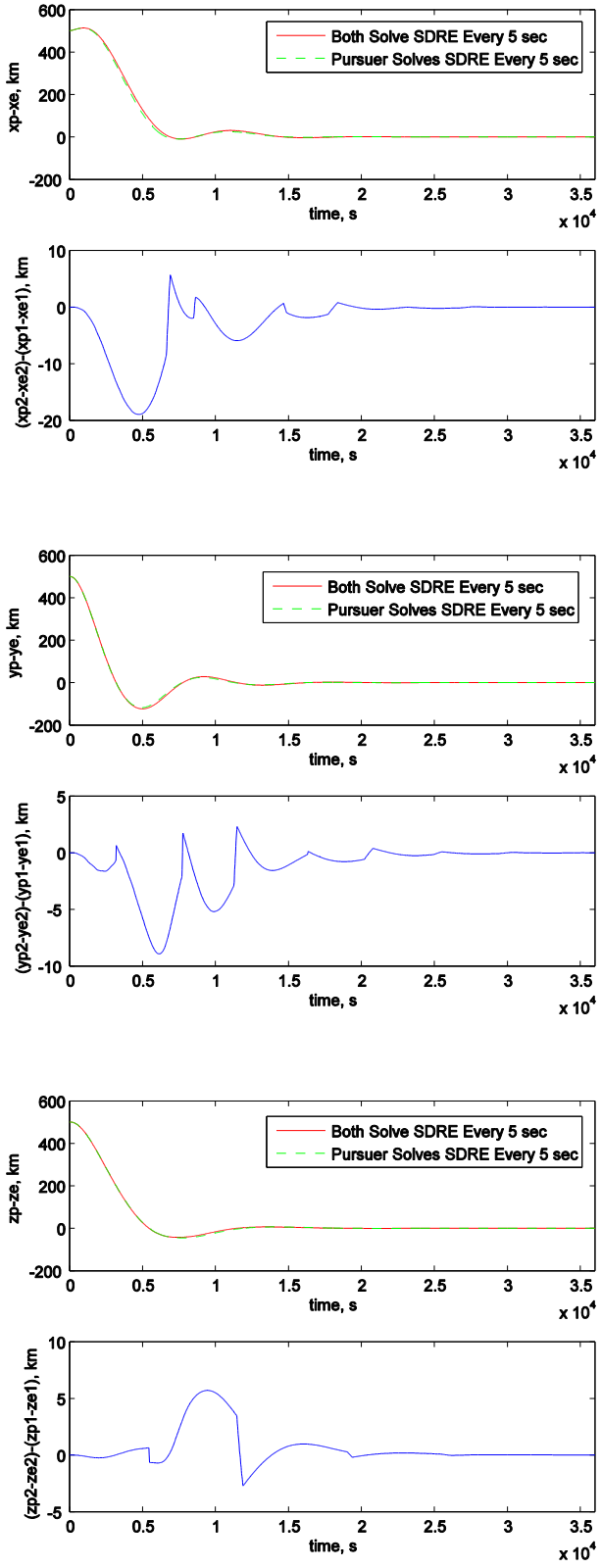

Figure 4.28: Game State Comparison for Scenario 1 and 2

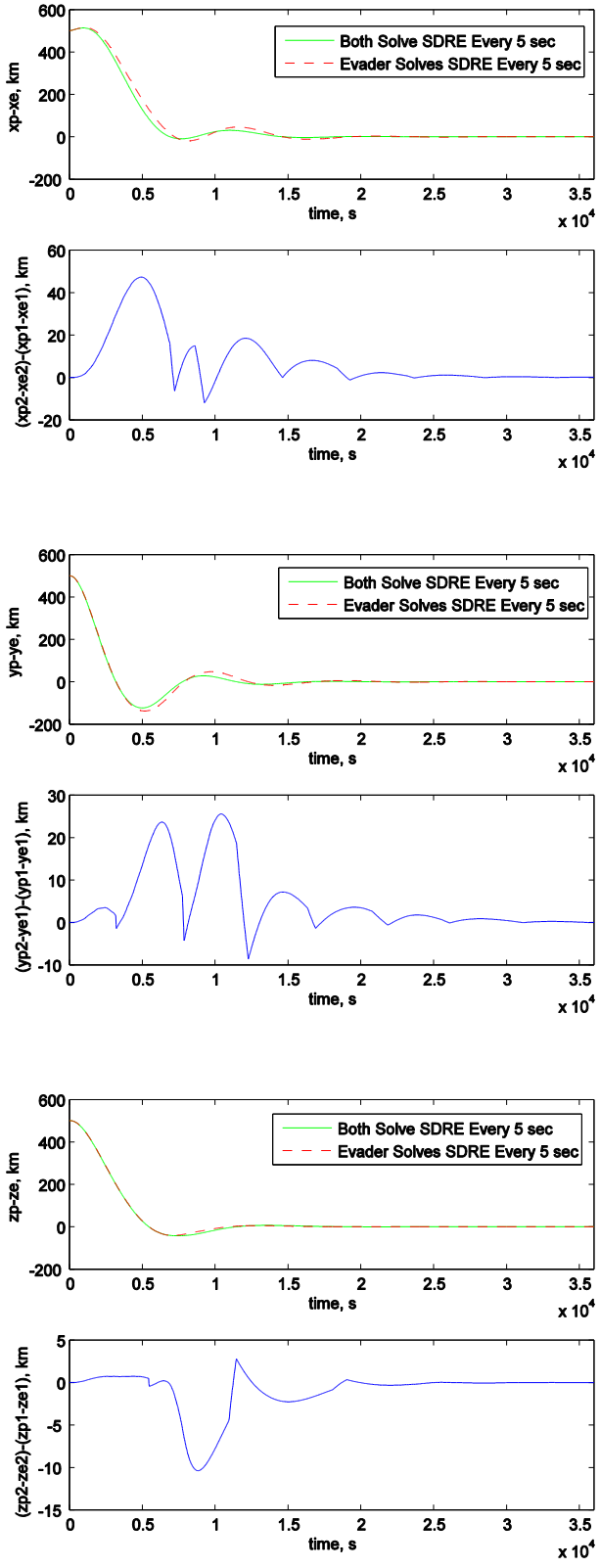

Figure 4.29: Game State Comparison for Scenario 1 and 3

CHAPTER 5

SPACECRAFT RELATIVE MOTION CONTROL USING ANGLES-ONLY NAVIGATION: SEPARATION PRICIPLE

Autonomous spacecraft rendezvous is a critical aspect of many current and future space missions. Autonomous rendezvous does not need cooperation between two spacecraft and is of particular importance to missions involving targets that are malfunctioning, uncooperative, or hostile. Relative navigation is an important aspect of autonomous rendezvous as the precision in the knowledge of the system state directly impacts mission success. The common measurement types for relative navigation are range and line-of-sight (LOS) angles. Range is the distance from the target to the chaser, and the angles are the azimuth and the elevation. The precision of navigation systems using both range and angle measurements is good but they require additional mass, power, and volume resources. For autonomous rendezvous, however, light weight, low power, compact navigation systems are desirable. For this purpose angles-only navigation has been explored. Angles-only navigation does not require range sensors, making it an attractive option from a logistics point-of-view but it is limited by its inability to extract range information.

The concept of angles-only navigation has played an important role in naval applications, target tracking, orbit determination, interplanetary navigation, formation flying of unmanned aerial vehicles, etc.[32] LOS measurements had a role in the earliest

orbital rendezvous and proximity operations as well. Both Gemini and Apollo missions used angle measurements in addition to other instruments for range measurement. In these missions the angle measurements were acquired by the human eye. Recently there have been many studies investigating autonomous orbital rendezvous missions using small, compact unmanned spacecraft. These missions are typically intended for uncooperative space objects and angles-only measurements acquired by an optical camera are considered for navigation purposes.

Angles-only navigation, due to lack of direct range measurements, can be ill-conditioned for orbital rendezvous and proximity operations from a system observability perspective. Observability means that the system state can be uniquely determined from observations of the system output over some time interval. As mentioned in Chapter 2, the linear HCW equations are the most frequently used equations of spacecraft relative motion. Reference 32 formulated an analytical criterion for observability using angles-only navigation and demonstrated that the system is unobservable when the HCW equations are used. This is because there is a family of linear relative trajectories described by the homogeneous HCW equations that are proportional to each other. These trajectories possess identical LOS histories and thus the range of the trajectory cannot be uniquely determined, making the system unobservable. There have been several attempts to overcome this limitation. The NERM have been used to describe the relative dynamics, and it is shown that; under certain geometric conditions on the relative configuration between the chief and the deputy, the system is observable from angles-only measurements.[33] It has also been shown that the range can be determined if angle measurements are taken from two cooperating spacecraft.[34] There have been attempts to

improve angles-only navigation by changing the coordinate system[35] and by combining angle measurements with other measurements.[36] In Reference 37 the authors discuss the observability conditions of angles-only relative navigation based on the observability matrix.

In Reference 38 the observability of the angles-only navigation system in various orbital rendezvous trajectories is studied both analytically and through linear covariance modeling. There it is shown that the range information can be generated from the angle measurements alone if assisted by appropriate maneuvers. It was concluded that maneuvers generating motion normal to the LOS achieve system observability. The analytical criterion formulated in Reference 32 also revealed that the relative position and velocity can be uniquely determined with angle measurements if a calibrated thrust maneuver is executed. It was shown that the maneuvers which alter the homogeneous LOS history guarantee observability. This is because the trajectory resulting from the maneuver has a different LOS history from the identical LOS histories of homogeneous HCW trajectories. This facilitates the unique determination of range. Reference 32 demonstrated system observability using impulsive maneuvers. Reference 39 demonstrated observability using continuous low-thrust maneuvers. In Reference 39, a 6 degree-of-freedom simulation was performed. An EKF was implemented such that the dynamics model was an inertial two-body model, whereas the guidance law and the LQR control law were derived based on the HCW relative dynamics. Observability, or the level of range knowledge, was indicated by 3-σ bounds of range components.

APPLICATION OF SEPARATION PRINCIPLE

This dissertation also investigates the observability of angles-only navigation using continuous-thrust maneuvers, but from a different perspective than previous studies. In this dissertation, a 3 degree-of-freedom simulation is performed and there is no guidance law or pre-selected trajectory. The filter is implemented such that both the dynamics model and the LQR control law are based on the HCW relative dynamics. Control strategy for such problems can be derived on the basis of the separation principle or the certainty equivalence principle.[23] According to this principle, the solution of a state feedback control problem with incomplete state knowledge is given by the solution of two separate sub-problems: 1) the estimation problem of obtaining a state estimate from noisy measurements and 2) the problem of deriving the feedback control law. The separation of the overall control design involves the eigenvalue separation property which states that the eigenvalues of the overall closed-loop system are given by the eigenvalues of the LQR system together with those of the state estimator system. The feedback control law then can be implemented using the state estimate.

The separation principle is based on the assumption that the control and estimation processes are decoupled. This assumption is in fact an optimal approach for linear systems with quadratic performance criterion and Gaussian noise. For linear systems, LQR control and the KF are combined leading to a linear quadratic Gaussian (LQG) control strategy. The separation principle, however, may not hold for systems involving nonlinearities such as the nonlinear angles-only measurement model considered here. In such systems, the control and estimation processes may be coupled.

Thus, the control action in addition to affecting the state of the system may also affect its observability and hence the accuracy of its estimation. This is called the dual effect of control.

In this chapter, LQG control implementing both a linear measurement model (for comparison purposes) and the nonlinear angles-only measurement model is investigated. It is found, as expected, that the control and estimation processes are decoupled in the LQG control implementing the linear measurement model. The magnitude of state weighting in the performance criterion and hence the magnitude of control input has no effect on the performance of the LQG control. The control and estimation processes are found to be coupled in the LQG control implementing the angles-only measurement model. When the magnitude of the state weighting is low, the magnitude of control input is also low and the LQG control performs well. When the magnitude of the state weighting is high, the magnitude of control input is also high and the LQG control fails. Simulations for LQG control implementing both the linear measurement model and the angles-only measurement model are performed later in this Chapter.

HCW SYSTEM DYNAMICS MODEL

The HCW equations are used as the system dynamics model. The HCW equations along with control accelerations can be written as follows.

$$\ddot{x} - 3n^2x - 2n\dot{y} = u_x$$

$$\ddot{y} + 2n\dot{x} = u_y$$

$$\ddot{z} + n^2z = u_z$$

$$\dot{\mathbf{x}} = \mathbf{A}_{HCW}\mathbf{x}(t) + \mathbf{B}\mathbf{u}(t) \tag{5.1}$$

LINEAR MEASUREMENT MODEL

Assuming that the y and z position components can be measured directly using sensors, the linear measurement model is given as follows.

$$\mathbf{y} = \begin{bmatrix} y \\ z \end{bmatrix} = \begin{bmatrix} 0 & 1 & 0 & 0 & 0 & 0 \\ 0 & 0 & 1 & 0 & 0 & 0 \end{bmatrix} \mathbf{x} = \mathbf{C}\mathbf{x} \tag{5.2}$$

The observability matrix given by $\mathbf{O} = [\mathbf{C} \quad \mathbf{C}\mathbf{A}_{\mathrm{HCW}} \quad \mathbf{C}\mathbf{A}_{\mathrm{HCW}}{}^{\mathbf{2}} \quad \ldots \quad \mathbf{C}\mathbf{A}_{\mathrm{HCW}}{}^{\mathbf{n-1}}]^{\mathrm{T}}$ is full rank.

ANGLES-ONLY MEASUREMENT MODEL

Figure 5.1 shows the schematic of angles-only measurements depicting the LOS angles of azimuth (AZ) and elevation (El).

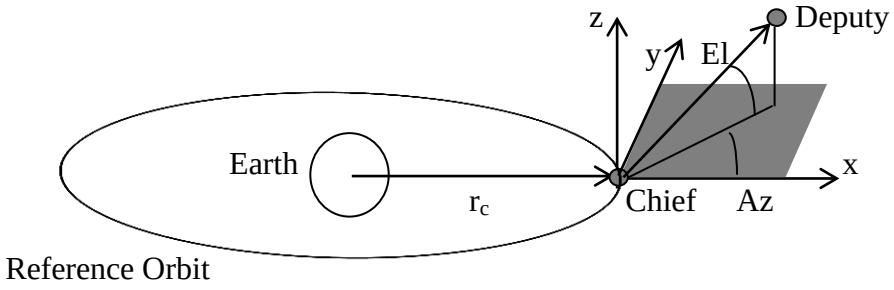

Figure 5.1: Line-of-Sight Measurements

According to the above schematic the nonlinear measurement model is given as follows.

$$\mathbf{y} = \mathbf{h}(\mathbf{x}) = \begin{bmatrix} \mathrm{Az} \\ \mathrm{El} \end{bmatrix} = \begin{bmatrix} \operatorname{atan}\left(\frac{y}{x}\right) \\ \operatorname{atan}\left(\frac{z}{\rho_{xy}}\right) \end{bmatrix}, \quad \rho_{xy} = \sqrt{x^2 + y^2} \tag{5.3}$$

The measurement sensitivity matrix **H** in the EKF is given as follows.

$$\mathbf{H} = \left(\frac{\partial \mathbf{h}}{\partial \mathbf{x}}\right)_{\hat{\mathbf{x}}} = \begin{bmatrix} \frac{\partial \mathrm{Az}}{\partial x} & \frac{\partial \mathrm{Az}}{\partial y} & \frac{\partial \mathrm{Az}}{\partial z} & \frac{\partial \mathrm{Az}}{\partial \dot{x}} & \frac{\partial \mathrm{Az}}{\partial \dot{y}} & \frac{\partial \mathrm{Az}}{\partial \dot{z}} \\ \frac{\partial \mathrm{El}}{\partial x} & \frac{\partial \mathrm{El}}{\partial y} & \frac{\partial \mathrm{El}}{\partial z} & \frac{\partial \mathrm{El}}{\partial \dot{x}} & \frac{\partial \mathrm{El}}{\partial \dot{y}} & \frac{\partial \mathrm{El}}{\partial \dot{z}} \end{bmatrix}_{\hat{\mathbf{x}}}$$

$$\mathbf{H} = \begin{bmatrix} \frac{-\hat{y}}{\hat{x}^2+\hat{y}^2} & \frac{\hat{x}}{\hat{x}^2+\hat{y}^2} & 0 & 0 & 0 & 0 \\ \frac{-\hat{x}\times\hat{z}}{\hat{\rho}^2\times\sqrt{\hat{x}^2+\hat{y}^2}} & \frac{-\hat{y}\times\hat{z}}{\hat{\rho}^2\times\sqrt{\hat{x}^2+\hat{y}^2}} & \frac{\sqrt{\hat{x}^2+\hat{y}^2}}{\hat{\rho}^2} & 0 & 0 & 0 \end{bmatrix} \tag{5.4}$$

$$\hat{\rho} = \sqrt{\hat{x}^2+\hat{y}^2+\hat{z}^2}$$

LQR CONTROL

An optimal feedback control law is obtained by solving the LQR control problem as follows.

Minimize: $$J_{LQR} = \frac{1}{2}\int_{t_0}^{\infty} (\mathbf{x}^T(t)\mathbf{Q_c}\mathbf{x}(t) + \mathbf{u}^T(t)\mathbf{R_c}\mathbf{u}(t))dt$$

Subject to: $$\dot{\mathbf{x}} = \mathbf{A}_{HCW}\mathbf{x}(t) + \mathbf{B}\mathbf{u}(t)$$

The control is given as follows.

$$\mathbf{u}_{LQR}(t) = -\mathbf{R_c}^{-1}\mathbf{B}^T\mathbf{P_c}\mathbf{x}(t) = -\mathbf{K}_c\mathbf{x}(t) \tag{5.5}$$

The symmetric matrix $\mathbf{P_c}$ is obtained by solving the ARE.

$$\mathbf{A}_{HCW}{}^T\mathbf{P_c} + \mathbf{P_c}\mathbf{A}_{HCW} + \mathbf{Q_c} - \mathbf{P_c}\mathbf{B}\mathbf{R_c}^{-1}\mathbf{B}^T\mathbf{P_c} = \mathbf{0}$$

MATLAB function "*lqr*" is used to solve for $\mathbf{K_c}$.

LQG CONTROL

The LQR control law is derived assuming full-state availability. However, it is not practical to assume full-state availability. Thus, the system state needs to be estimated using a filter. The state estimate given by the filter can then be used in implementation of the LQR control law leading to the LQG control law. The cost function for the LQG control problem is the expected value of the cost function for the LQR control problem.

$$J_{LQG} = E\left\{\frac{1}{2}\int_{t_0}^{\infty}\left(\mathbf{x}^T(t)\mathbf{Q}_c\mathbf{x}(t) + \mathbf{u}^T(t)\mathbf{R}_c\mathbf{u}(t)\right)dt\right\} \tag{5.6}$$

It should be noted that the HCW dynamics is used as the dynamics model of the filter. Thus, for the linear measurement model the filter is simply the KF. For the angles-only measurement model, the filter is only a partial EKF as only the measurement sensitivity matrix **H** is evaluated at the current state estimate whereas the HCW dynamics is obtained by linearizing the NERM about the origin instead of the current state estimate. Most physical systems involve continuous-time dynamic models and discrete-time measurements taken from a digital signal processor. The steps for the LQG control which uses a continuous-discrete KF for implementing the linear measurement model are given below.

Initialize: $\mathbf{x}(t_0) = \mathbf{x}_0, \hat{\mathbf{x}}(t_0) = \hat{\mathbf{x}}_0, \mathbf{P}_e(t_0) = \mathbf{P}_{e,0}$

Control: $\mathbf{u}_{LQG} = -\mathbf{K}_c\hat{\mathbf{x}}$

Model: $\dot{\mathbf{x}} = \mathbf{A}_{HCW}\mathbf{x} + \mathbf{B}\mathbf{u}_{LQG} + \mathbf{w}$

$\mathbf{y}_k = \mathbf{C}\mathbf{x}_k + \mathbf{v}$

Gain: $\mathbf{K}_k = \mathbf{P}_{e,k}{}^{-}\mathbf{C}^T\left[\mathbf{C}\mathbf{P}_{e,k}{}^{-}\mathbf{C}^T + \mathbf{R}_v\right]^{-1}$

Update: $\hat{\mathbf{x}}_k{}^{+} = \hat{\mathbf{x}}_k{}^{-} + \mathbf{K}_k[\mathbf{y}_k - \mathbf{C}\hat{\mathbf{x}}_k{}^{-}]$

$\mathbf{P}_{e,k}{}^{+} = [\mathbf{I} - \mathbf{K}_k\mathbf{C}]\mathbf{P}_{e,k}{}^{-}$

Propagate: $\dot{\hat{\mathbf{x}}} = \mathbf{A}_{HCW}\hat{\mathbf{x}} + \mathbf{B}\mathbf{u}_{LQG}$

$\dot{\mathbf{P}}_e = \mathbf{P}_e\mathbf{A}_{HCW}{}^{T} + \mathbf{A}_{HCW}\mathbf{P}_e + \mathbf{Q}_w$

The steps for the LQG control which uses a continuous-discrete EKF for implementing the angles-only measurement model are given below.

Initialize: $\mathbf{x}(t_0) = \mathbf{x}_0, \hat{\mathbf{x}}(t_0) = \hat{\mathbf{x}}_0, \mathbf{P}_e(t_0) = \mathbf{P}_{e,0}$

Control: $\mathbf{u}_{LQG} = -\mathbf{K}_c\hat{\mathbf{x}}$

Model: $\dot{\mathbf{x}} = \mathbf{A}_{HCW}\mathbf{x} + \mathbf{B}\mathbf{u}_{LQG} + \mathbf{w}$

$\mathbf{y}_k = \mathbf{h}(\mathbf{x}_k) + \mathbf{v}$

Gain: $\mathbf{K}_k = \mathbf{P}_{e,k}{}^{-}\mathbf{H}^T\left[\mathbf{H}\mathbf{P}_{e,k}{}^{-}\mathbf{H}^T + \mathbf{R}_v\right]^{-1}, \mathbf{H} = \frac{\partial \mathbf{h}}{\partial \mathbf{x}}\Big|_{\hat{\mathbf{x}}_k{}^{-}}$

Update: $\hat{\mathbf{x}}_k{}^{+} = \hat{\mathbf{x}}_k{}^{-} + \mathbf{K}_k[\mathbf{y}_k - \mathbf{h}(\hat{\mathbf{x}}_k{}^{-})]$

$\mathbf{P}_{e,k}{}^{+} = [\mathbf{I} - \mathbf{K}_k\mathbf{H}]\mathbf{P}_{e,k}{}^{-}$

Propagate: $\dot{\hat{\mathbf{x}}} = \mathbf{A}_{HCW}\hat{\mathbf{x}} + \mathbf{B}\mathbf{u}_{LQG}$

$\dot{\mathbf{P}}_e = \mathbf{P}_e\mathbf{A}_{HCW}{}^{T} + \mathbf{A}_{HCW}\mathbf{P}_e + \mathbf{Q}_w$

NUMERICAL EXAMPLES

MATLAB simulations for the LQG control implementing both linear measurement model and angles-only measurement model are performed. Various parameters used in the numerical simulations are given in Table 5.1. The RK4 numerical integration method is used to propagate the dynamics. A time step of 1 second is used. The duration of simulations is 5828 seconds which is the period of the chief orbit.

Linear LQG

Simulations are performed for the LQG control implementing the linear measurement model for both low state weighting as well as high state weighting cases. For the low-weight case, plots comparing the time history of true and estimated position vector components of the chaser are shown in Figure 5.2. It can be seen that, by the end of the simulation time, the state has been regulated very close to the origin and that the state estimate has converged on the true state. Plots of the control vector components of

Parameter	Value
r_c (km)	7000
Low Weight $\mathbf{Q}_c$	$\mathbf{I}_{6\times6}$
High Weight $\mathbf{Q}_c$	$\mathbf{I}_{6\times6} \times 10^4$
$\mathbf{R}_c$	$\mathbf{I}_{3\times3} \times 10^{11}$
Process Noise Standard Deviation σ_p (m/s^2)	10^{-4}
$\mathbf{Q}_w$	$\begin{bmatrix} \mathbf{0}_{3\times3} & \mathbf{0}_{3\times3} \\ \mathbf{0}_{3\times3} & \mathbf{I}_{3\times3} \end{bmatrix} \times {\sigma_p}^2$
Linear Model Standard Deviation σ_l (m)	5
Linear Model $\mathbf{R}_v$	$\mathbf{I}_{2\times2} \times {\sigma_l}^2$
Nonlinear Model Standard Deviation σ_n (rad)	10^{-3}
Nonlinear Model $\mathbf{R}_v$	$\mathbf{I}_{2\times2} \times {\sigma_n}^2$
$\mathbf{x}_0$	[1000 1000 1000 10 10 10]
$\hat{\mathbf{x}}_0$	$2\mathbf{x}_0$
$\mathbf{P}_{e,0}$	$[\hat{\mathbf{x}}_0 - \mathbf{x}_0]^T[\hat{\mathbf{x}}_0 - \mathbf{x}_0]$

Table 5.1: LQG Simulation Parameters

the chaser are shown in Figure 5.3. Plots comparing the filter errors with the $\pm 3\sigma$ standard deviation bounds are shown in Figure 5.4. It can be seen that, at all times, the filter errors are within the $\pm 3\sigma$ standard-deviation bounds indicating range observability. The uncertainty in the y and z components reduces very quickly as measurements for these components are available. Hence, a magnified view of the $\pm 3\sigma$ plots of these components is also given.

For the high-weight case, plots comparing the time history of true and estimated position vector components of the chaser are shown in Figure 5.5. It can be seen that the state has been regulated to the origin much earlier than the low-weight case and that the state estimate has converged on the true state. Plots of the control vector components of the chaser are shown in Figure 5.6. Plots comparing the filter errors with the $\pm 3\sigma$ standard deviation bounds are shown in Figure 5.7. It can be seen that, at all times, the filter errors are within the $\pm 3\sigma$ standard-deviation bounds indicating range observability.

Thus, the control and estimation processes are decoupled in the LQG control implementing the linear measurement model. The magnitude of state weighting in the performance criterion and hence the magnitude of control input has no effect on the performance of the KF estimation. This may be attributed to the observability property of linear systems. According to this property, an n-dimensional linear system is observable if the observability matrix given by $\mathbf{O} = [\mathbf{C} \quad \mathbf{CA}_{\mathrm{HCW}} \quad \mathbf{CA}_{\mathrm{HCW}}{}^{\mathbf{2}} \quad \ldots \quad \mathbf{CA}_{\mathrm{HCW}}{}^{\mathrm{n-1}}]^{\mathrm{T}}$ is full rank.[23] Thus, the system observability depends only on the system dynamics matrix ($\mathbf{A}_{\mathrm{HCW}}$) and the measurement model matrix ($\mathbf{C}$) and not on the control input.

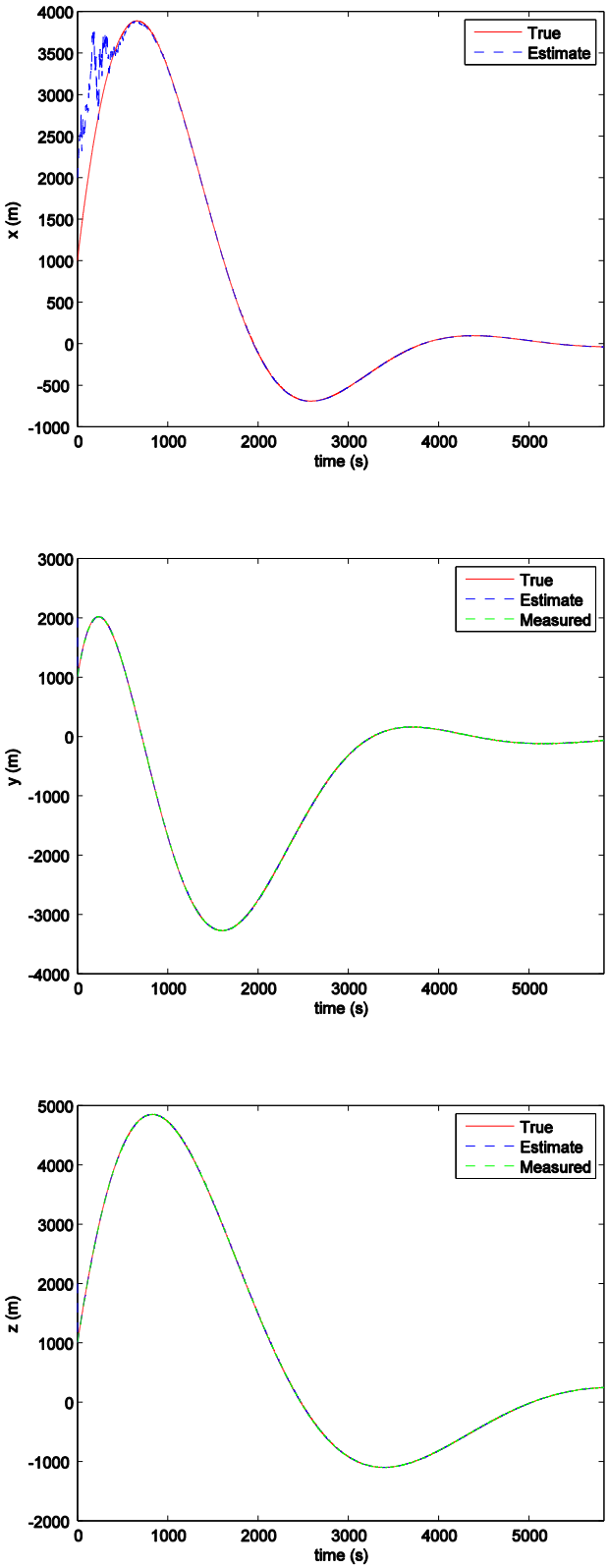

Figure 5.2: Linear LQG Low-Weight Case: Position Vector Components

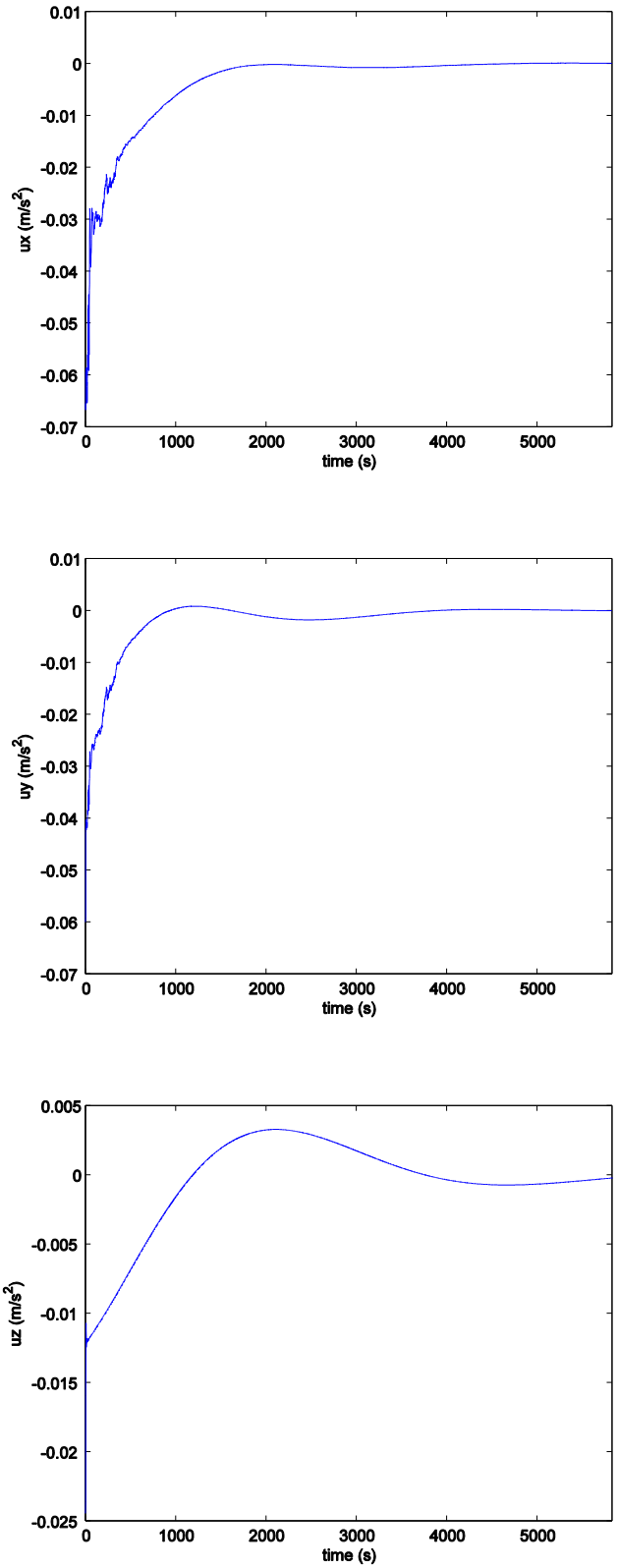

Figure 5.3: Linear LQG Low-Weight Case: Control Vector Components

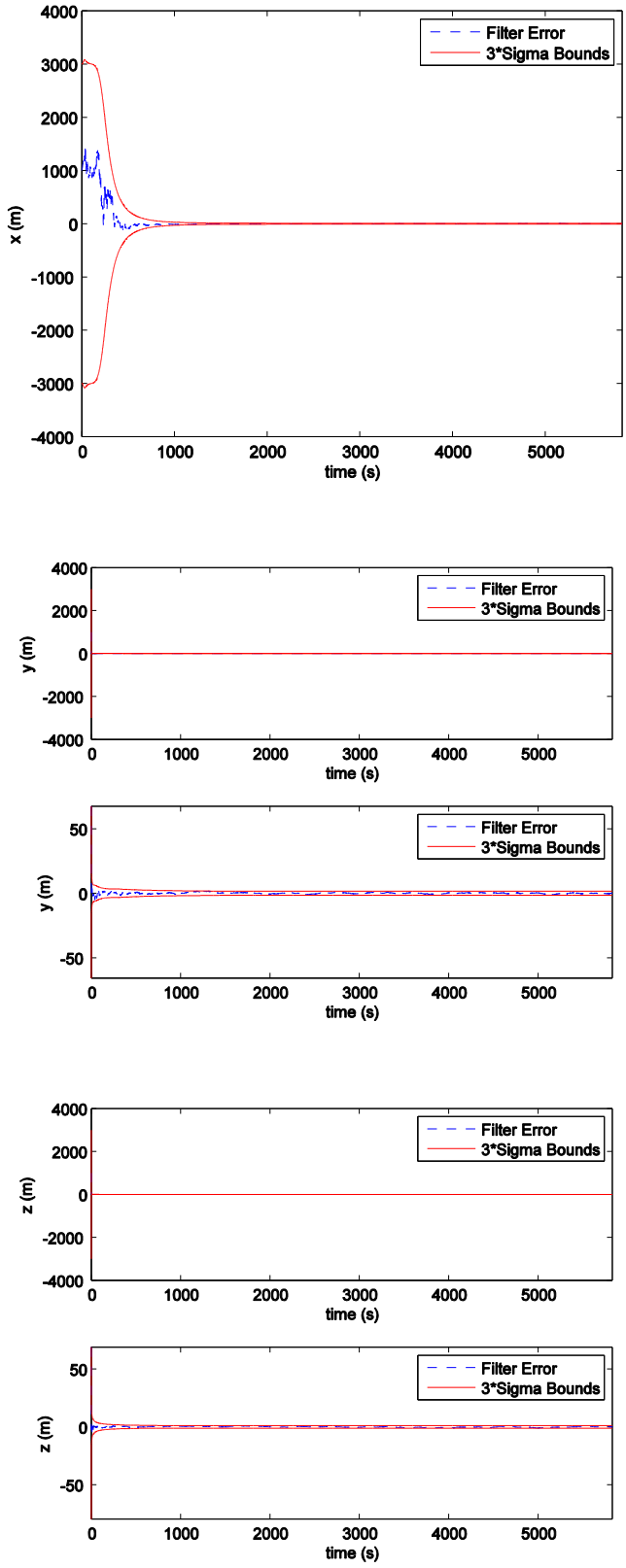

Figure 5.4: Linear LQG Low-Weight Case: Filter Error and 3-σ Bounds

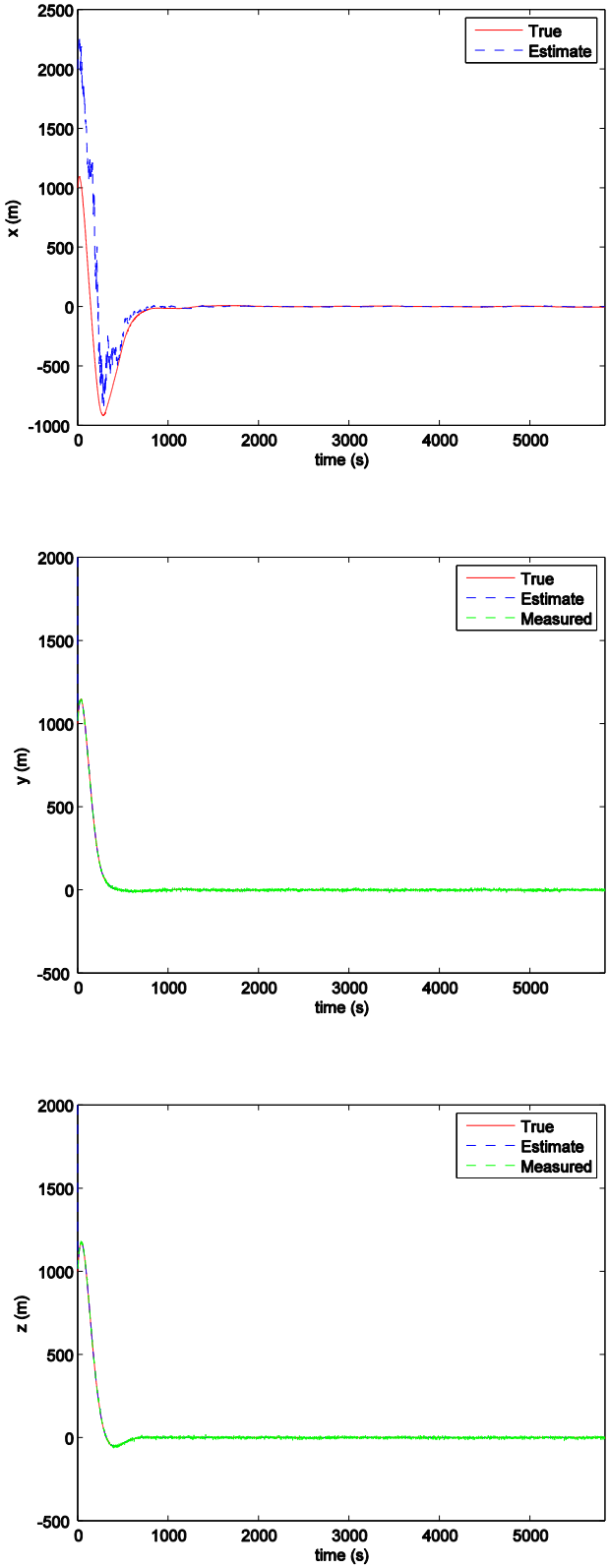

Figure 5.5: Linear LQG High-Weight Case: Position Vector Components

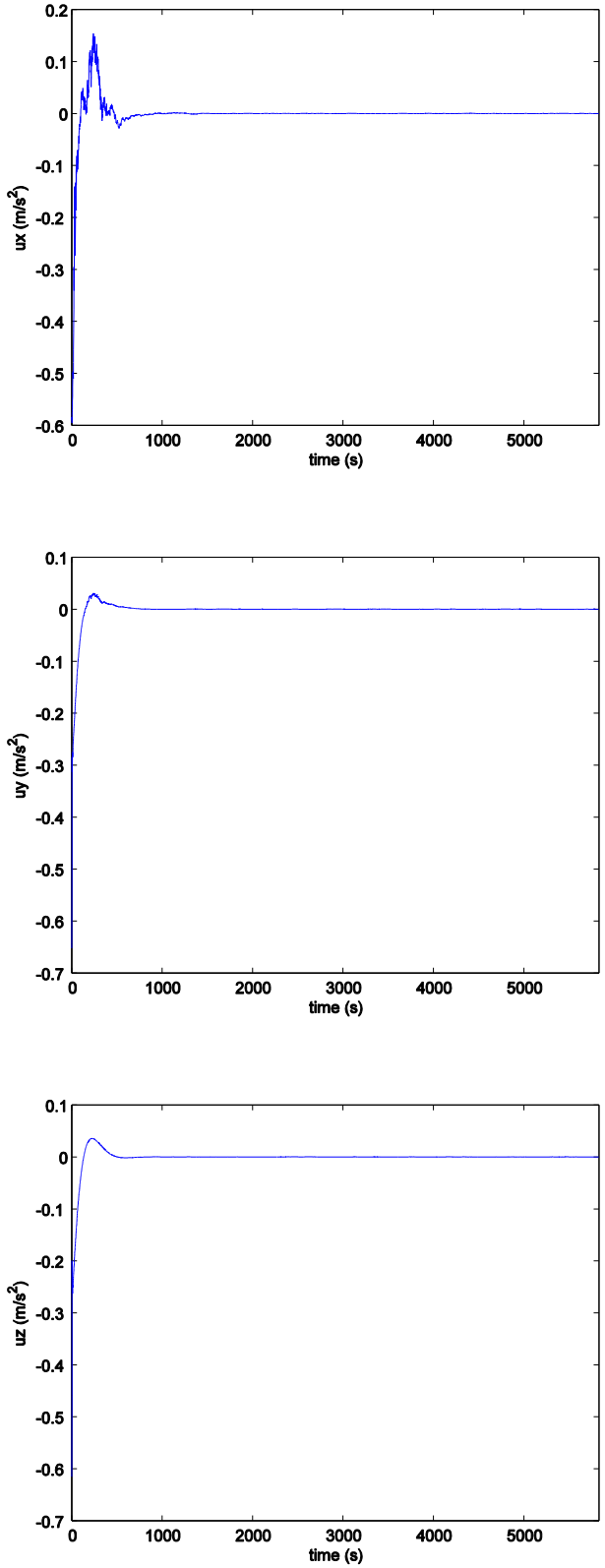

Figure 5.6: Linear LQG High-Weight Case: Control Vector Components

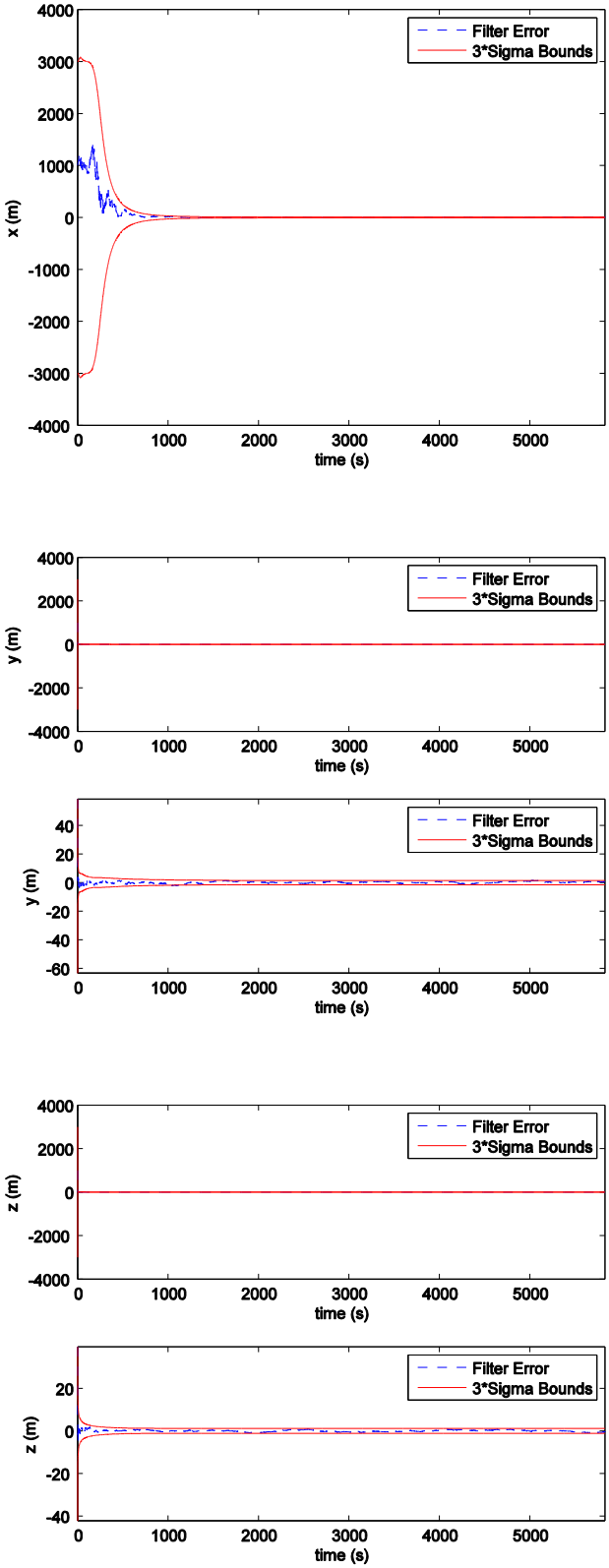

Figure 5.7: Linear LQG High-Weight Case: Filter Error and 3-σ Bounds

Nonlinear LQG

Simulations are performed for the LQG control implementing the angles-only measurement model for both low state weighting as well as high state weighting cases. As mentioned earlier, the LQG control performs well in the low-weight case and fails in the high-weight case.

For the low-weight case, plots comparing the time history of true and estimated position vector components of the chaser are shown in Figure 5.8. It can be seen that, by the end of the simulation time, the state has been regulated very close to the origin and that the state estimate has converged on the true state. Plots of the control vector components of the chaser are shown in Figure 5.9. Plots comparing the filter errors with the $\pm 3\sigma$ standard deviation bounds are shown in Figure 5.10. It can be seen that, at all times, the filter errors are within the $\pm 3\sigma$ standard-deviation bounds indicating range observability.

For the high-weight case, by virtue of the stochastic nature of the LQG control, two different behaviors have been observed. In some simulation runs, initially, the state estimate seems to converge on the true state and the true state seems to go to the origin but later the true state diverges whereas the state estimate is regulated to the origin. In other simulation runs, the state estimate never converges on the true state. The true state diverges whereas the state estimate is regulated to the origin.

For the first type of LQG failure, plots comparing the time history of true and estimated position vector components of the chaser are shown in Figure 5.11. It can be seen that, initially, the state estimate has converged on the true state but later the true state has diverged and the state estimate has been regulated to the origin. Plots of the

control vector components of the chaser are shown in Figure 5.12. It can be seen that the control history is not well-behaved. Plots comparing the filter errors with the $\pm 3\sigma$ standard deviation bounds are shown in Figure 5.13. It can be seen that the filter errors are large as a result of the true state diverging and are not within the $\pm 3\sigma$ standard-deviation bounds.

For the second type of LQG failure, plots comparing the time history of true and estimated position vector components of the chaser are shown in Figure 5.14. It can be seen that the state estimate never converges on the true state. The state estimate has been regulated to the origin but the true state has diverged. Plots of the control vector components of the chaser are shown in Figure 5.15. Plots comparing the filter errors with the $\pm 3\sigma$ standard deviation bounds are shown in Figure 5.16. It can be seen that the filter errors are large as a result of the true state diverging and are not within the $\pm 3\sigma$ standard-deviation bounds.

An attempt was made to understand why the LQG control fails for the high-weight case. When the simulation run time is extended to multiple periods of the chief orbit, it is seen that while the state estimate has been regulated to the origin, the true state is following a trajectory resembling an orbit described by homogeneous HCW equations with secular drift along y direction. For both types of LQG failure, this is demonstrated in Figures 5.17 and 5.18 respectively where plots comparing the time history of true and estimated position vector components of the chaser for simulation time equal to three periods of the chief orbit are shown. An insight into why the true state is following a trajectory resembling a homogeneous HCW trajectory may be gained by looking at the

homogeneous HCW dynamics and the LQG state estimator and true state dynamics. The homogeneous HCW dynamics is written as follows.

$$\dot{\mathbf{x}} = \mathbf{A}_{\mathrm{HCW}}\mathbf{x}$$

The LQG state estimator dynamics is written as follows.

$$\dot{\hat{\mathbf{x}}} = \mathbf{A}_{\mathrm{HCW}}\hat{\mathbf{x}} + \mathbf{B}\mathbf{u}_{\mathrm{LQG}} = \mathbf{A}_{\mathrm{HCW}}\hat{\mathbf{x}} - \mathbf{B}\mathbf{K}_c\hat{\mathbf{x}} = \mathbf{A}_{\mathrm{LQR}}\hat{\mathbf{x}} \tag{5.7}$$

Thus, the estimator dynamics is closed-loop and hence the state estimate is regulated to the origin. The LQG true state dynamics is written as follows.

$$\dot{\mathbf{x}} = \mathbf{A}_{\mathrm{HCW}}\mathbf{x} + \mathbf{B}\mathbf{u}_{\mathrm{LQG}} + \mathbf{w} = \mathbf{A}_{\mathrm{HCW}}\mathbf{x} - \mathbf{B}\mathbf{K}_c\hat{\mathbf{x}} + \mathbf{w} \tag{5.8}$$

The high magnitude of state weighting leads to high control input. This causes the state estimate to be regulated quickly to the origin making the term $\mathbf{B}\mathbf{K}_c\hat{\mathbf{x}}$ vanish quickly. This makes the true state dynamics follow a trajectory resembling an orbit described by homogeneous HCW equations.

For the LQG control implementing the nonlinear angles-only measurement model, the magnitude of state weighting in the performance criterion and hence the magnitude of control input has an effect on the performance of the EKF estimation. Whereas in the low-weight case the LQG control performs well and provides range observability, in the high-weight the LQG control fails. This failure can be attributed to the high control usage initially. Thus, in the case of nonlinear LQG control, the processes of efficient control and reliable estimation are coupled. There is a need for a control strategy which attempts to address this coupling between the control and estimation processes such that, initially, the control usage is reasonable and the two processes work in sync. Two such strategies are explored in the next chapter.

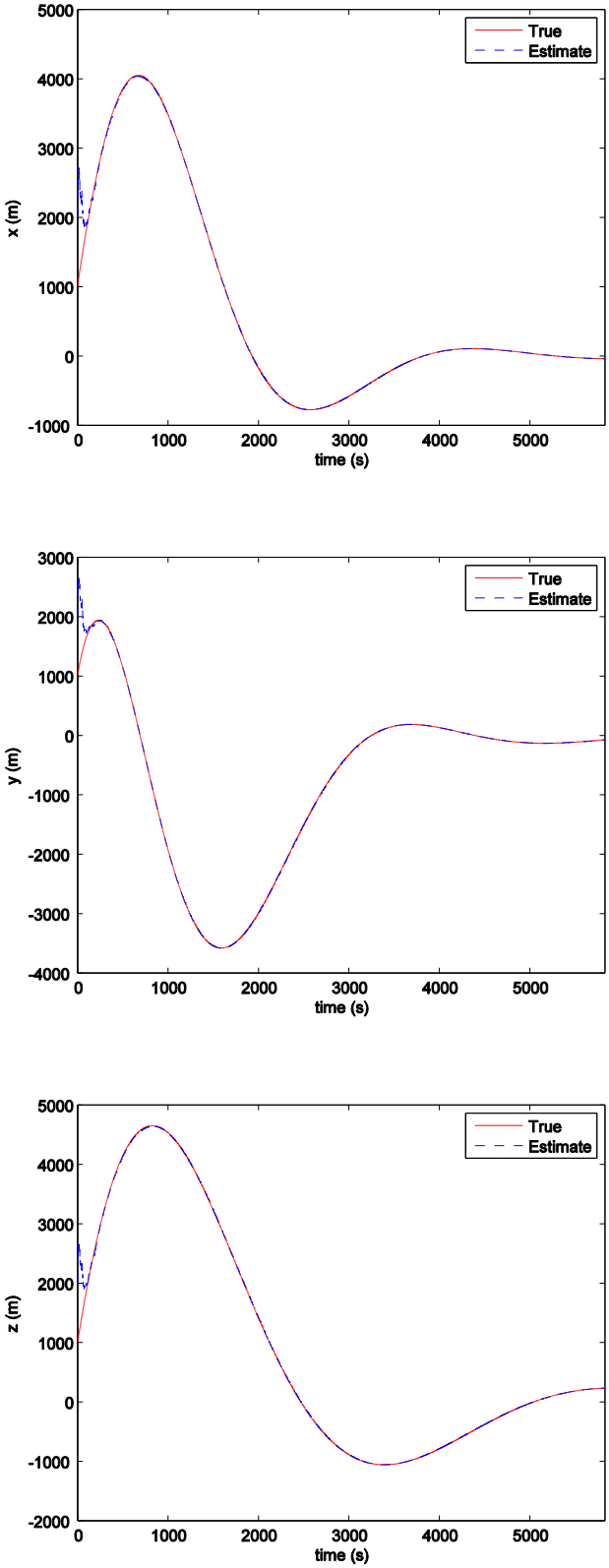

Figure 5.8: Nonlinear LQG Low-Weight Case: Position Vector Components

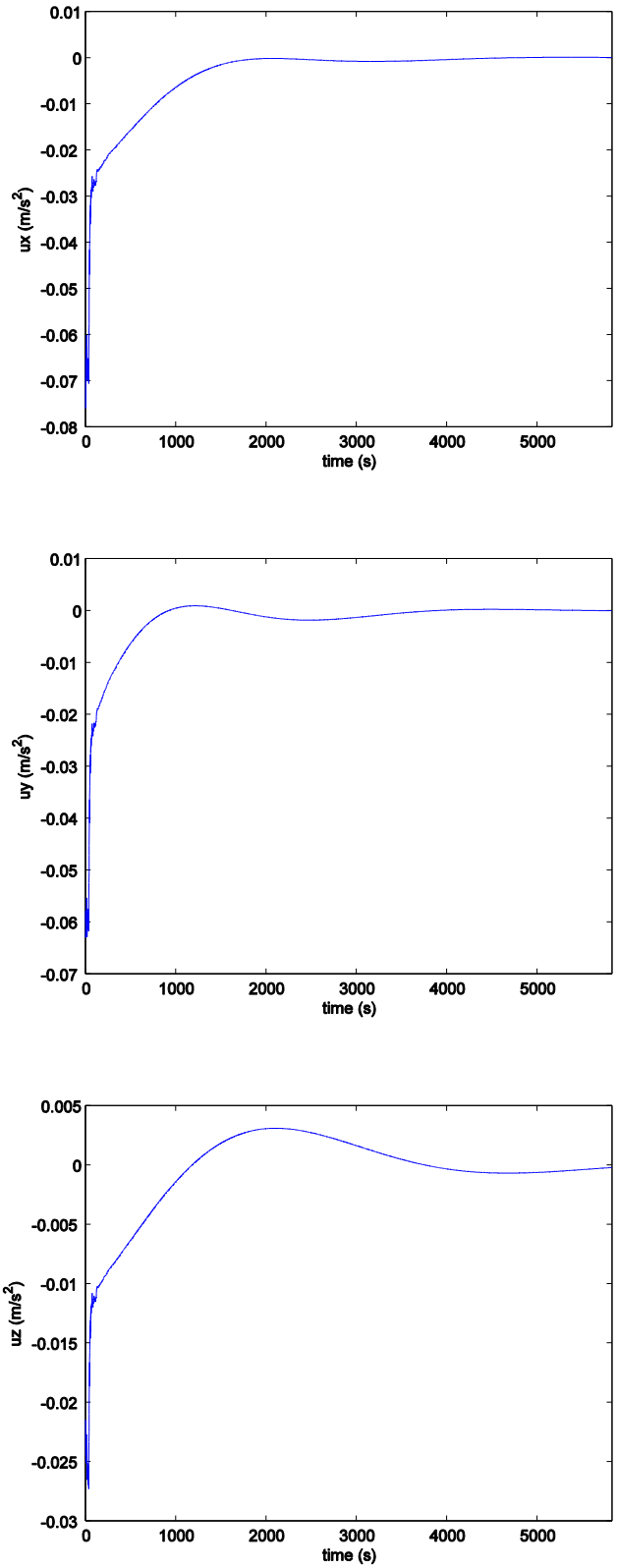

Figure 5.9: Nonlinear LQG Low-Weight Case: Control Vector Components

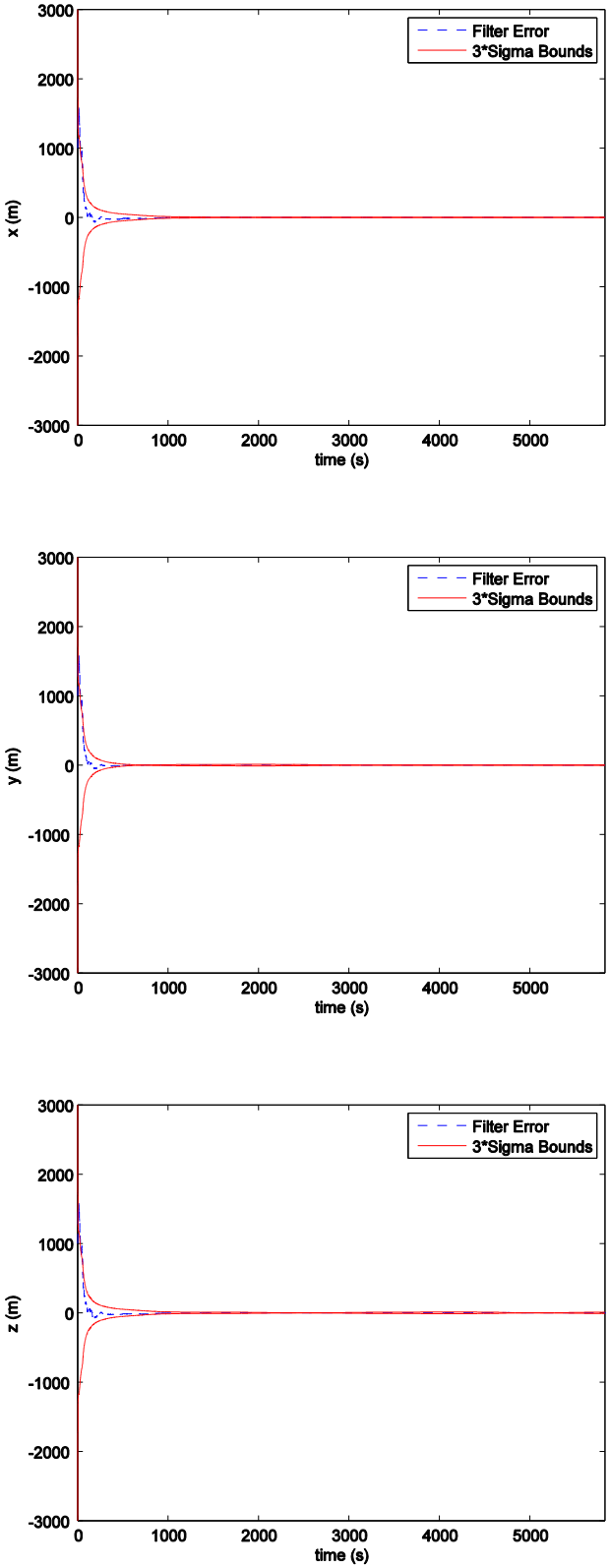

Figure 5.10: Nonlinear LQG Low-Weight Case: Filter Error and 3-σ Bounds

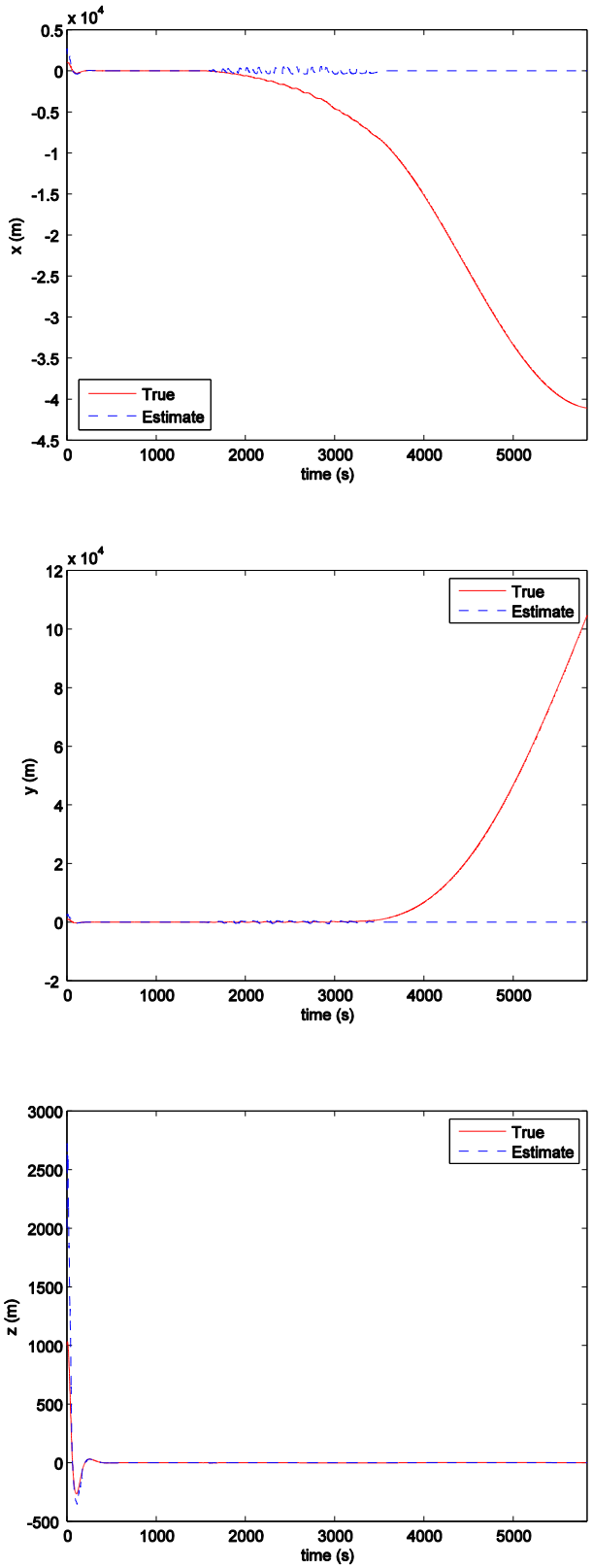

Figure 5.11: Nonlinear LQG High-Weight Case Type 1: Position Vector Components

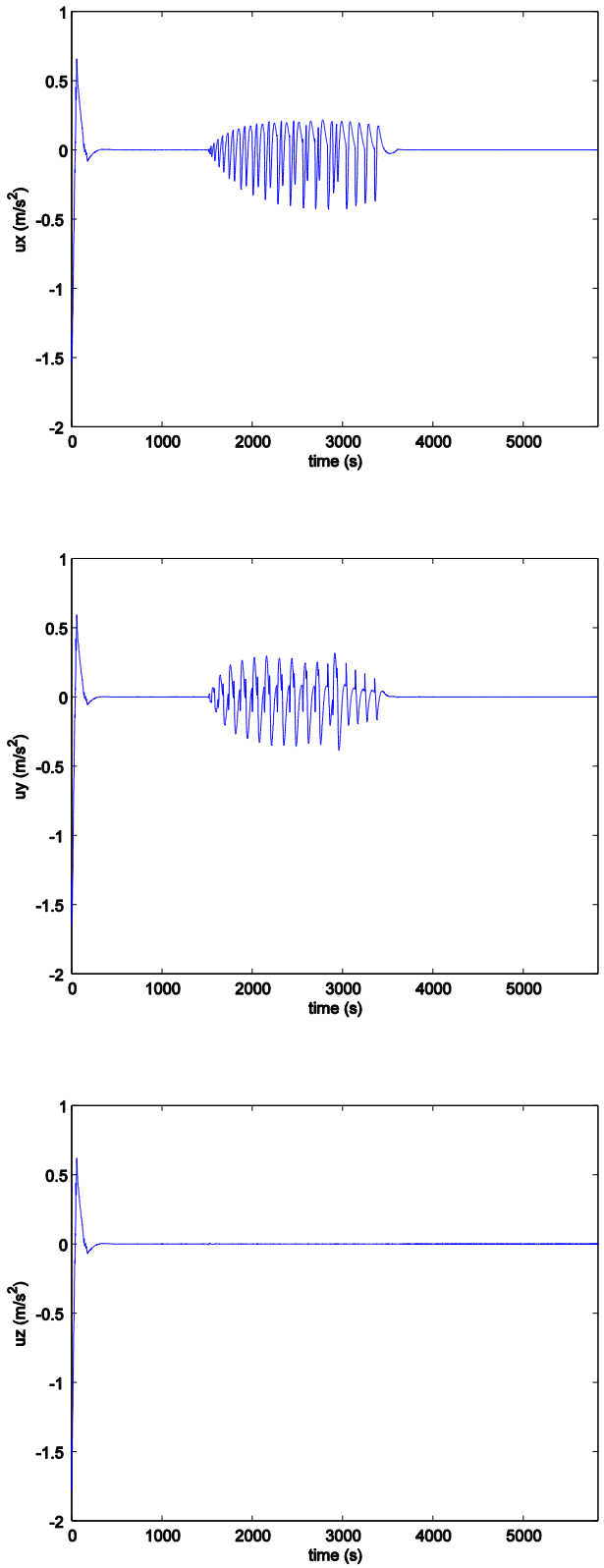

Figure 5.12: Nonlinear LQG High-Weight Case Type 1: Control Vector Components

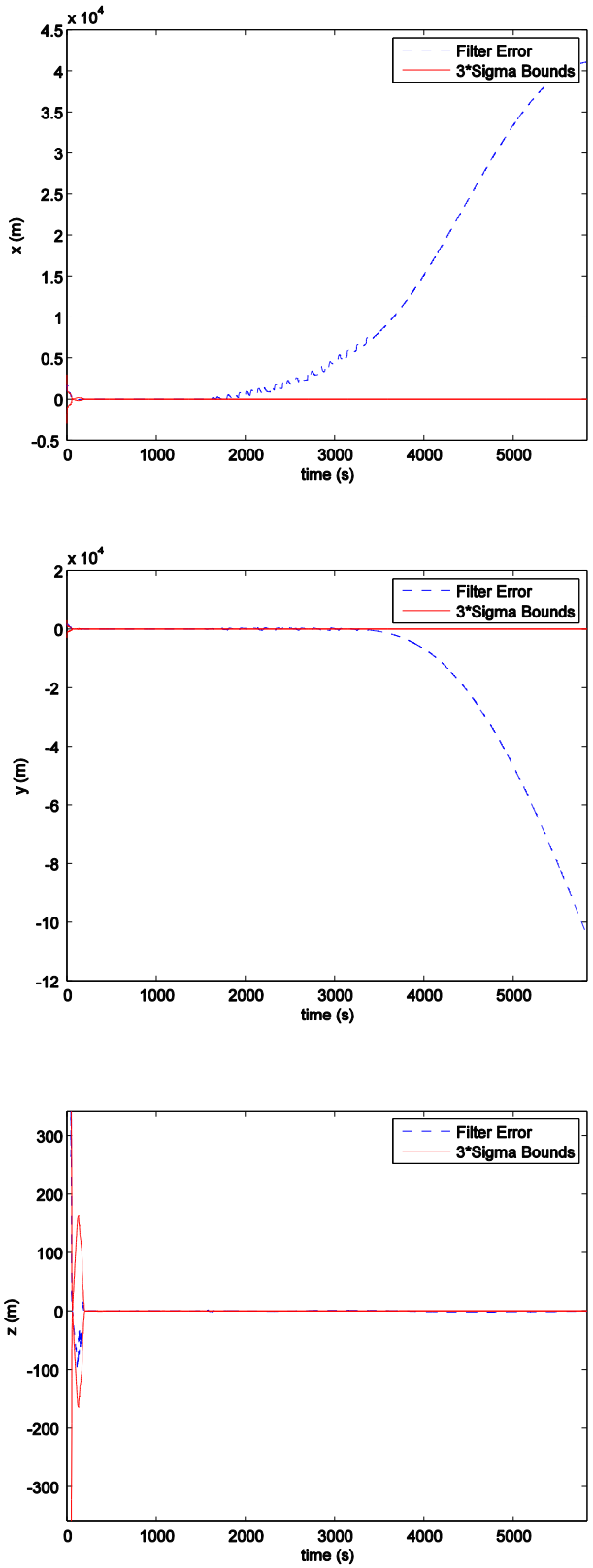

Figure 5.13: Nonlinear LQG High-Weight Case Type 1: Filter Error and 3-σ Bounds

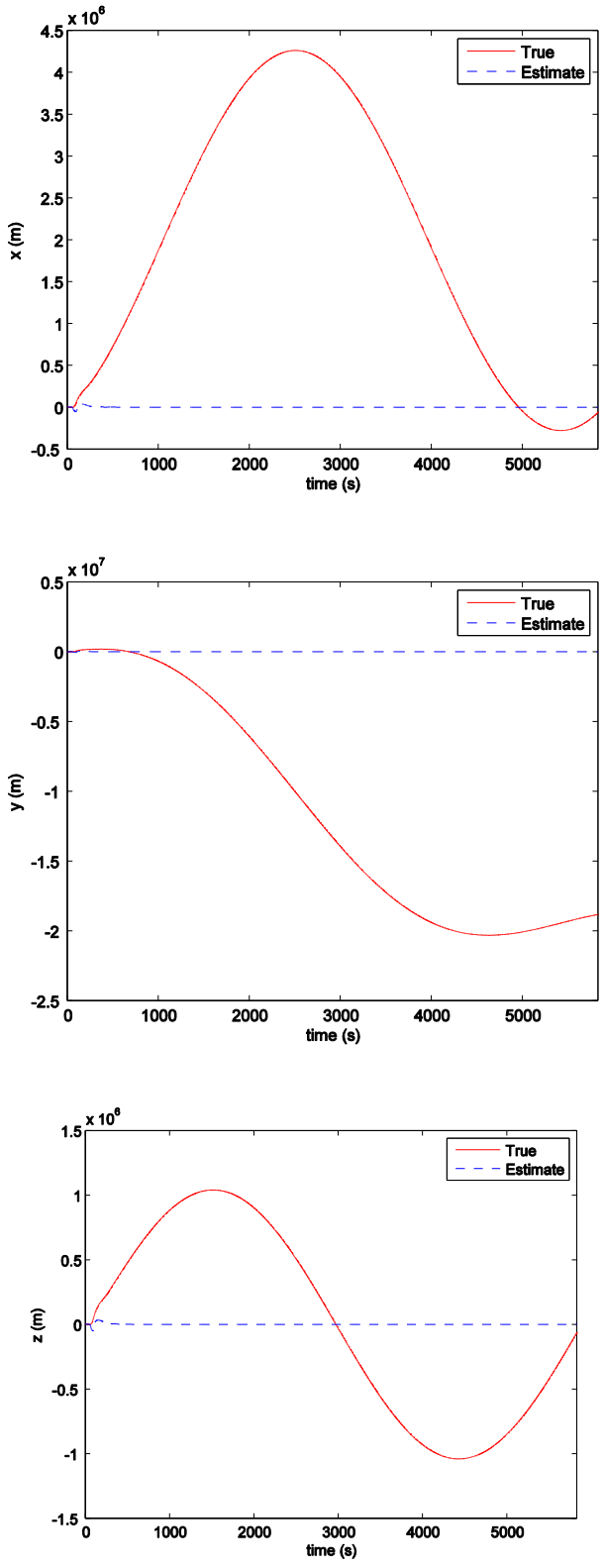

Figure 5.14: Nonlinear LQG High-Weight Case Type 2: Position Vector Components

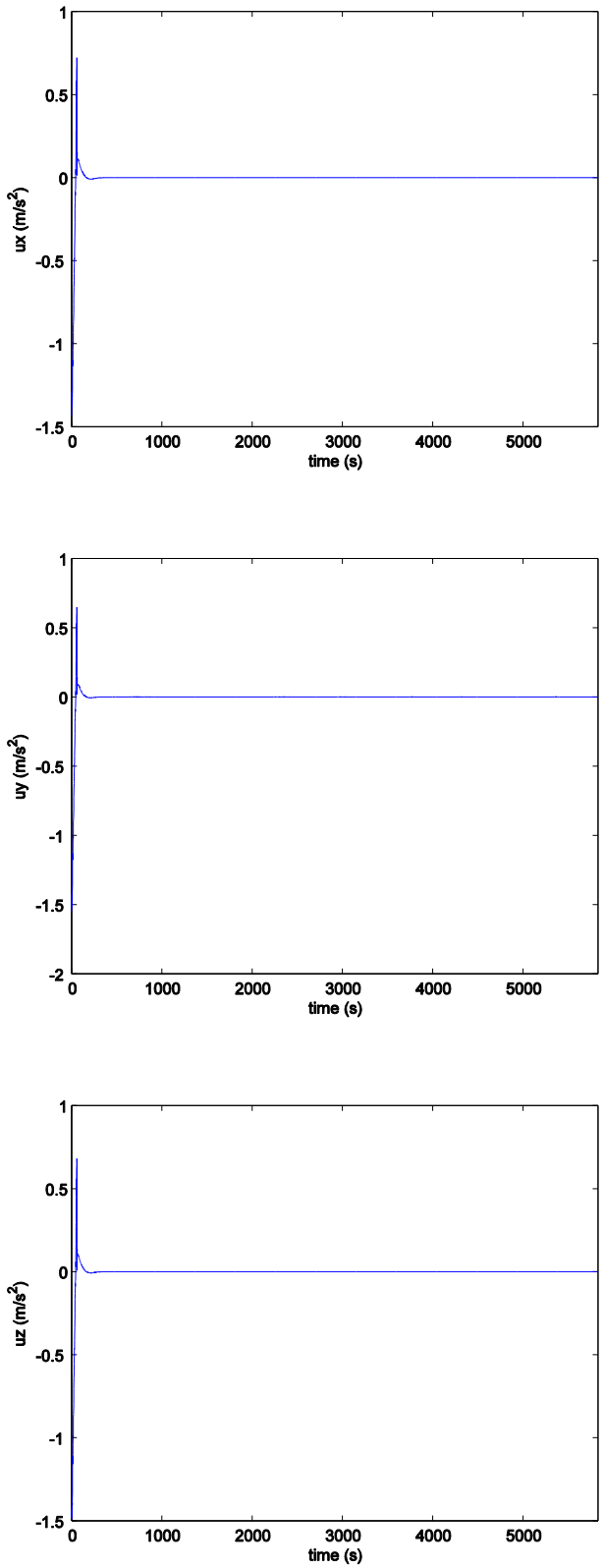

Figure 5.15: Nonlinear LQG High-Weight Case Type 2: Control Vector Components

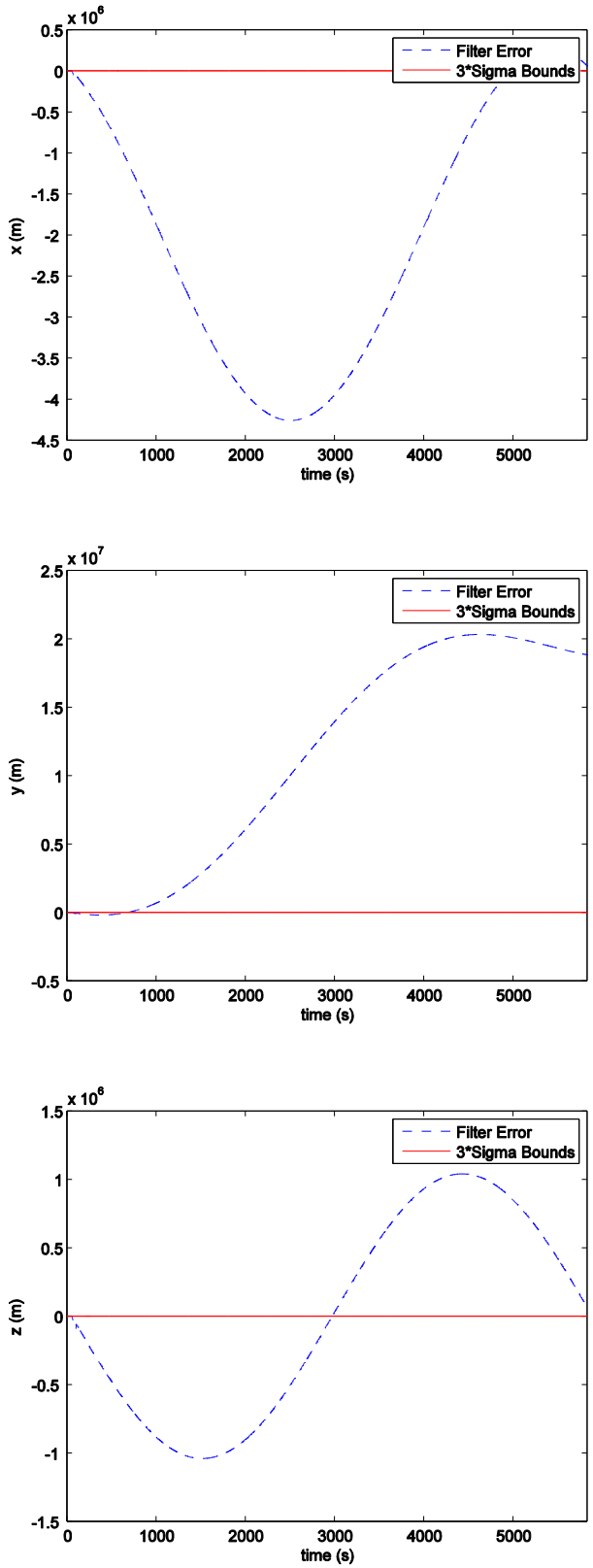

Figure 5.16: Nonlinear LQG High-Weight Case Type 2: Filter Error and 3-σ Bounds

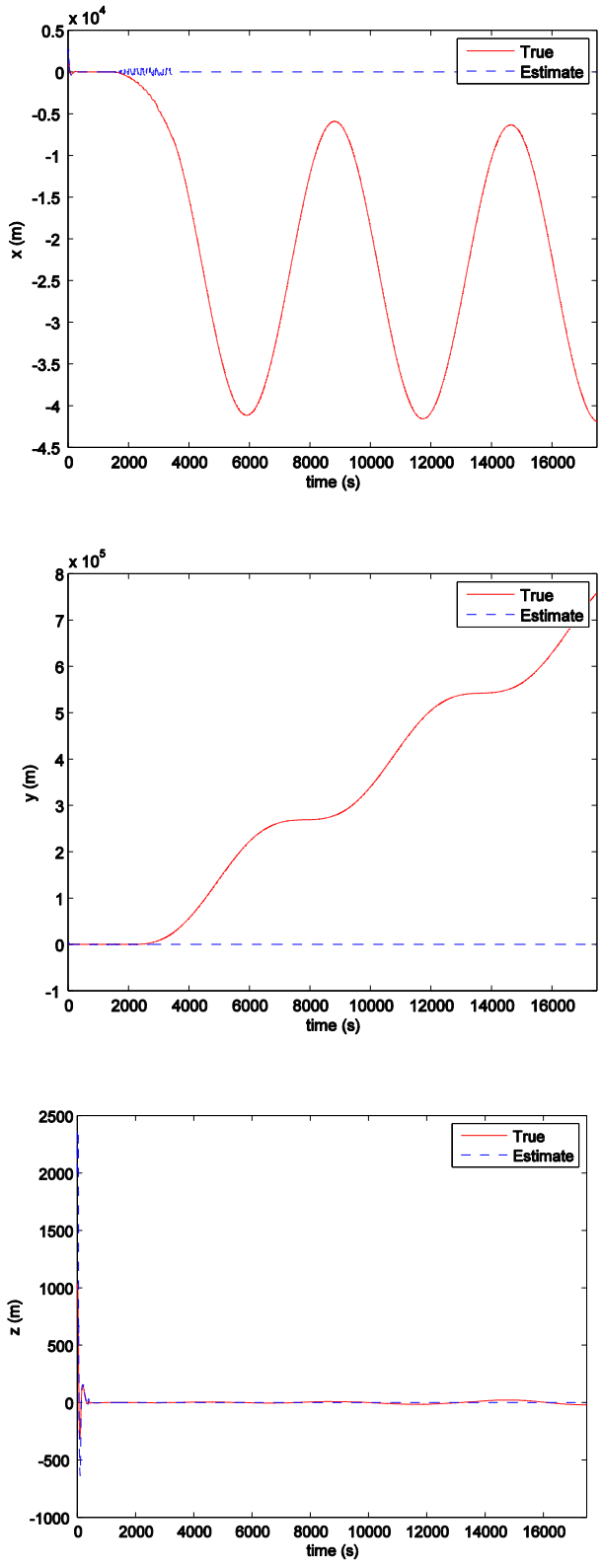

Figure 5.17: Nonlinear LQG High-Weight Case Type 1: Position Vector Components for 3 Orbits of Chief

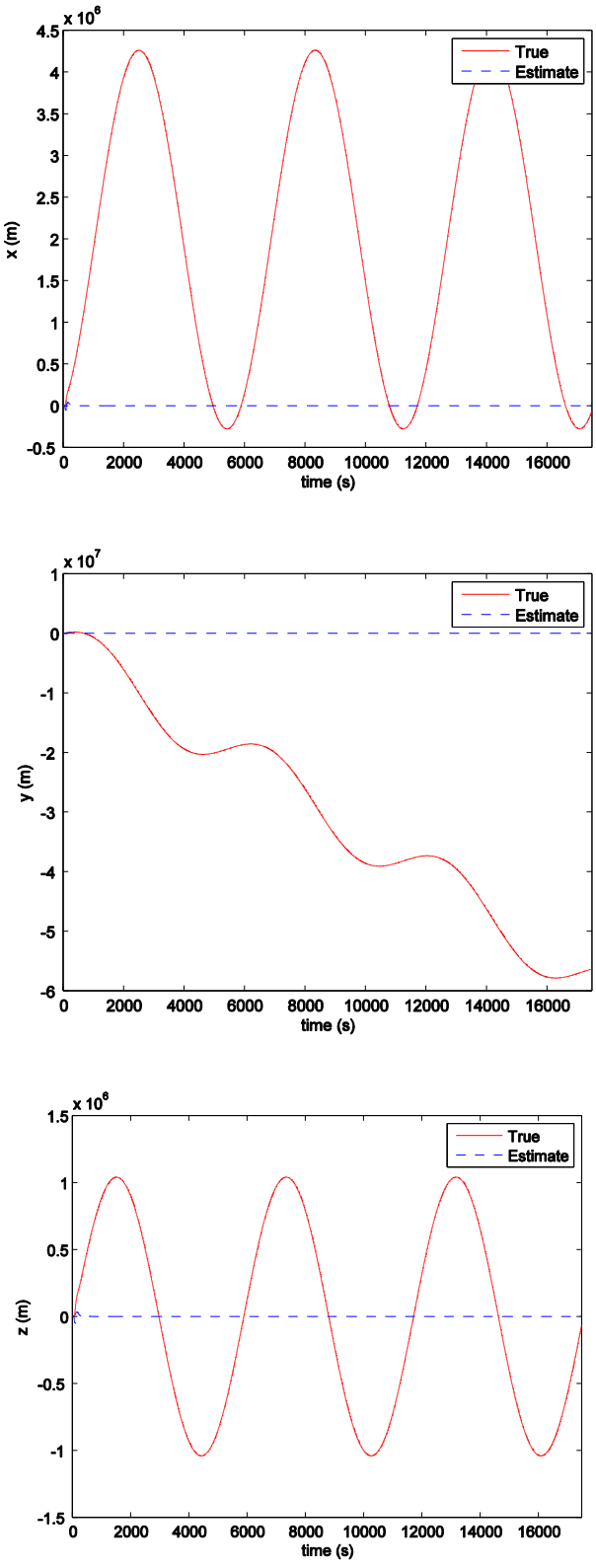

Figure 5.18: Nonlinear LQG High-Weight Case Type 2: Position Vector Components for 3 Orbits of Chief

CHAPTER 6

SPACECRAFT RELATIVE MOTION CONTROL USING ANGLES-ONLY NAVIGATION: DUAL CONTROL AND INFORMATION-WEIGHTD LQG

This chapter explores two approaches to address the coupling between the processes of efficient control and reliable estimation in the LQG control implementing the nonlinear angles-only measurement model. The first approach, an existing one in the dual control theory literature, is the linear quadratic dual control method. Problems involving coupling between the control and estimation processes are often addressed using the dual control theory. There are two common dual control methods found in the literature.[40] The first method is to add a perturbation signal or a probing input to improve the observability of the system.

$$\mathbf{u}_{\text{new}} = \mathbf{u}_{\text{LQR}} + \mathbf{u}_{\text{obs}} \tag{6.1}$$

The second method is to form a cost function that is a sum of the standard LQR cost and a term that penalizes the uncertainty in the system.

$$\mathrm{J}_{\text{new}} = \mathrm{J}_{\text{LQR}} + \mathrm{J}_{\text{obs}} \tag{6.2}$$

The first method is heuristic-based and the second one requires computationally expensive methods for solution such as dynamic programming or search-based techniques. Thus, these methods are often not feasible for on-board applications. An alternative dual control method was explored in Reference 41 and was applied to the automatic docking problem for an unmanned wheeled rover with a monocular vision

sensor. This method augments the state of the system to include uncertainty states. The LQR cost function is also augmented to include a quadratic function of the uncertainty states which penalizes the uncertainty in the system state. The control input then consists of two parts. One control input regulates the system state while the other attempts to reduce the uncertainty in the system state estimate. This method is known as the linear quadratic dual control approach. An attractive feature of this approach, as the name suggests, is that the new augmented problem has linear-quadratic-like structure and hence this approach is chosen in this dissertation.

The second approach is the information-weighted LQG control method which is a new approach explored in this dissertation. The information-weighted LQG control approach differs from the LQG control of previous chapter in the manner in which the state weighting matrices are chosen. In the LQG control of previous chapter, both the low state weighting and the high state weighting matrices were constant. The state weighting matrix in the information-weighted LQG control approach is not constant and is dependent on the accuracy of the state estimate. The Fisher information matrix is used for this purpose such that as the accuracy of the state estimate increases the state weighting becomes higher.

LINEAR QUADRATIC DUAL CONTROL

The linear quadratic dual (LQD) control approach uses the continuous-time form of the EKF. The equation for the state estimate covariance matrix can be given as follows.

$$\dot{\mathbf{P}}_{\mathrm{e}} = \mathbf{P}_{\mathrm{e}}\mathbf{A}^{\mathrm{T}}{}_{\mathrm{HCW}} + \mathbf{A}_{\mathrm{HCW}}\mathbf{P}_{\mathrm{e}} + \mathbf{Q}_{\mathrm{w}} - \mathbf{P}_{\mathrm{e}}\mathbf{H}^{\mathrm{T}}\mathbf{R}_{\mathrm{v}}{}^{-1}\mathbf{H}\mathbf{P}_{\mathrm{e}} \tag{6.3}$$

Matrix $\mathbf{P}_e$ can be written as $\mathbf{P}_e = \mathbf{S}\mathbf{S}^T$. The matrix $\mathbf{S}$ is set to be in lower triangular form.

$$\mathbf{S} = \begin{bmatrix} s_{11} & 0 & 0 & \dots & 0 \\ s_{21} & s_{22} & 0 & \dots & 0 \\ s_{31} & s_{32} & s_{33} & \dots & 0 \\ \vdots & \vdots & \vdots & \ddots & 0 \\ s_{n1} & s_{n2} & s_{n3} & \dots & s_{nn} \end{bmatrix} \tag{6.4}$$

The nonlinear matrix differential equation for $\mathbf{S}$ can be obtained from the differential equation for $\mathbf{P}_e$ and after some simple algebra is given as follows.

$$\dot{\mathbf{S}} = \left(\mathbf{A}_{HCW} - \frac{1}{2}\mathbf{S}\mathbf{S}^T\mathbf{H}^T{\mathbf{R}_d}^{-1}\mathbf{H}\right)\mathbf{S} + \frac{1}{2}\mathbf{Q}_d\mathbf{S}^{-T} \tag{6.5}$$

A couple of issues with Equation (6.5) deserve mention. The first, as stated in Reference 41, is the need for careful treatment when propagating $\mathbf{S}$ in time because $\dot{\mathbf{S}}$ may not be lower triangular even though $\mathbf{S}$ is. In this dissertation, the same method given in Reference 41 is implemented for computing $\dot{\mathbf{S}}$ in a lower triangular form.

The second is of inconsistent matrix dimensions which may arise due to choice of matrices $\mathbf{Q}_d$ and $\mathbf{R}_d$. Since the $\dot{\mathbf{S}}$ equation is derived from the $\dot{\mathbf{P}}_e$ equation, matrices $\mathbf{Q}_d$ and $\mathbf{R}_d$ should technically be the noise covariance matrices $\mathbf{Q}_w$ and $\mathbf{R}_v$. However, in Reference 37 matrices $\mathbf{Q}_d$ and $\mathbf{R}_d$ are chosen to be the state and control weighting matrices $\mathbf{Q}_c$ and $\mathbf{R}_c$. This choice seems curious because of the inconsistency in matrix dimensions that may arise. In order for Equation (6.5) to be dimensionally consistent, matrix $\mathbf{R}_d$ must have the same dimensions as that of matrix $\mathbf{R}_v$. So in order to choose $\mathbf{R}_d = \mathbf{R}_c$, matrix $\mathbf{R}_c$ must have the same dimensions as that of matrix $\mathbf{R}_v$ which is not true for every problem. For the problem addressed in Reference 37, matrix $\mathbf{R}_c$ has the same dimensions as that of matrix $\mathbf{R}_v$, so the issue of inconsistent matrix dimensions does not arise. However, for the problem addressed in this dissertation, measurement model is 2-dimensional and control vector is 3-dimesional which leads to the issue of

inconsistent matrix dimensions. However, $\mathbf{Q}_d$ and $\mathbf{R}_d$ may also be treated as tuning parameters[42], and in this dissertation matrices are chosen after trial and error.

The nonzero elements of $\mathbf{S}$ can be written as a vector. For an n-dimensional system this vector has $\frac{n(n+1)}{2}$ elements.

$$\mathbf{y} = [s_{11} \quad s_{21} \quad \dots \quad s_{nn}]^T, \qquad \dot{\mathbf{y}} = [\dot{s}_{11} \quad \dot{s}_{21} \quad \dots \quad \dot{s}_{nn}]^T, \qquad \dot{s}_{ij} = \dot{\mathbf{S}}(i,j)$$

The augmented state vector can be written as follows.

$$\mathbf{x}_a = \begin{bmatrix} \mathbf{x} \\ \mathbf{y} \end{bmatrix}$$

The augmented LQR cost function can be written as follows.

$$J_{LQD} = \frac{1}{2}\int_{t_0}^{\infty} \left(\mathbf{x}^T(t)\mathbf{Q}_c\mathbf{x}(t) + \mathbf{u}^T(t)\mathbf{R}_c\mathbf{u}(t) + \mathbf{y}^T(t)\mathbf{Q}_y\mathbf{y}(t)\right)dt$$

The augmented cost function can be written in terms of the augmented state as follows.

$$J_{LQD} = \frac{1}{2}\int_{t_0}^{\infty} \left(\mathbf{x}_a{}^T(t)\mathbf{Q}_a\mathbf{x}_a(t) + \mathbf{u}^T(t)\mathbf{R}_c\mathbf{u}(t)\right)dt, \qquad \mathbf{Q}_a = \begin{bmatrix} \mathbf{Q}_c & \mathbf{0} \\ \mathbf{0} & \mathbf{Q}_y \end{bmatrix} \tag{6.6}$$

The augmented control problem is as follows.

Minimize: $$J_{LQD} = \frac{1}{2}\int_{t_0}^{\infty} \left(\mathbf{x}_a{}^T(t)\mathbf{Q}_a\mathbf{x}_a(t) + \mathbf{u}^T(t)\mathbf{R}_c\mathbf{u}(t)\right)dt$$

Subject to: $$\dot{\mathbf{x}}_a = \begin{bmatrix} \dot{\mathbf{x}} \\ \dot{\mathbf{y}} \end{bmatrix} = \mathbf{f}_a(\mathbf{x}_a) + \mathbf{B}_a\mathbf{u}, \qquad \mathbf{B}_a = \begin{bmatrix} \mathbf{B} \\ \mathbf{0}_{\frac{n(n+1)}{2}\times 3} \end{bmatrix}$$

Even though the dynamics for $\mathbf{x}$ were linear, $\mathbf{y}$ obeys nonlinear dynamics. The sub-optimal full-state feedback control law is given as follows.

$$\mathbf{u}_{LQD}(t) = -\mathbf{R}_c{}^{-1}\mathbf{B}_a{}^T\mathbf{P}_a\mathbf{x}_a(t) = -\mathbf{K}_a\mathbf{x}_a(t) = -\mathbf{K}_x\mathbf{x} - \mathbf{K}_y\mathbf{y}, \qquad \mathbf{K}_a = [\mathbf{K}_x \; \mathbf{K}_y] \tag{6.7}$$

MATLAB function "*lqr*" is used to solve for $\mathbf{K}_a$. The full-state feedback control law can then be implemented using the state estimate.

$$\mathbf{u}_{\mathrm{LQD}}(t) = -\mathbf{K}_x\hat{\mathbf{x}} - \mathbf{K}_y\mathbf{y} \tag{6.8}$$

The symmetric matrix $\mathbf{P}_a$ is obtained by solving the ARE at each time step.

$$\mathbf{A}_a{}^T\mathbf{P}_a + \mathbf{P}_a\mathbf{A}_a + \mathbf{Q}_a - \mathbf{P}_a\mathbf{B}_a\mathbf{R}_c{}^{-1}\mathbf{B}_a{}^T\mathbf{P}_a = \mathbf{0}, \qquad \mathbf{A}_a = \left.\frac{\partial \mathbf{f}_a}{\partial \mathbf{x}_a}\right|_{\mathbf{x}_a} \tag{6.9}$$

Thus, the LQD control approach is quasi-LQG as it requires numerically solving the nonlinear differential equation for **S**. The augmented control problem is solved as an LQR control problem where the system matrix is obtained by taking the partial derivative of the nonlinear dynamics.

INFORMATION-WEIGHTED LQG CONTROL

The LQG control implementing the nonlinear angles-only measurement model in the previous chapter worked for the constant low state weighting case and failed for the constant high state weighting case. Thus, a scheme where the state weighting is not constant but increases gradually from low to high is sought. The information-weighted LQG (IWLQG) control approach is such that the state weighting is dependent on the accuracy of the state estimate. The Fisher information matrix (FIM), which is the inverse of the state estimation covariance matrix ($\mathbf{P}_e{}^{-1}$), is used for this purpose. Thus, initially when the accuracy of the state estimate is low, the state weighting is also low. This leads to small control input. As the state estimate gets better as a result of the filtering process, the state weighting increases which leads to higher control input causing faster state regulation. At each time step of propagation the state weighting matrix $\mathbf{Q}_{\mathrm{IW}}$ is chosen to

be a function of the instantaneous FIM. The matrix $\mathbf{Q}_{IW}$ at each time step is defined as follows.

$$\mathbf{Q}_{IW} = \mathbf{V}\frac{q}{\pi}\begin{bmatrix} \tan^{-1}\lambda_1 & 0 & 0 & 0 & 0 & 0 \\ 0 & \tan^{-1}\lambda_2 & 0 & 0 & 0 & 0 \\ 0 & 0 & \tan^{-1}\lambda_3 & 0 & 0 & 0 \\ 0 & 0 & 0 & \tan^{-1}\lambda_4 & 0 & 0 \\ 0 & 0 & 0 & 0 & \tan^{-1}\lambda_5 & 0 \\ 0 & 0 & 0 & 0 & 0 & \tan^{-1}\lambda_6 \end{bmatrix}\mathbf{V}^T \quad (6.10)$$

Here, $\mathbf{V}$ matrix contains the eigenvectors of the FIM and $\lambda_1, \ldots, \lambda_6$ are the eigenvalues of the FIM. Parameter q is varied for varying state weighting. The inverse tangent function facilitates smooth transition from low state weighting to high state weighting.

NUMERICAL EXAMPLES

Linear Quadratic Dual Control

MATLAB simulations are performed for LQD control approach with low as well as high state weighting. As mentioned earlier, the LQD control approach uses continuous-time form of the EKF. A time step 0.1 seconds is used for propagation. Various parameters used in the simulations are given in Table 6.1.

For the low state weighting LQD control, plots comparing the time history of true and estimated position vector components of the chaser are shown in Figure 6.1. It can be seen that, by the end of the simulation time, the state has been regulated very close to the origin and that the state estimate has converged on the true state. Plots of the control vector components of the chaser are shown in Figure 6.2. Spikes in the control history should be noted. Plots comparing the filter errors with the $\pm 3\sigma$ standard deviation bounds are shown in Figure 6.3. It can be seen that, at all times, the filter errors are within the $\pm 3\sigma$ standard-deviation bounds indicating range observability.

Parameter	Value
r_c (km)	7000
Low Weight $\mathbf{Q}_a$	$\mathbf{I}_{27\times27}$
High Weight $\mathbf{Q}_a$	$\mathbf{I}_{27\times27} \times 10^2$
$\mathbf{R}_c$	$\mathbf{I}_{3\times3} \times 10^{11}$
Process Noise σ_p (m/s^2)	10^{-4}
Process Noise $\mathbf{Q}_w$	$\begin{bmatrix} \mathbf{0}_{3\times3} & \mathbf{0}_{3\times3} \\ \mathbf{0}_{3\times3} & \mathbf{I}_{3\times3} \end{bmatrix} \times {\sigma_p}^2$
Nonlinear Measurement Model σ_n (rad)	10^{-1}
Nonlinear Measurement Model $\mathbf{R}_v$	$\mathbf{I}_{2\times2} \times {\sigma_n}^2$
$\mathbf{Q}_d$	$\mathbf{I}_{6\times6}$
$\mathbf{R}_d$	$\mathbf{I}_{2\times2}$
$\mathbf{x}_0$	[1000 1000 1000 10 10 10]
$\hat{\mathbf{x}}_0$	$2\mathbf{x}_0$
$\mathbf{P}_{e,0}$	$[\hat{\mathbf{x}}_0 - \mathbf{x}_0]^T[\hat{\mathbf{x}}_0 - \mathbf{x}_0]$

Table 6.1: LQD Control Simulation Parameters

For the high state weighting LQD control, plots comparing the time history of true and estimated position vector components of the chaser are shown in Figure 6.4. It can be seen that the state has been regulated to the origin quicker compared to the low state weighting case and that the state estimate has converged on the true state. Plots of the control vector components of the chaser are shown in Figure 6.5. Spikes in the control history should be noted. Plots comparing the filter errors with the $\pm 3\sigma$ standard deviation bounds are shown in Figure 6.6. It can be seen that, at all times, the filter errors are within the $\pm 3\sigma$ standard-deviation bounds indicating range observability. Thus, the LQD control has addressed the coupling between the control and estimation processes.

It should be noted that the simulation time for high state weighting case is not one complete orbit of the chief. This is due to the failure of the MATLAB "*lqr*" function at that time. Although, by this time the state has been regulated to the origin, the MATLAB solver fails to further solve the augmented control problem. The error given by MATLAB indicates that, at that time, the solver failed to stabilize the system.

Although the LQD control has made the control and estimation processes work in sync, it may be limited in terms of direct application to angles-only orbital navigation problem. The dynamics associated with orbital motion makes the problem more complex than the problem studied in Reference 41. Solving the dual control problem is computationally intensive. The control history is not particularly well behaved and the spikes in control history could not be pinpointed. All these issues may make potential use of the LQD control method in a real-time feedback system questionable.

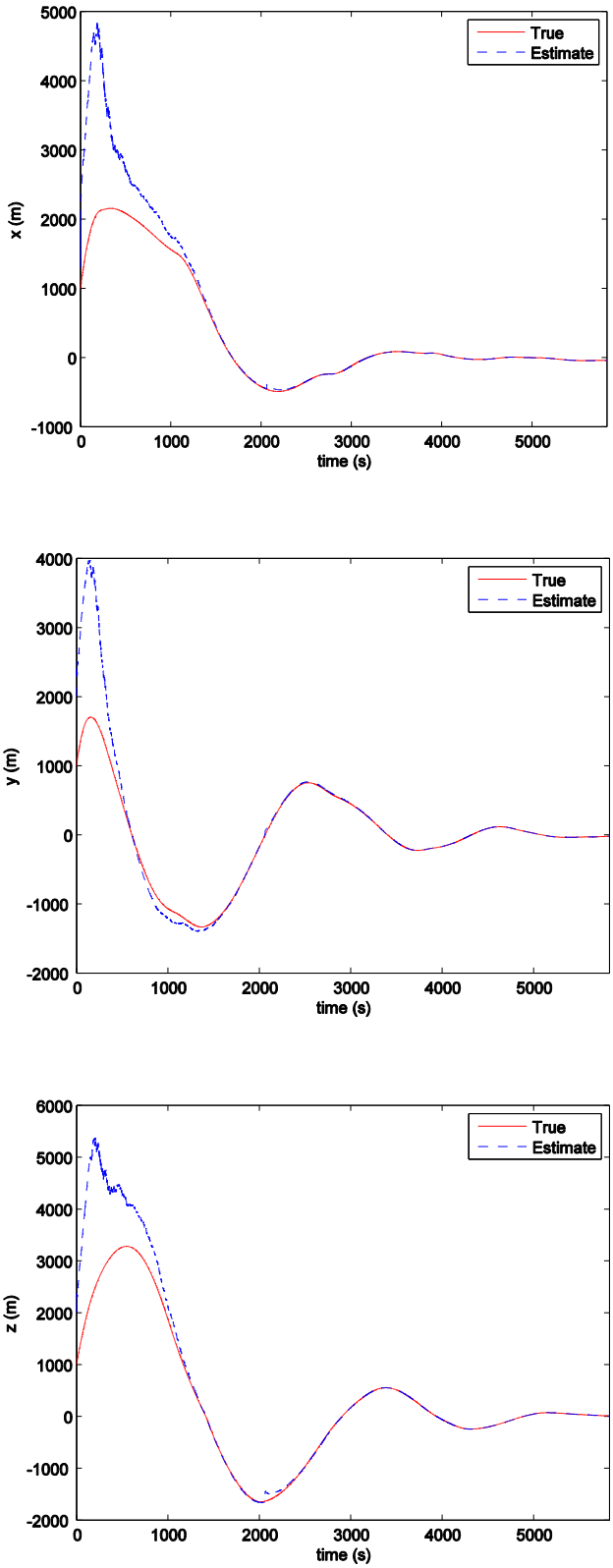

Figure 6.1: LQD Low Weight Case: Position Vector Components

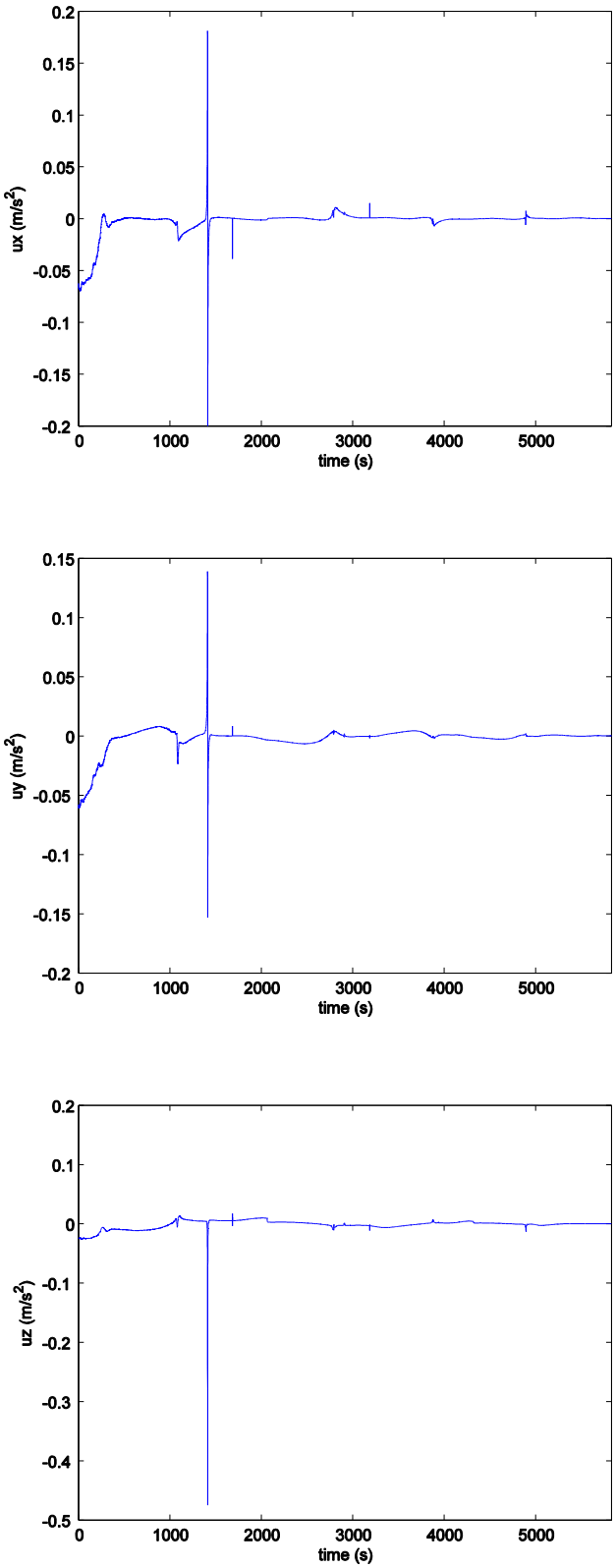

Figure 6.2: LQD Low Weight Case: Control Vector Components

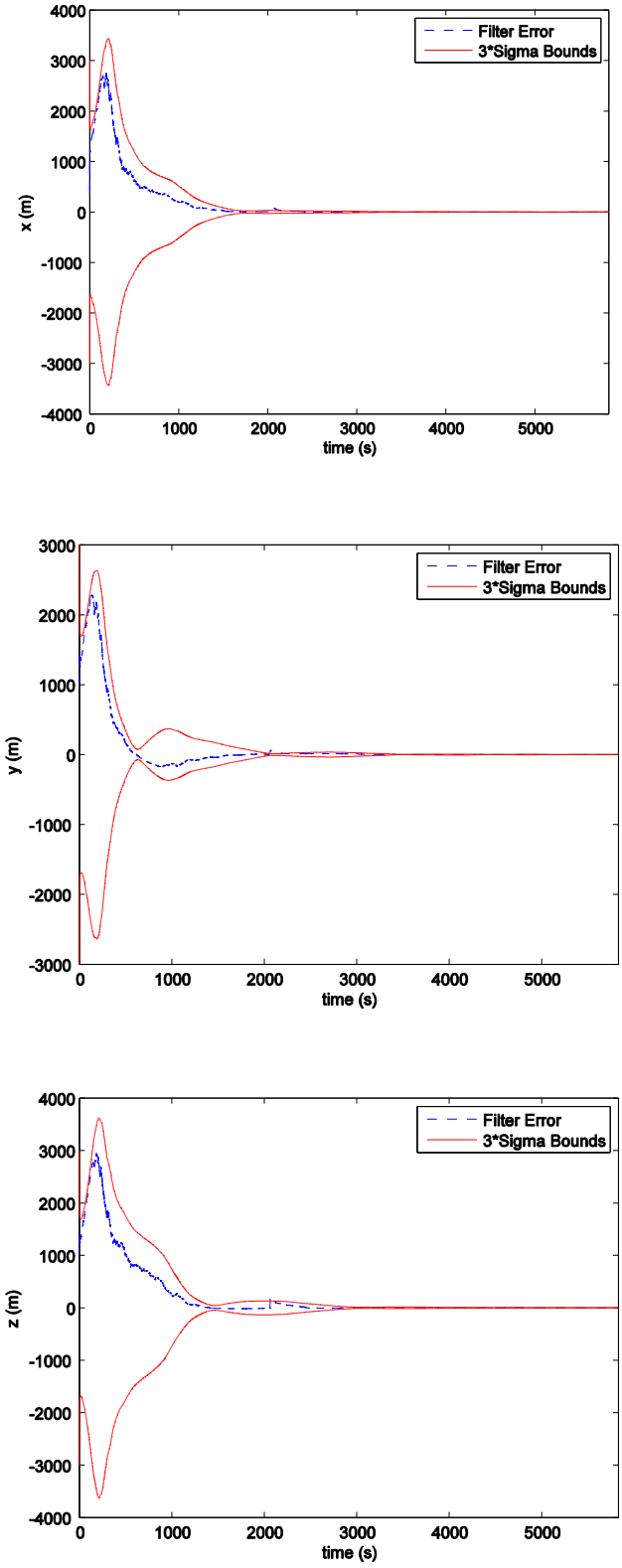

Figure 6.3: LQD Low Weight Case: Filter Error and 3-σ Bounds

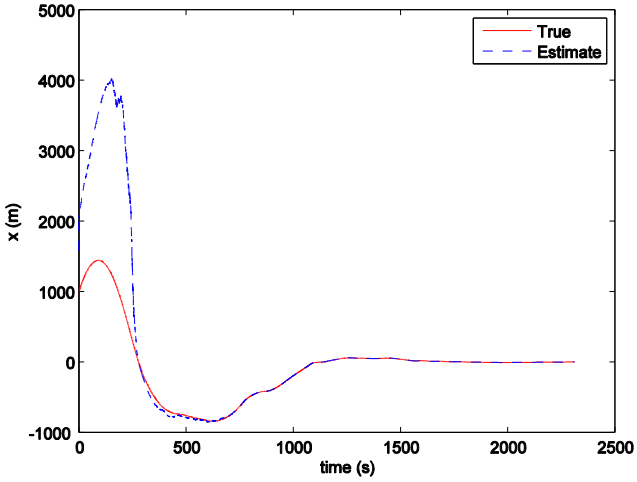

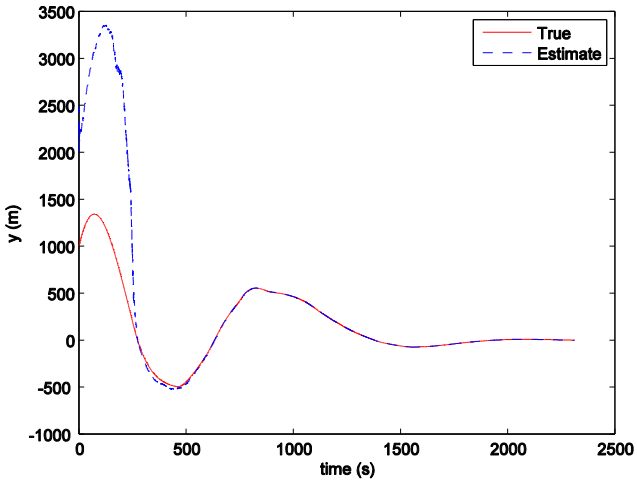

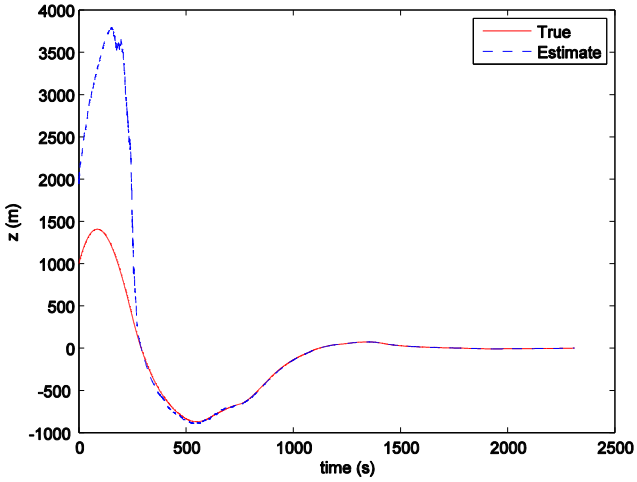

Figure 6.4: LQD High Weight Case: Position Vector Components

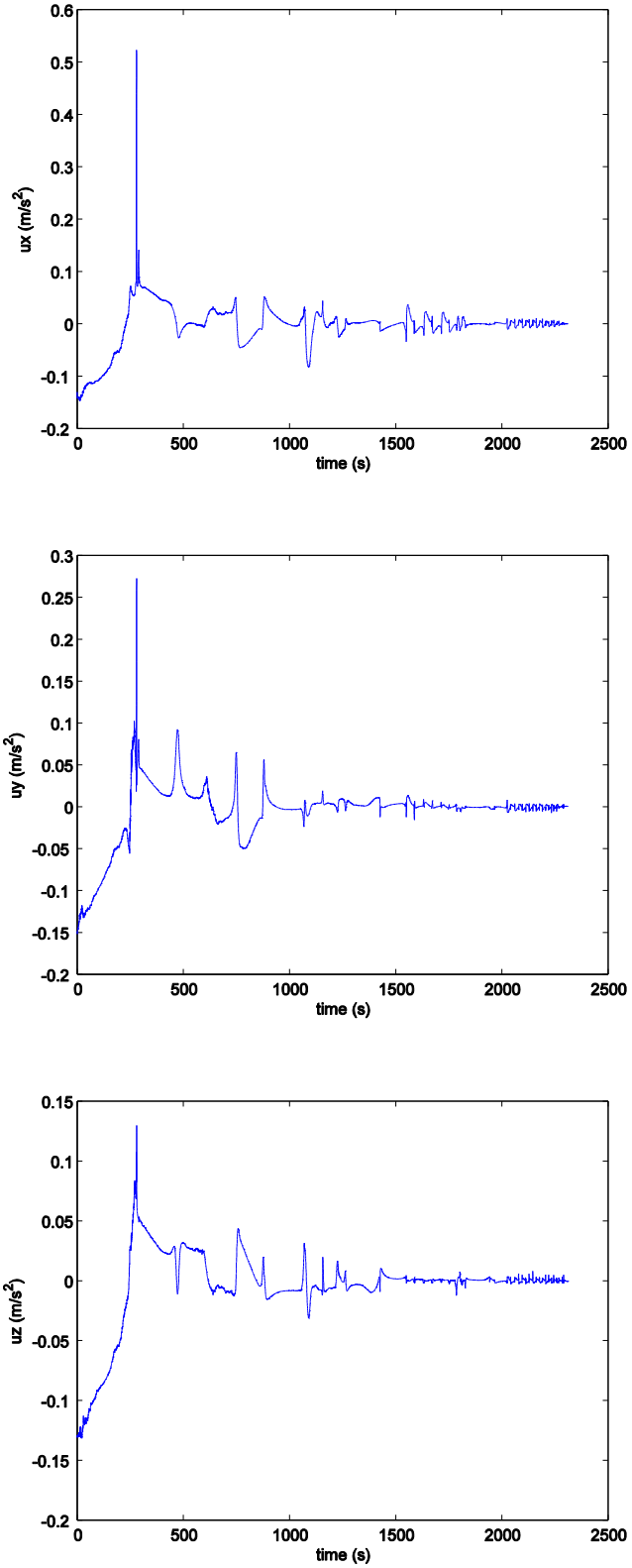

Figure 6.5: LQD High Weight Case: Control Vector Components

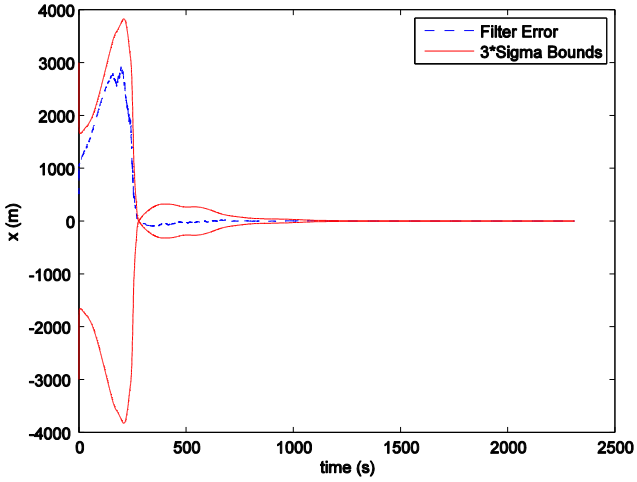

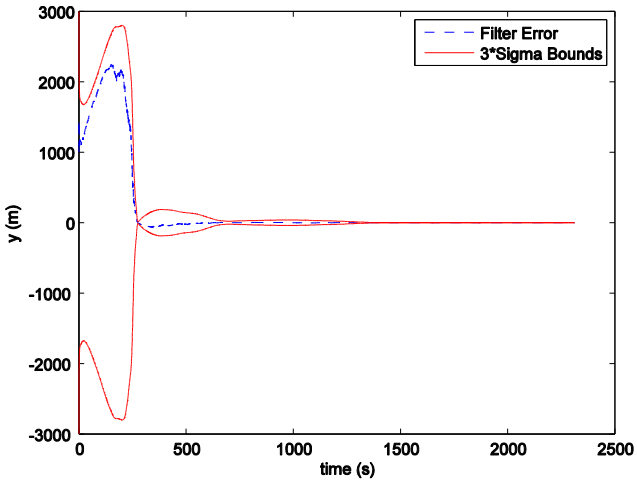

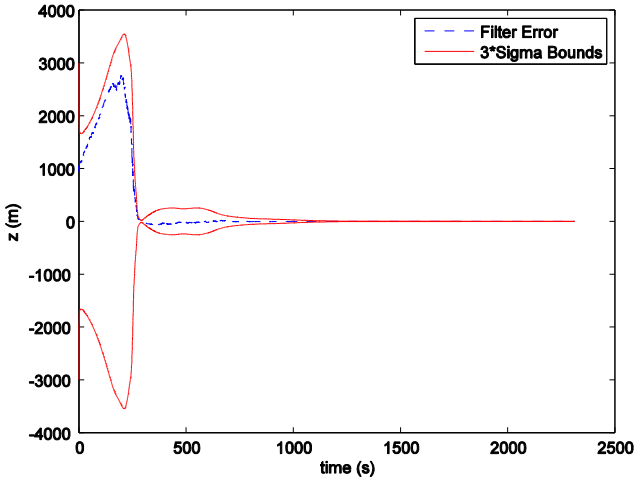

Figure 6.6: LQD High Weight Case: Filter Error and 3-σ Bounds

Information-Weighted LQG Control

MATLAB simulations are performed for IWLQG control approach for two values of q. The IWLQG control approach uses continuous-discrete form of the EKF. A time step of 1 second is used for propagation. Various parameters used in the simulations are given in Table 6.2.

Parameter	Value
r_c (km)	7000
q_1	10^2
q_2	10^4
$\mathbf{R}_c$	$\mathbf{I}_{3\times3} \times 10^{11}$
Process Noise σ_p (m/s^2)	10^{-4}
Process Noise $\mathbf{Q}_w$	$\begin{bmatrix} \mathbf{0}_{3\times3} & \mathbf{0}_{3\times3} \\ \mathbf{0}_{3\times3} & \mathbf{I}_{3\times3} \end{bmatrix} \times {\sigma_p}^2$
Nonlinear Measurement Model σ_n (rad)	10^{-3}
Nonlinear Measurement Model $\mathbf{R}_v$	$\mathbf{I}_{2\times2} \times {\sigma_n}^2$
$\mathbf{x}_0$	[1000 1000 1000 10 10 10]
$\hat{\mathbf{x}}_0$	$2\mathbf{x}_0$
$\mathbf{P}_{e,0}$	$[\hat{\mathbf{x}}_0 - \mathbf{x}_0]^T[\hat{\mathbf{x}}_0 - \mathbf{x}_0]$

Table 6.2: IWLQG Control Simulation Parameters

For $q = 10^2$, plots comparing the time history of true and estimated position vector components of the chaser are shown in Figure 6.7. It can be seen that the state has been regulated to the origin fairly quickly and that the state estimate has converged on the true state. Plots of the control vector components of the chaser are shown in Figure 6.8. Plots comparing the filter errors with the $\pm 3\sigma$ standard deviation bounds are shown in Figure 6.9. It can be seen that, at all times, the filter errors are within the $\pm 3\sigma$ standard-deviation bounds indicating range observability.

For $q = 10^4$, plots comparing the time history of true and estimated position vector components of the chaser are shown in Figure 6.10. It can be seen that the state has been regulated to the origin very quickly and that the state estimate has converged on

the true state. Plots of the control vector components of the chaser are shown in Figure 6.11. Plots comparing the filter errors with the $\pm 3\sigma$ standard deviation bounds are shown in Figure 6.12. It can be seen that, at all times, the filter errors are within the $\pm 3\sigma$ standard-deviation bounds indicating range observability.

In both cases, the state of the system is regulated quickly to the origin and the state estimate has converged on the true state. Thus, the IWLQG control has addressed the coupling between the processes of efficient control and reliable estimation. The IWLQG control scheme does not have the limitations of the LQD control scheme. It does not introduce any nonlinearity or increase the dimension of the problem. Thus, the IWLQG control scheme can be feasible for real-time applications.

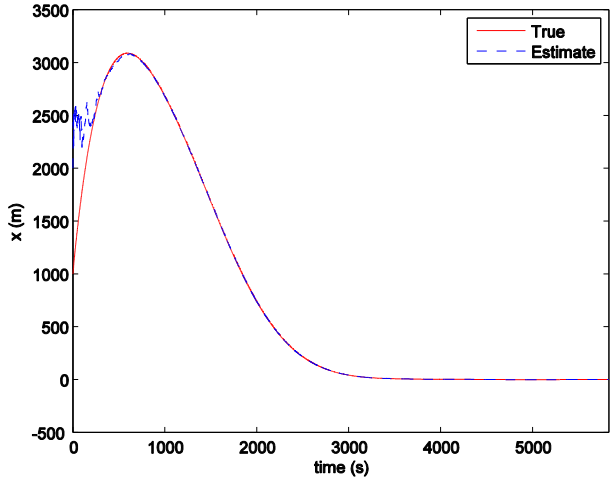

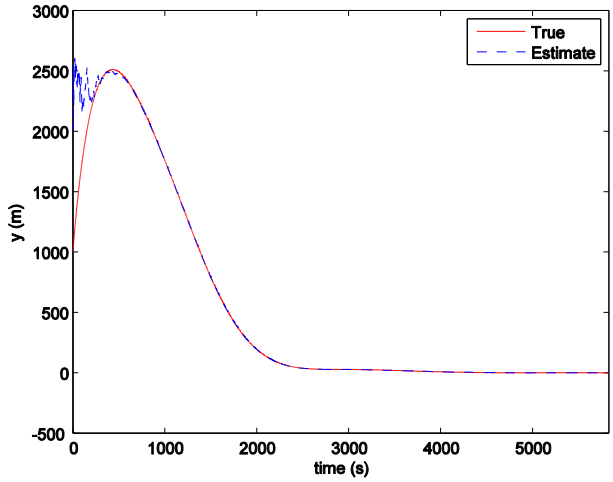

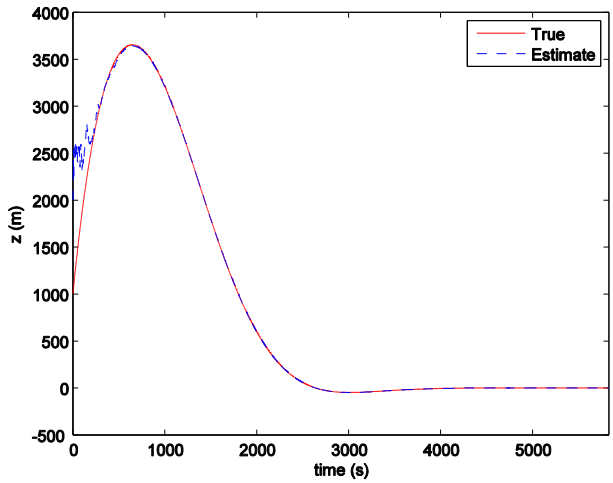

Figure 6.7: IWLQG $q = 10^2$: Position Vector Components

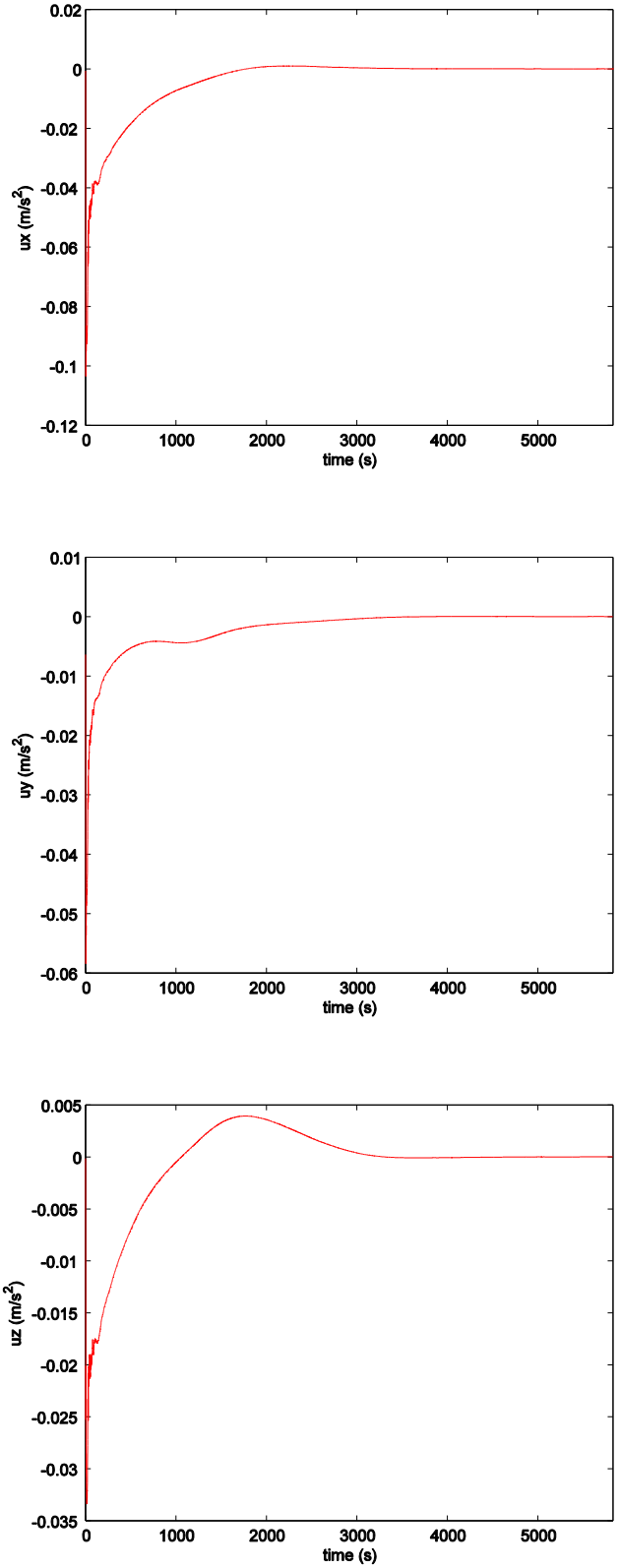

Figure 6.8: IWLQG q = 10^2: Control Vector Components

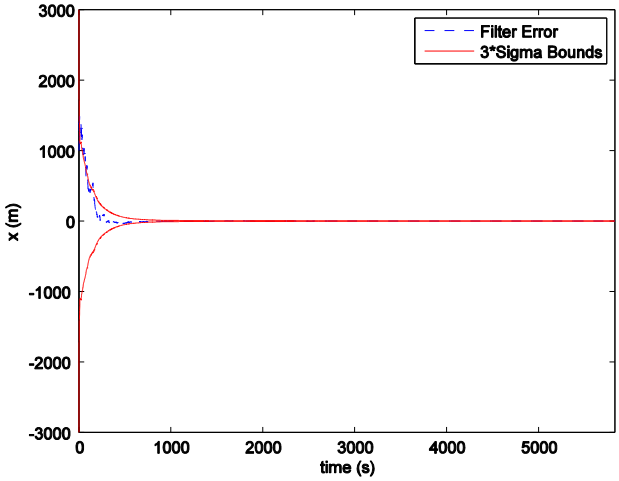

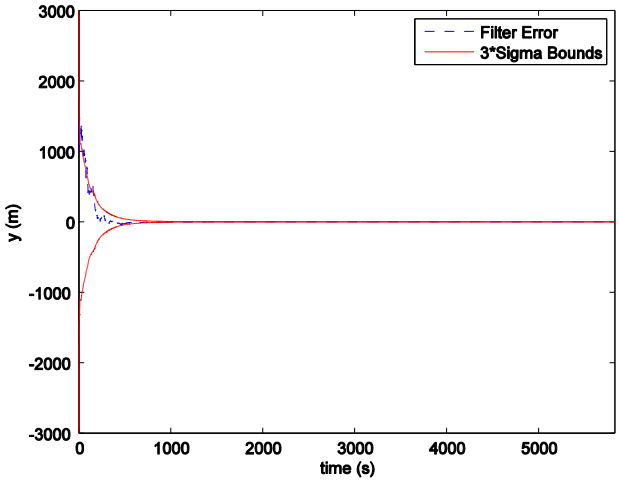

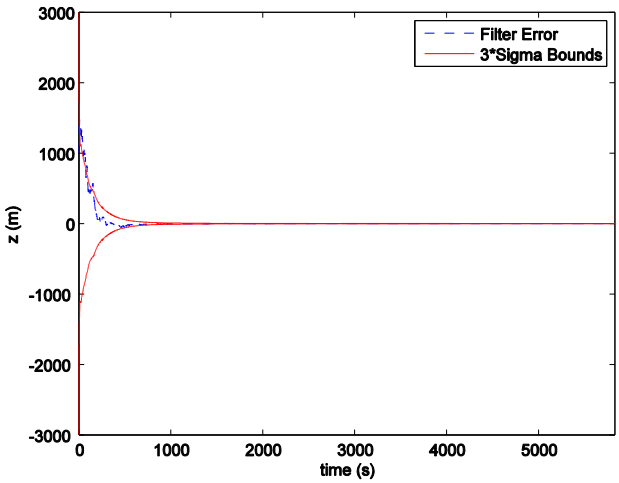

Figure 6.9: IWLQG $q = 10^2$: Filter Error and 3-σ Bounds

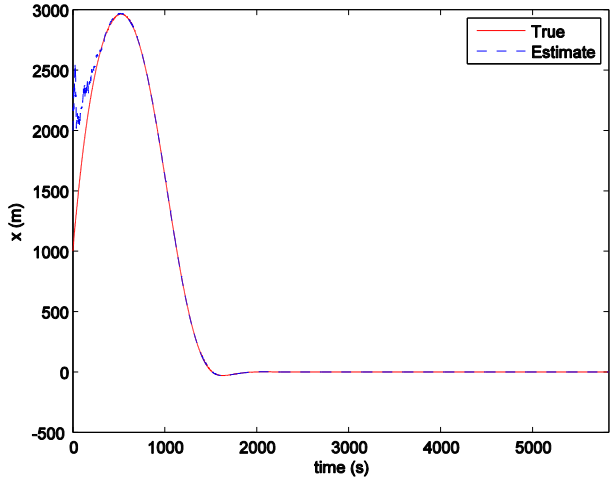

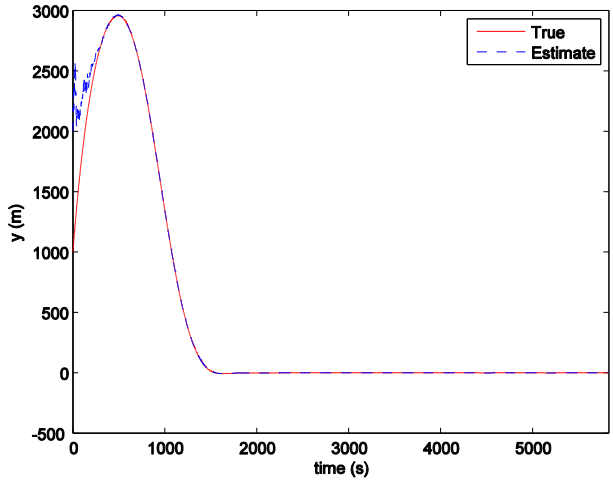

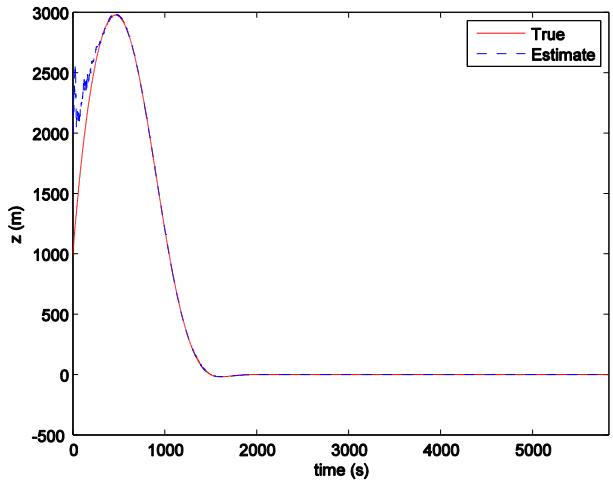

Figure 6.10: IWLQG $q = 10^4$: Position Vector Components

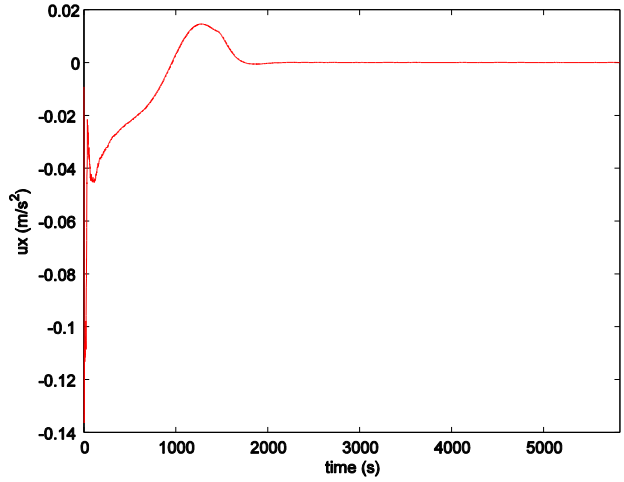

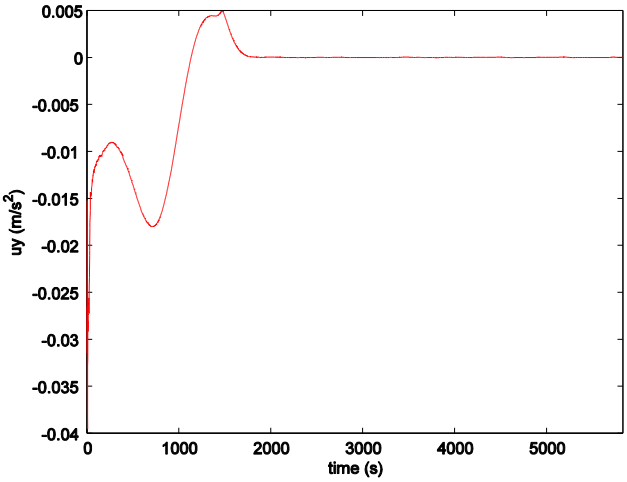

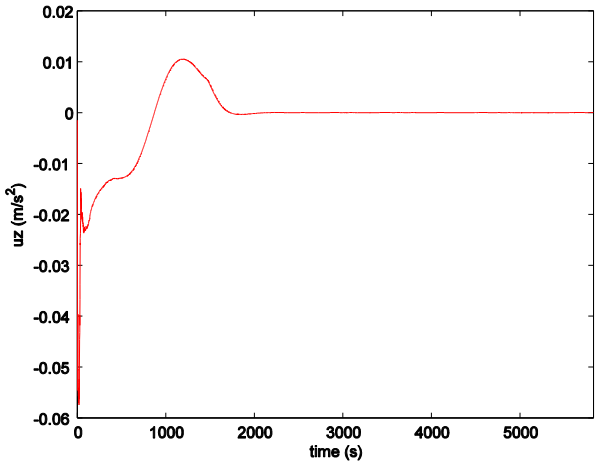

Figure 6.11: IWLQG q = 10^4: Control Vector Components

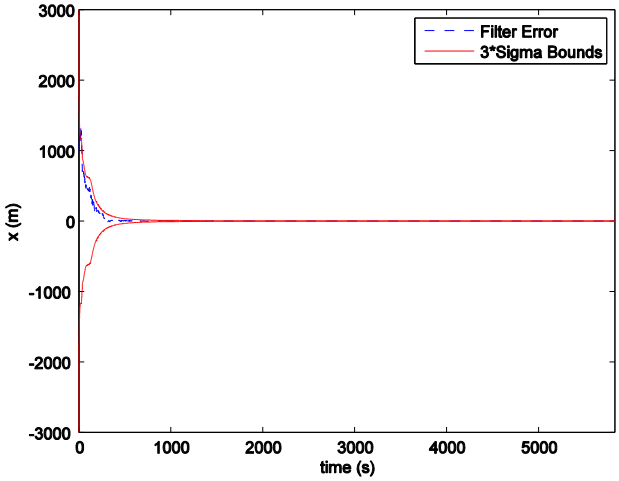

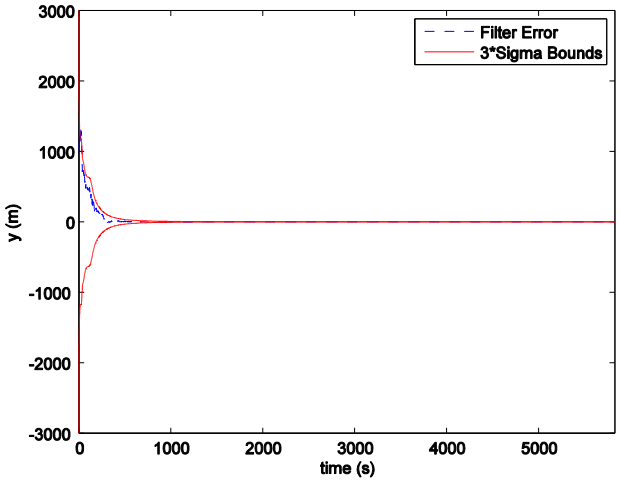

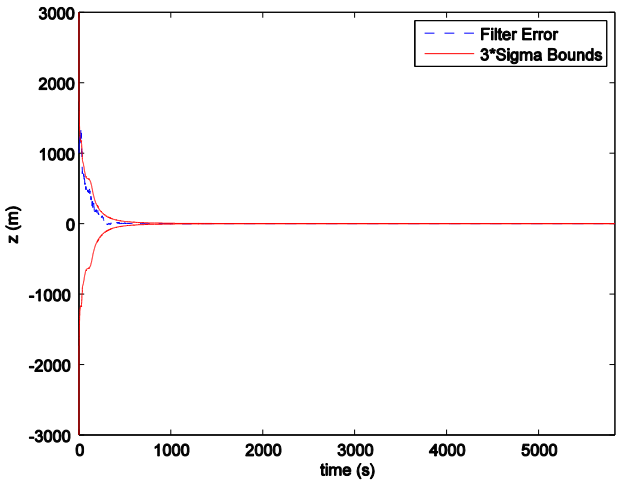

Figure 6.12: IWLQG $q = 10^4$: Filter Error and 3-σ Bounds

CHAPTER 7

CONCLUSION

In the first part of the dissertation, feedback control laws forming a saddle point solution to the spacecraft PE game are derived. The dynamics of the game are described in the space-based EH reference frame rather than the Earth-centered reference frame. Linear feedback control laws are derived for the LQ PE game using the LQ differential game theory. The SDRE method is used to write nonlinear game dynamics in linear-like non-unique SDC form. The application of the LQ differential game theory is then extended to LQ-like nonlinear PE game. The nonlinear feedback control laws derived may be near-optimal.

The near-optimal nonlinear feedback control laws, however, are obtained by solving an algebraic SDRE rather than solving an HJI PDE or a TPBVP which give optimal solutions, but are difficult to solve. Moreover, for larger separations, the efficacy of the near-optimal nonlinear control laws is superior to that of the linear control laws. Thus, the near-optimal nonlinear feedback control laws are a good substitute for computationally expensive optimal solution of an HJI PDE or a TPBVP as well as for the linear control laws.

In future, this work can be extended in a few avenues. The nonlinear control laws can be implemented using the game dynamics which include perturbations. Putting a constraint on the control usage, instead of a cost, so that each player has limited amount

of fuel to spend could be explored. Finally, PE games using impulsive thrusts could be explored.

In the second part of the dissertation, when the nonlinear angles-only measurement model is used to estimate the relative state of a spacecraft for control purposes, a coupling between the control and estimation processes is found to exist. In the LQG control implementing the angles-only measurement model, when constant high state weighting leads to a higher control effort, true state diverges from the state estimate which leads to the failure of the LQG control.

To address this issue two approaches are explored. The first approach is the LQD control approach. In this approach, the state and the performance criterion of the LQR/LQG problem are augmented to include uncertainty terms. The resulting control law has two parts. One part performs the system state regulation and the other attempts to reduce the uncertainty in the system state. This two-part control law is found to have addressed the coupling between the processes of efficient control and reliable estimation.

The second approach is the IWLQG control approach where the state weighting is not constant but is a function of the Fisher information matrix making the state weighting dependent on the accuracy of the state estimate. This variation in the state weighting is found to have addressed the coupling between the processes of efficient control and reliable estimation.

Thus, both approaches facilitate observability of linear spacecraft relative-motion state when angles-only navigation model is used and one of the spacecraft undergoes continuous-thrust maneuvers. The LQD control approach has some limitations. The augmented system is nonlinear and increases the dimension of the problem.

The solution is computationally intensive. The IWLQG approach avoids these issues. It is simpler and is viable for real-time applications.

REFERENCES

1. Alfriend, K. T., Vadali, S. R., Gurfil, P., How, J. P., and Breger, L. S., *Spacecraft Formation Flying*, Elsevier, 2010.
2. Bate R., Mueller D., White J., *Fundamentals of Astrodynamics*, Dover Publications, New York, 1971.
3. http://ase.tufts.edu/cosmos/print_images.asp?id=43
4. Chao C., *Applied Orbit Perturbation and Maintenance*, The Aerospace Press, El Segundo, CA, 2005.
5. Curtis, Howard D., *Orbital Mechanics for Engineering Students*, Elsevier Butterworth-Heinemann, 2009.
6. http://mathworld.wolfram.com/EccentricAnomaly.html
7. Tschauner, J. and Hempel, P., "Rendezvous zu einem in elliptischer Bahn unlaufenden Ziel," Acta Astronautica, Vol. 11, No. 2, 1965, pp. 104–109.
8. Clohessy, W. H. and Wiltshire, R. S., "Terminal Guidance System for Satellite Rendezvous," Journal of Guidance, Control, and Dynamics, Vol. 27, No. 9, 1960, pp. 653–658.
9. Hill, G. W., "Researches in the Lunar Theory," American Journal of Mathematics, Vol. 23, No. 1, 1878, pp. 5–26.
10. Schaub, H. and Junkins J. L., *Analytical Mechanics of Space Systems*, AIAA, 2009.
11. Kirk, Donald E., *Optimal Control Theory: An Introduction*, Dover Publications, 2004.
12. Isaacs, R., *Differential Games*, John Wiley & Sons, New York, 1965.

13. Basar, T. and Olsder, G. J., *Dynamic Noncooperative Game Theory*, Academic Press, London, 1982.
14. Engwerda J., *LQ Dynamic Optimization and Differential Games*, John Wiley & Sons, England, 2005.
15. Cimen, T., "State-Dependent Riccati Equation (SDRE) Control: A Survey," *Proceedings of the 17th IFAC World Congress*, 2008, pp. 3761–3775.
16. Cimen, T., "Systematic and Effective Design of Nonlinear Feedback Controllers via the State-Dependent Riccati Equation (SDRE) Method," *Annual Reviews in Control*, Vol. 34, No. 1, 2010, pp. 32–51.
17. Cimen, T., "Survey of State-Dependent Riccati Equation in Nonlinear Optimal Feedback Control Synthesis", *Journal of Guidance, Control, and Dynamics*, Vol. 35, No. 4, 2012, pp. 1025-1047.
18. Cloutier, J. R., D'Souza, C. N., and Mracek, C. P., "Nonlinear Regulation and Nonlinear H_∞ Control via the State-Dependent Riccati Equation Technique: Part 1, Theory," *1st International Conference on Nonlinear Problems in Aviation and Aerospace*, Embry-Riddle Aeronautical Univ. Press, Daytona Beach, FL, 1996, pp. 117–130.
19. Cloutier, J. R., D'Souza, C. N., and Mracek, C. P., "Nonlinear Regulation and Nonlinear H_∞ Control via the State-Dependent Riccati Equation Technique: Part 2, Examples," *1st International Conference on Nonlinear Problems in Aviation and Aerospace*, Embry-Riddle Aeronautical Univ. Press, Daytona Beach, FL, 1996, pp. 131–141.

20. Hammett, K. D., “Control of Nonlinear Systems via State Feedback State-Dependent Riccati Equation Techniques,” Ph.D. Dissertation, Air Force Inst. of Technology, Wright-Patterson AFB, OH, 1997.
21. Park, Han-Earl., Park, Sang-Young., Choi, Kyu-Hong., “Satellite Formation Reconfiguration and Station-keeping Using State-Dependent Riccati Equation Technique,” *Aerospace Science and Technology*, Vol. 15, No.6, 2011, pp. 440-452.
22. Kalman, R. E., “A New Approach to Linear Filtering and Prediction Problems,” *ASME Journal of Basic Engineering*, Vol. 82, No. 1, 1960, pp. 35–45.
23. Crassidis, J. L. and Junkins, J. L., *Optimal Estimation of Dynamics Systems*, Chapman and Hall/CRC Applied Mathematics and Nonlinear Science Series, 2004.
24. Woodward R. H., “Pursuit-Evasion Games Between Two Spacecraft in Near-Earth Orbits,” M.S. Thesis, Air Force Institute of Technology, Wright-Patterson AFB, Ohio, USA, 1972.
25. Bohn, G. D., “Application of a Near-Optimal Closed Loop Control Law to a Pursuit-Evasion Game Between Two Spacecraft,” M.S. Thesis, Air Force Institute of Technology, Wright-Patterson AFB, Ohio, USA, 1975.
26. Pontani, M., and Conway, B. A., “Numerical Solution of the Three-Dimensional Orbit Pursuit Evasion Game,” *Journal of Guidance, Control, and Dynamics*, Vol. 32, No. 2, 2009, pp. 474-487.
27. Menon, P. K. A., and Calise, A. J., “Guidance Laws for Spacecraft Pursuit-Evasion and Rendezvous," *AIAA Guidance, Navigation, and Control Conference*, Minneapolis, MN, 1988, pp. 688-697.

28. Kelley, H. J., Cliff, E. M., and Lutze, F. H., "Pursuit–Evasion in Orbit," *Journal of the Astronautical Sciences,* Vol. 29, No. 3, 1981, pp. 277–288.
29. Stupik, J., Pontani, M., Conway, B., "Optimal Pursuit/Evasion Spacecraft Trajectories in the Hill Reference Frame," *AIAA/AAS Astrodynamics Specialist Conference*, Minneapolis, MN, 2012.
30. Bernhard, P., "Linear-quadratic, Two-person, Zero-sum Differential Games: Necessary and Sufficient Conditions," *Journal of Optimization Theory and Applications,* Vol. 27, No. 1, 1979, pp. 51–69.
31. Basar, T., Bernhard, P., *H_∞ Optimal Control and Related Minimax Design Problems: A Dynamic Game Approach*, Birkhauser, Boston, 1991.
32. Woffinden, D., "Angles-Only Navigation for Autonomous Orbital Rendezvous," Ph.D. Dissertation, Utah State University, Logan, Utah, USA, 2008.
33. Lovell, T. A., and Lee, T., "Nonlinear Observability for Relative Satellite Orbits With Angles-Only Measurements," *24th International Symposium on Space Flight Dynamics*, Laurel, Maryland, USA, 5 - 9 May, 2014.
34. Chen, T. and Xu, S., "Double Line-of-Sight Measuring Relative Navigation for Spacecraft Autonomous Rendezvous," *Acta Astronautica*, Vol. 67, July-August 2010, pp. 122-134.
35. Tombasco, J., "Orbit Estimation of Geosynchronous Objects via Ground-Based and Space-Based Optical Tracking," Ph.D. Dissertation, University of Colorado, Boulder, CO, USA, 2011.

36. Hablani, H. B., Tapper, M. L., and Dana-Bashian, D. J., "Guidance and Relative Navigation for Autonomous Rendezvous in a Circular Orbit," *Journal of Guidance, Control, and Dynamics*, Vol. 25, No. 3, 2002, pp. 553–562.
37. Hablani, H. B., "Autonomous Relative Navigation, Attitude Determination, Pointing and Tracking for Spacecraft Rendezvous," AIAA 2003-5355, *AIAA Guidance, Navigation, and Control Conference Exhibit*, Austin, TX, 2003.
38. Chari, R. J. V., "Autonomous Orbital Rendezvous Using Angles-Only Navigation," M.S. Thesis, Massachusetts Institute of Technology, Cambridge, MA, 2001.
39. Gillis, R. W., "Low-Thrust Assisted Angles-Only Navigation," M.S. Thesis, Utah State University, Logan, Utah, USA, 2011.
40. Wittenmark, B., "Adaptive Dual Control Methods: An Overview," *5th IFAC Symposium on Adaptive Systems in Control Signal Processing*, Budapest, Hungary, 1995, pp. 62-72.
41. Kim, J., "Dual Control Approach for Automatic Docking Using Monocular Vision," Ph.D. Dissertation, Stanford University, USA, 2007.
42. Personal communication with Dr. Jinwhan Kim.